THE UNIVERSITY OF QUEENSLAND

AUSTRALIA

Novel methods for predicting clinical outcome in neonates from clinical electroencephalography recordings

Kartik K. Iyer

A thesis submitted for the degree of Doctor of Philosophy at
The University of Queensland in 2015

School of Medicine

Abstract

In this doctoral thesis I investigate a key issue in neonatal intensive care monitoring - the prediction of clinical outcome for infants soon after preterm or compromised full-term birth. With an ever increasing need for robust and reliable bedside monitoring, this dissertation develops a set of novel methods to quantify the electrical activity of the neonatal brain. In particular, I draw upon concepts established in physics and neuroscience known as criticality and crackling noise. These concepts, observed in many other dynamic natural systems, are used here to characterize bursts of cortical activity that are present in the neonatal electroencephalogram (EEG). Henceforth, in this thesis I test two related hypotheses: First, that cortical bursts in neonatal EEG yield important insights into critical brain states and underlying neurophysiology; Second, I propose that the robust characterization of these cortical bursts yield predictive markers of clinical outcome soon after birth, in those neonates at risk of poor outcome.

Previous studies of complex natural systems, such as earthquakes, have drawn upon analyses of stochastic, bursty activity known formally as "crackling noise". These analyses characterize the statistical distribution of the bursts (their area and duration) as well as the average shape of the bursts across a hierarchy of time scales. Furthermore, the study of crackling noise processes allow one to determine whether the bursts have a characteristic scale, or whether they are scale-free and consistent with criticality. In this thesis, I apply both these techniques – analyses of statistical distribution and of average burst shape to quantify the temporal progression of cortical bursts in EEG, from birth to recovery periods in the neonatal intensive care unit.

The data driven methods developed in this thesis are henceforth specifically aimed at analyzing the durations, areas and average shapes of EEG bursts in two neonatal populations; 1) Full-term neonates following birth asphyxia, and 2) Extremely preterm infants. In both cohorts, I characterize empirical data features present in neonatal EEG, i.e. durations and areas of cortical bursts by analyzing their probability distributions. Statistical quantifiers of average burst shapes - such as burst symmetry and sharpness - are used to distinguish between healthy and abnormal brain states. The analysis of statistical distributions of bursts and the quantification of average burst shapes leads to an automated metric for outcome prediction.

The key, original contributions of this thesis are that EEG bursts following full-term hypoxia and preterm birth are inherently scale-free, that is, their statistical distributions have no characteristic scales and robustly conform to the theoretical exponentially truncated power-law. In full-term

hypoxic infants, burst shapes are nearly scale-invariant although show changes in symmetry and sharpness for longer burst durations. These scale-free distributions and average shapes reflect fundamental, stochastic properties of critical brain states that provide insight into important neurobiological processes. For example, following recovery from hypoxia, average burst shapes in full-term neonates become symmetrical and scale invariant across all time scales. I study simulations of stochastic models to investigate possible mechanisms underlying the resumption of healthy cortical activity states such as recovery from metabolic depletion. In the preterm neonate, average shapes reveal a temporal progression in cortical bursts with respect to gestational age, and significantly pre-empt the occurrence of intra-ventricular brain hemorrhage.

In these cohort studies, I present the utility of novel methods developed to predict acute brain injury and long-term neurodevelopment. This work establishes statistically significant differences between burst shape indices in healthy versus poor clinical outcomes in both full-term hypoxic and preterm populations. These findings indicate a practical use for prediction and classification of at-risk neonates not readily available in current clinical settings. Moreover, the fundamental understanding of the neonatal brain is enriched by presenting unique features and insights into cortical burst generation, allowing a better understanding of neonatal neurophysiology.

Declaration by author

This thesis is composed of my original work, and contains no material previously published or written by another person except where due reference has been made in the text. I have clearly stated the contribution by others to jointly-authored works that I have included in my thesis.

I have clearly stated the contribution of others to my thesis as a whole, including statistical assistance, survey design, data analysis, significant technical procedures, professional editorial advice, and any other original research work used or reported in my thesis. The content of my thesis is the result of work I have carried out since the commencement of my research higher degree candidature and does not include a substantial part of work that has been submitted to qualify for the award of any other degree or diploma in any university or other tertiary institution. I have clearly stated which parts of my thesis, if any, have been submitted to qualify for another award.

I acknowledge that an electronic copy of my thesis must be lodged with the University Library and, subject to the policy and procedures of The University of Queensland, the thesis be made available for research and study in accordance with the Copyright Act 1968 unless a period of embargo has been approved by the Dean of the Graduate School.

I acknowledge that copyright of all material contained in my thesis resides with the copyright holder(s) of that material. Where appropriate I have obtained copyright permission from the copyright holder to reproduce material in this thesis.

Publications during candidature

Peer-reviewed papers:

Iyer K.K., Roberts J.A., Metsäranta M., Finnigan S., Breakspear, M., Vanhatalo S., Title: Novel features of early burstsuppression EEG predict outcome after birth asphyxia Published, *Annals of Clinical & Translational Neurology*, 2014

Roberts, J.A., **Iyer K.K.**, Finnigan S., Vanhatalo S., Breakspear M., Title: Scale-Free Bursting in Human Cortex following Hypoxia at Birth. Published, *Journal of Neuroscience*, 2014

Roberts J.A., **Iyer K.K**., Vanhatalo S., Breakspear, M. Title: Critical role for resource constraints in neural models Published, *Frontiers in Neuroscience*, 2014

Iyer K.K., Roberts J.A., Hellstrom-Westas L, Wikstrom S, Hansen-Pupp I, Ley D, Vanhatalo S, Breakspear M

Title: Cortical burst dynamics predict clinical outcome early in extremely preterm infants Under Review, 2014

Iyer K.K., Roberts J.A., Hellstrom-Westas L, Wikstrom S, Hansen-Pupp I, Ley D, Breakspear M, Vanhatalo S

Title: Early cortical bursts are acute markers of preterm intraventricular hemorrhage Under Review, 2014

Iyer K.K., Roberts J.A., Palmu K., Breakspear, M., Vanhatalo S.,

Title: Emerging methods for burst detection in neonatal brain monitoring In preparation, review paper, 2015

Conference abstracts:

Roberts, J.A., **Iyer K.K**., Finnigan S., Vanhatalo S., Breakspear M. Crackling noise in cortex after perinatal hypoxia. Society for Neuroscience Annual Meeting , USA. 2012

Roberts, J.A**., Iyer K.K**., Finnigan S., Vanhatalo S., Breakspear M. Scale-free dynamics in human neonatal cortex following perinatal hypoxia. 22nd Annual Computational Neuroscience Meeting, , France. 2013

Roberts, J.A., **Iyer K.K**., Finnigan S., Vanhatalo S., Breakspear M. Scale-free dynamics in cortex after perinatal hypoxia. NeuroEng 6th Australian Workshop on Computational Neuroscience, Melbourne, Australia. 2013

Publications included in this thesis

Roberts, J. A., Iyer, K. K., Finnigan, S., Vanhatalo, S., & Breakspear, M. (2014). Scale-free bursting in human cortex following hypoxia at birth. The Journal of Neuroscience, 34(19), 6557-6572. Incorporated as part of Chapter 3

Contributor	Statement of contribution
Kartik Iyer (Candidate)	Analyzed data (40%) Designed experiments (10%) Data extraction (50%) Wrote and edited the paper (15%)
James Roberts	Designed experiments (10%) Analyzed data (60%) Wrote and edited paper (30%)
Simon Finnigan	Wrote and edited the paper (5%)
Sampsa Vanhatalo	Designed experiments (50%) Data extraction (50%) Wrote and edited the paper (10%)
Michael Breakspear	Designed experiments (30%) Wrote and edited paper (40%)

Iyer, K. K., Roberts, J. A., Metsäranta, M., Finnigan, S., Breakspear, M., & Vanhatalo, S. (2014). Novel features of early burst suppression predict outcome after birth asphyxia. Annals of Clinical and Translational Neurology,1(3), 209-214. Incorporated as Chapter 4

Contributor	Statement of contribution
Kartik Iyer (Candidate)	Analyzed data (90%) Data extraction (50%) Wrote the paper (60%)
James Roberts	Analyzed data (10%) Wrote and edited paper (10%)
Marjo Metsäranta	Wrote and edited paper (5%)
Michael Breakspear	Wrote and edited paper (10%)
Sampsa Vanhatalo	Data extraction (50%) Wrote and edited paper (15%)

Iyer K.K., Roberts J.A., Hellstrom-Westas L, Wikstrom S, Hansen-Pupp I, Ley D, Vanhatalo S, Breakspear M, Cortical burst dynamics predict clinical outcome early in extremely preterm infants, Brain (published, advance access), 2015. Incorporated as Chapter 5

Contributor	Statement of contribution
Kartik Iyer (Candidate)	Analyzed data (80%) Data extraction (50%) Wrote the paper (50%)
James Roberts	Analyzed data (10%) Wrote and edited paper (10%)
Lena Hellstrom-Westas	Wrote and edited paper (5%)
Sverre Wikstrom	Analyzed data (10%)
Ingrid Hansen-Pupp	Designed experiments (40%) Wrote and edited paper (5%)
David Ley	Designed experiments (40%) Wrote and edited paper (5%)
Sampsa Vanhatalo	Designed experiments (20%) Data extraction (50%) Wrote and edited paper (10%)
Michael Breakspear	Wrote and edited paper (15%)

Iyer K.K., Roberts J.A., Hellstrom-Westas L, Wikstrom S, Hansen-Pupp I, Ley D, Breakspear M, Vanhatalo S, Early cortical bursts are acute markers of preterm intraventricular hemorrhage

In press, Critical Care Medicine, 2014. Incorporated as Chapter 6

Contributor	Statement of contribution
Kartik Iyer (Candidate)	Analyzed data (80%) Data extraction (50%) Wrote the paper (50%)
James Roberts	Analyzed data (10%) Wrote and edited paper (10%)
Lena Hellstrom-Westas	Wrote and edited paper (5%)
Sverre Wikstrom	Analyzed data (10%)
Ingrid Hansen-Pupp	Designed experiments (40%) Wrote and edited paper (5%)
David Ley	Designed experiments (40%) Wrote and edited paper (5%)
Michael Breakspear	Wrote and edited paper (10%)
Sampsa Vanhatalo	Designed experiments (20%) Data extraction (50%) Wrote and edited paper (15%)

Contributions by others to the thesis

Iyer K.K., Roberts J.A., Metsäranta M., Finnigan S., Breakspear, M., Vanhatalo S., Title: Novel features of early burstsuppression EEG predict outcome after birth asphyxia Published, *Annals of Clinical & Translational Neurology*, 2014

Vanhatalo S, Metsäranta M., were responsible for planning, implementing and collection of the infant data analysed within the study.

Breakspear, M., Roberts J.A. Finnigan S., Vanhatalo S, contributed to the design of experiments, analysis, and drafting of the paper

Iyer K.K. was involved with all of the above and the remainder of the work.

Roberts J.A., **Iyer K.K**., Finnigan S., Vanhatalo S., Breakspear M., Title: Scale-Free Bursting in Human Cortex following Hypoxia at Birth. Published, *Journal of Neuroscience*, 2014

Vanhatalo S, Roberts, J.A., Breakspear M., were responsible for planning, implementing and collection of the infant data analysed within the study.

Breakspear, M., Roberts J.A. Finnigan S., Vanhatalo S, to the design of experiments, analysis, and drafting of the paper

Iyer K.K. was involved with all of the above and the remainder of the work.

Roberts J.A., **Iyer K.K**., Vanhatalo S., Breakspear, M. Title: Critical role for resource constraints in neural models Published, *Frontiers in Neuroscience*, 2014

Roberts, J.A., Breakspear M., were responsible for conception of the paper, design of experiments and drafting

Vanhatalo S, was involved with the editing of the paper

Iyer K.K. was involved with simulation results and editing of the paper

Iyer K.K., Roberts J.A., Hellstrom-Westas L, Wikstrom,S, Hansen-Pupp I, Ley D., Vanhatalo S., Breakspear M

Title: Cortical burst dynamics predict clinical outcome early in extremely preterm infants Under Review, 2014

Hansen-Pupp I, Ley D., Hellstrom-Westas L., Wikstrom,S., Vanhatalo S, were responsible for planning, implementing and collection of the infant data analysed within the study.

Breakspear, M., Roberts J.A. Iyer, K.K, Hellstrom-Westas L., Vanhatalo S, contributed to the design of experiments, analysis, and drafting of the paper

Iyer K.K. was involved with all of the above and the remainder of the work.

Iyer K.K., Roberts J.A., Hellstrom-Westas L., Wikstrom,S., Hansen-Pupp I, Ley D., Breakspear, M., Vanhatalo S.

Title: Early cortical bursts are acute markers of preterm intraventricular hemorrhage Under Review, 2014

Hansen-Pupp I, Ley D., Hellstrom-Westas L., Wikstrom,S., Vanhatalo S, were responsible for planning, implementing and collection of the infant data analysed within the study.

Breakspear, M., Roberts J.A. Iyer, K.K, Hellstrom-Westas L., Vanhatalo S, contributed to the design of experiments, analysis, and drafting of the paper

Iyer K.K. was involved with all of the above and the remainder of the work.

Iyer K.K., Roberts J.A., Palmu K., Breakspear, M., Vanhatalo S.,

Title: Emerging methods for burst detection in neonatal brain monitoring In preparation, *Clinical Neurophysiology*, 2015

Iyer K.K., Palmu K., Vanhatalo S., were responsible for planning, and collection of relevant literature

Iyer K.K., Roberts J.A., Palmu K., Breakspear, M., Vanhatalo S., contributed to the drafting of the paper

Iyer K.K. was involved with all of the above and the remainder of the work.

Statement of parts of the thesis submitted to qualify for the award of another degree

None

Acknowledgements

First and foremost, thank you to my primary supervisor Michael Breakspear for giving me a wonderful opportunity to be involved in this research project. I am deeply thankful for your tutelage and advice during the whole course of the journey. Thank you for giving me a formal exposure to neuroscience and clinical research. As a mentor, you have given me a great motivation to pursue new frontiers in science. I am grateful for all the constructive feedback on many paper drafts, oral presentations and of course, the editing of this thesis. Personally, I have enjoyed your warm sense of humour throughout, the kind heartedness you have shown me and overall positive attitude you instil. Away from work, I have enjoyed our conversations on family, your usual recount of how good the surf was, cricket and your nostalgia for the '80s. Overall, I have genuinely admired your philosophy towards scientific pursuits and life outside of the 'research bubble' and will continue to influence me for a long time.

To Sampsa Vanhatalo, thank you for being associate supervisor to this project and allowing this fruitful collaboration. Your genuine enthusiasm for this project, knowledge of clinical neurophysiology and insight into modern clinical research is remarkable and very much appreciated. Professionally, you have given me a great formal exposure to clinical research and taught me well about the challenges of translating "super heavy mathematical analysis" to common bedside monitoring measures. Personally, I have enjoyed our many talks ranging from science, philosophy, culture and in general, the way of things in life – these were wonderful conversations. Thank you for your kind hospitality during my stay in Finland and the experience of working with you is one that I will never forget. Getting to know you well, and your family, visiting your country will no doubt be treasured memories of mine.

To James Roberts, thank you for your supervision and mentorship throughout this project. I am incredibly thankful and appreciative for all the technical lessons you gave me and elevating for my abilities for analysis and scientific writing. From an academic point of view, your eye for detail and insights into science are qualities that I admire and sincerely hope to emulate. Personally, I consider you a very good friend and will miss your quasi-professorial quips such as "I have my doubts about this", whilst stroking one's chin. Thank you for our casual conversations in cricket (more specifically, cricket statistics), the best bargains a man can buy on any given day, and for offering plentiful, sage advice for a career in research – these chats were most welcome and greatly assisted in my overall output.

To Simon Finnigan, thank you for your involvement and early supervision in this project. I am deeply thankful for meeting you when I did those years ago as it has given me great experiences, both academically and personally.

You have all been wonderful mentors throughout this project and I sincerely hope to continue future collaboration.

Thanks to all the folks at the SNG Lab as well. Matt Hyett, Anton Lord, Leonardo Gollo, I've got to know well you over the years and I am thankful for our continued friendship. To Sascha Frydman, Tamara Powell, Matt Aburn, at various stages you helped my research progress and for that I am thankful. To Christine Guo as well for some astute advice for a career in research, I thank you for guidance early in my final year.

Thank you to QIMR Berghofer Medical Research Institute, the business development team, Matthew Spitzer and Professor Frank Gannon for supporting and funding an overseas study trip in Finland. Thanks to Karen Moran and the Moran family, including grandson Calvin for their support in raising funds towards this trip and research into causes of cerebral palsy - I wish Calvin and family all the best. This trip greatly enhanced the academic contributions of this thesis, and has resulted in a successful ongoing collaboration with European partners.

Thank you to Angela Trieu from QIMR Berghofer Medical Research Institute and the School of Medicine (UQ) research office for their support and assistance during my candidature.

Last but not least, thank you to my family for their love and support over the years. To my parents, thank you for encouraging and supporting me to pursue my interests. To my Father, it is said that causality has its many interpretations, but as a child growing up and watching you devote yourself to the pursuit of scientific discovery inspired me to think differently and develop a scientific mind. To my Mother, childhood teachings of reading, writing and clarity when communicating are lifelong lessons that I hold dear and have held me in good stead thus far. To my younger brother Guru, thank you for your much appreciated sense of humour and genuine interest in my research, it was most welcome and offered a great relief. Lastly, to my wife Sushma, thank you for sharing in this journey with me, your love and warmth throughout inspired and motivated me to keep chipping away.

Keywords

Scale-free brain activity, crackling noise, neonate, cortical bursts, full-term hypoxia, preterm birth, clinical outcome prediction, power-law, average shapes, criticality

Australian and New Zealand Standard Research Classifications (ANZSRC)

ANZSRC code: 110904, Neurology and Neuromuscular Diseases, 70% ANZSRC code: 029901, Biological physics, 30%

Fields of Research (FoR) Classification

FoR code: 1109, Neurosciences, 100%

Table of Contents

List of Figures & Tables

List of Abbreviations used in the thesis

aEEG – amplitude-integrated electroencephalographyBMS – Bayesian Model Selection

BS – Burst Suppression

BSID-II – Bayley Scales of Infant and Toddler Development, Second version

CNS – Central nervous system

CTS – Continuous EEG

EEG – Electroencephalography

GA – Gestational age

GABA - gamma-Aminobutyric acid

HIE – Hypoxic ischemic-encephalopathy

IBI – Inter-burst Interval

IVH – Intraventricular hemorrhage

MDI – Mental Development Index

NICU – Neonatal Intensive Care Unit

PDI – Psychomotor Development Index

PVL – Periventricular leukomalacia

REM – Rapid eye movement

SATs – Spontaneous activity transients

WHO – World Health Organization

1.0 INTRODUCTION

ABSTRACT

This introductory chapter provides a short overview of the fundamental structure and function of the neonatal brain. To provide a background, this chapter firstly summarizes the developmental aspects of the healthy neonate brain briefly introducing brain development, the proliferation of cortical pathways and basic neural circuitry. It elaborates the growth processes involved early in gestation and further into the intricate signalling networks in the brain. These networks form the basis for rapid cortical electrical bursting patterns. This leads to the focus of this thesis which is quantifying cortical activity from the electroencephalogram (EEG) in full-term hypoxic infants and preterm infants. The associated neurological sequelae in both populations are foregrounded by a summary into current epidemiology and common clinical practices. Finally, this chapter briefly highlights recent advances in physics and neuroscience, such as criticality, scale-free dynamics and crackling noise. These concepts introduce novel techniques to answering the fundamental hypotheses tested in this body of work – of developing rapid and reliable predictors of outcome for full-term and preterm neonates after birth.

1.1 THE NEONATAL BRAIN: CONCEPTION TO POSTNATAL DEVELOPMENT

The human brain is an incredibly complex and diversely structured organ. It is the core of the human nervous system in which movement, cognition and overall biological well-being is developed, determined and maintained. From early stages of conception in the womb, through to childhood and adulthood, tremendous changes in overall brain size, structure and connectivity take place. In this section I overview the neurodevelopment of an infant, including the basis for brain formation and how the structure of the brain is wired for growth and communication.

1.1.1 FORMATION OF THE BRAIN

The brain begins to form early in the embryonic period, beginning at three weeks post-conception, with a process known as neural induction in the neural tube – the foundation of the central nervous system (CNS) (Stiles and Jernigan 2010). The neural tube is a fundamental structure in the vertebrate embryo, carrying highly proliferative cells which provide the building blocks for organs and vasculature. As the neural tube closes, these proliferative cells are contained within a hollow tube-type structure. This structure allows for neural induction, which is initiated when two of three germ layers of cells in the neural tube, the mesoderm (middle layer of cell tissue) induces the ectoderm (outer layer of cell tissue) to form the neural plate (Fig.1.1A). Whilst the exact mechanism of this induction is not fully understood, the folding of neural plates rapidly converges to form neural folds (Lagercrantz et al. 2010). Within these neural folds, major cells such as neurons and glia arise, allowing for connectivity and a foundation for basic homeostasis via the human brain (Merkle and Alvarez-Buylla 2006). As key mitotic (cell-dividing) processes occur in parallel with multiple layers of neural folding, the overall morphology of the human brain becomes more apparent, forming the overall structure identified as the cerebral cortex (Fig. 1.1B).

From this early perinatal period through to postnatal development, the cerebral cortex undergoes vast development in interconnectivity, growth and function. Towards the end of the embryonic period (eighth and ninth week gestation) leading to the end of gestation, there is rapid growth and elaboration of both cortical and subcortical structures including major fibre pathways that are crucial for synaptogenesis (Kostović and Jovanov-Milošević 2006). Early neuronal connections, which are controlled by growth processes, are aided by migration of neurons and more intricate expression of neuronal structures such as axons (connecting long fiber between neurons) and dendrites (short fibres at the end of axons). These pathways proliferate innumerably, with studies into the macaque prefrontal cerebral cortex (order *Primate*) indicative of up to 40000 new synapses per second during the perinatal period (Bourgeois 1997; Moser

1999). As these processes rapidly unfold within the cortex, the migration of neurons to specific 'local' clusters allow for communication between cortical columns (Lagercrantz et al. 2010). These basic cortical columns extend across and between cortical hemispheres, accompanied by long-range connections between thalamus (a small structure above the brainstem) and cortex (Kostović and Jovanov-Milošević 2006; Kostović and Judaš 2007). Long-range connections, such as thalamocortical and corticocortical projections, continue to proliferate up until 30 weeks gestation (Kostović and Judaš 2010) with the emergence of major inter-hemispheric short-range connections formed in the weeks leading up to 37-38 weeks gestation (Lagercrantz et al. 2010).

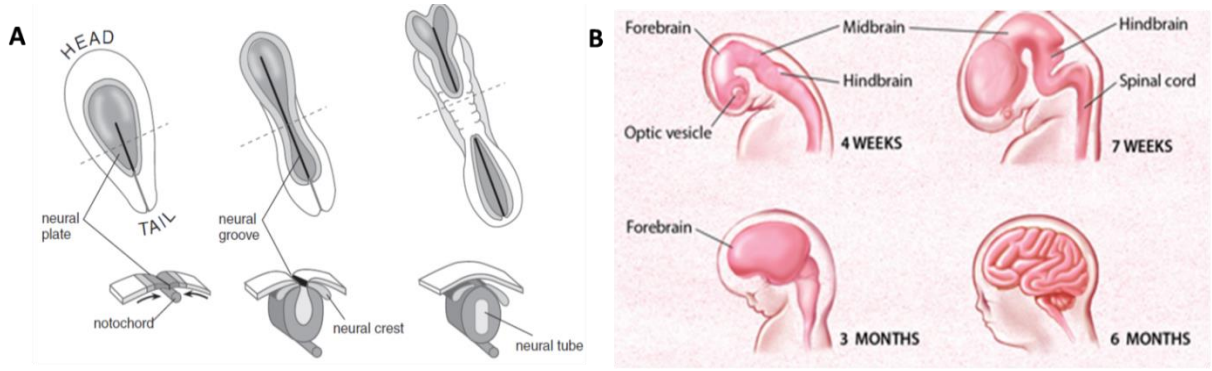

Figure 1.1 – From the embryo through to neural tube closure and cerebral cortex formation in-utero. (A) Embyronic period during which neural induction occurs (Lagercrantz et al. 2010). (B) From neural folding to cortex development (BrainFacts.org 2014)

After birth, brain growth and connectivity continues postpartum through to early childhood and adolescence. Cortical pathways proliferate until two years of age followed by increases in size and shape, before reaching 90% of adult volume by the age of six (Iwasaki et al. 1997; Lenroot and Giedd 2006). An inherently unique aspect of brain development in-utero is the high number of neurons and synapses produced – a level that far exceeds that which is seen during adult life (Innocenti and Price 2005). One of the mechanisms for this level of growth is the fetal brain being experience-independent, i.e. new connections are generated spontaneously in the absence of patterned stimuli from the external world (Lagercrantz et al. 2010). As the influence of experience-dependent activity is subsequently exerted upon the newborn (as early as its first awakening post-birth) connectivity processes are stemmed by competitive processes – an indication of early plasticity and intrinsic adaptation of the external world (Stiles and Jernigan 2010).

1.1.2 NEONATAL CORTICAL CONNECTIONS

The spread and growth of networks within the cerebral cortex, extending to the basal ganglia, thalamus and brainstem, establishes fundamental neurophysiological connections required for sensory perception and later cognition. As these networks differentiate into specific areas within the brain, they begin to institute key functions. By the end of the embryonic period, the

vertebrate embryo within the neural tube structure begins a prolonged and highly refined process of neural patterning (Stiles and Jernigan 2010; Sur and Rubenstein 2005). This process of neural patterning extends throughout the gestation period and is fundamental to the organization of the somatosensory network, motor cortex, and cognitive association areas of the human brain.

In parallel with brain formation, basic signal communication and networking is established through neuron-neuron interactions. In the fetal period (beginning at the ninth gestation week through to mid-gestation) neurons proliferate and migrate, allowing for prototypic connections between neuron 'chains' or *synapses*, resulting in formation of co-active networks via axons and dendrites (Stiles and Jernigan 2010). Arising from this period is the neocortex – a sub-structure within the cerebral cortex responsible for higher functions such as sensory perception, generation of motor commands and cognition. Vast amounts of activity relay through axons and dendrite 'chains' between the neocortex and sub-cortical nuclei takes place in the final trimester of pregnancy (Lagercrantz et al. 2010).

Previous studies have reported the emergence of myelin - a critical insulating layer of axons– during this period midway between conception and birth, becoming evident by the 24th week and continuing until two years of age (Lagercrantz et al. 2010; Stiles and Jernigan 2010; Van der Knaap and Valk 2005). The main function of these myelinated axons and dendrites is to receive and efficiently regulate the transmission of electrochemical signals (Stiles and Jernigan 2010). Thus, complex neural 'hubs' of communication arise from these key structures allowing for substantial neurodevelopment in the weeks leading up to birth.

Synaptic communication is an integral part of brain growth and function from the second trimester onwards through to postnatal development (Kostović and Jovanov-Milošević 2006). Critical feedback loops become established via thalamocortical and corticothalamic pathways from the neocortex to the thalamus. Here, the thalamocortical pathway transmits sensory and motor information from the receptors in the eye (retina), ear (cochlea) and muscle or skin to the sensorimotor regions of the neocortex via the thalamus (Stiles and Jernigan 2010). At 22 weeks, the thalamocortical pathway is not immediately established, but rather, forms its initial connections with a subplate layer of the cortex (Kostović and Jovanov-Milošević 2006). This subplate structure is unique and essential to prenatal brain development, without which normal connectivity patterns cannot exist (Stiles and Jernigan 2010).

Over a four week period, thalamocortical axons make connections with the subplate layer, and then eventually to the primary cortical layer by about 26 weeks (Fig. 1.2). Similarly, the same development pathway occurs for corticothalamic axons, where the subplate layer is intermediary

to eventual thalamic connectivity (Kostović and Jovanov-Milošević 2006). The feedback loop is completed via the corticothalamic pathway by transmitting information from cortex back to the thalamus. These early cortical connections have been thought to be the basis for neuronal circuitry in the human fetal cerebral cortex (Kostovic and Judas 2010) and further, a strong component of the electrical activity in the brain (Lagercrantz 2010).

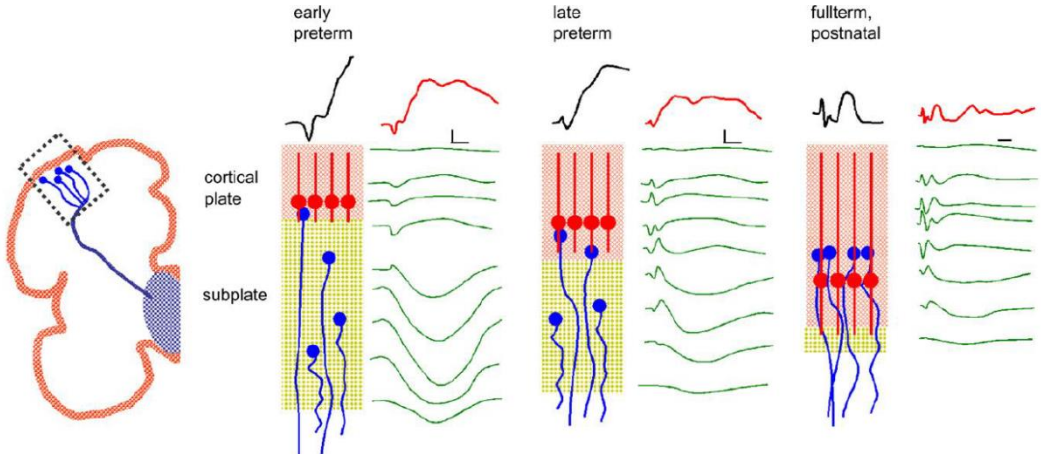

Figure 1.2 – Thalamocortical connections (blue fibres) with somatosensory evoked potentials (green trace) at different development stages. The red fibres indicate layer pyramidal neurons (Vanhatalo and Lauronen 2006)

The electrical activity of the mature human cortex, commonly measured via an electroencephalogram (EEG), reflects the functional state of the brain through cortical activity (Ernst Niedermeyer and da Silva 2005). Spontaneous, recurrent action potentials from the thalamic nucleus and cortical pyramidal cells (Mircea Steriade et al. 1990) form the basis for EEG activity in the cortex. Further, this activity reflects the synchronization of postsynaptic action potentials from large numbers of neurons. This synchronicity is maintained by recurrent connections between thalamocortical relay cells and the reticular thalamic nucleus (Lagercrantz et al. 2010). The neurophysiological basis for fetal EEG activity is relatively unknown. Research suggests that at the second trimester the cortical subplate is likely to be involved in modulating EEG activity (Kostović and Jovanov-Milošević 2006). It has been hypothesized that the subplate layer plays a large role in the emergence of spontaneous activity transients (SATs), a type of developmental activity that is present until an infant reaches term age (Vanhatalo and Kaila 2006). This type of activity is stereotypically distinct, with slow bursts of cortical activity followed by transient silent (inter-burst) periods. As the fetal brain's emerging cortical connectivity becomes established, cortical bursts reflected in EEG become mediated through synaptic networks and further mediated by neurotransmitters. By term age, the newborn undergoes further maturational changes through to early childhood (Fig. 1.3).

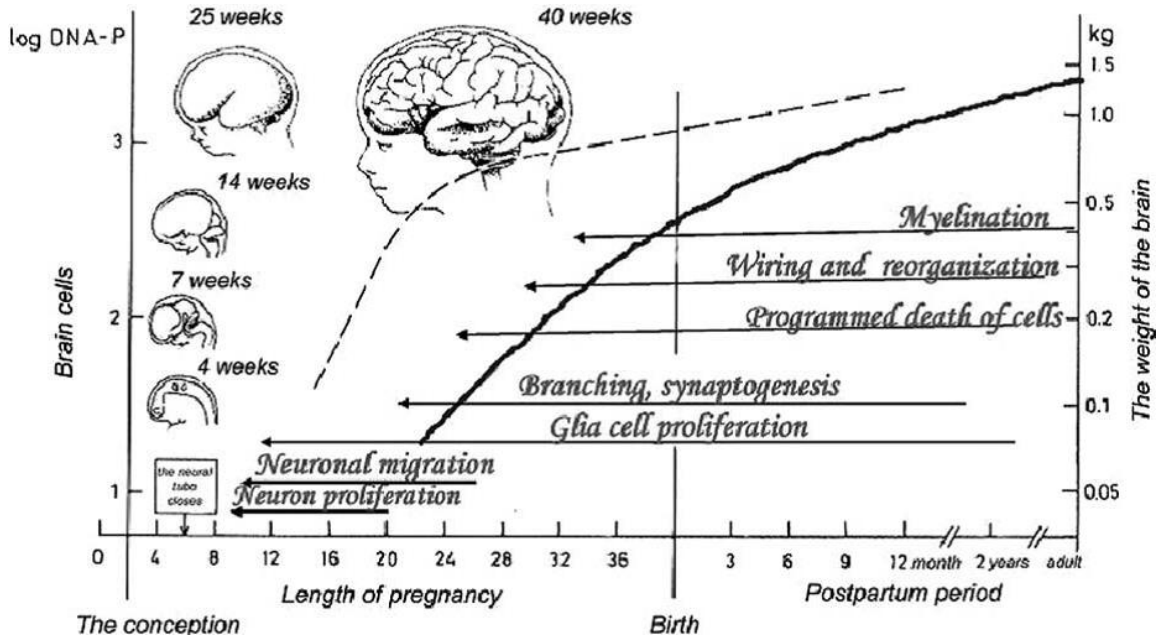

Figure 1.3 – Milestones of brain development processes from Lagercrantz (2010)

Complex dynamics within EEG activity such as sleep-wake cycles become more apparent during the third trimester (Graven and Browne 2008; Peirano et al. 2003). After birth, either preterm or at term, the EEG can be characterized as discontinuous or continuous. Background activity during discontinuous patterns display distinct periods of burst and inter-burst intervals, whereas in continuous patterns this distinction is less apparent. At term age, background EEG activity is predominantly continuous during wakefulness and active (REM) sleep, but discontinuous during quiet (non-REM) sleep (Peirano et al. 2003). In the preterm, cortical activity is typically characterized by a discontinuous (*trace discontinu*) EEG background (Hellström-Westas and Rosén 2005). The underlying neurophysiological mechanisms behind these EEG patterns of activity have been of immense interest in recent research (Feldman and Eidelman 2006; Graven and Browne 2008; Weisman et al. 2011). Neurotransmitters such as GABA (gamma-Aminobutyric acid), glutamate and ions such as chloride and extracellular calcium have been postulated as playing a major role in the excitation and inhibition of neuronal circuits (Kostović and Jovanov-Milošević 2006). This balance of excitation and inhibition in the brain is interrupted, either temporarily or irrevocably, by the presence of brain injury.

The presence of abnormal EEG activity patterns such as *trace discontinu* and burst suppression are acute reflections of the functional state of the human cortex. In this thesis I further explore these abnormal types of neonatal EEG and aim to provide further insight into prenatal and postnatal brain development.

1.2 BRIEF EPIDEMIOLOGY OF NEONATAL ENCEPHALOPATHY

During the period of tremendous growth and complexity involved in brain development processes, the human infant is exposed to the ever present risk of brain injury, particularly during the perinatal period. Whilst complex forms of encephalopathy – disease of the brain – exist, infant brain disorders can be categorized into those occurring at normal gestation (or term) and those affecting premature (or preterm) infant populations. In the following section, I briefly overview the incidence and risk of two common neonatal brain abnormalities: 1) hypoxic ischemic encephalopathy at term and 2) encephalopathy arising from preterm birth. The pathophysiological aspects of these abnormalities will be discussed in Chapter 2.

1.2.1 BIRTH ASPHYXIA AND HYPOXIC ISCHEMIC ENCEPHALOPATHY

The World Health Organisation (WHO) defines the criteria for the diagnosis of birth asphyxia as the "failure to establish breathing after birth" (Spector and Daga 2008). Despite major advances in neonatal monitoring, treatment and clinical management in perinatal medicine, birth asphyxia leading to hypoxia is still a leading cause of mortality and long term morbidity. Asphyxia at birth leads to two major physiological consequences: (1) hypoxic ischemia and (2) neonatal encephalopathy. A combination of diminished oxygen rich blood, the deprivation of energy producing metabolites and a disturbed neurological function of the newborn brain (Volpe 2001a) results in the condition hypoxic ischaemic encephalopathy (HIE).

Neonatal HIE has a significant prevalence worldwide and has a number of associated risk factors as the condition is complex in its diagnosis and clinical management. The condition is a significant pre-cursor to neurodevelopmental disorders and disability in infants. HIE infants have poor neurodevelopmental outcomes at 18 months of age (Sinclair et al. 1999), such as:

- Cerebral Palsy,
- Epilepsy,
- Blindness,
- Other motor development problems (e.g. hypotonia) & Learning difficulties.

Most infant death from acute HIE occurs within the first week of life, with infants suffering with severe neurologic impairment or even dying in their infancy from aspiration pneumonia or systemic infections (Morley 2005). The incidence of HIE worldwide is relatively high with birth asphyxia associated with mortality rates of 25-50% (Spector and Daga 2008). HIE occurs in 1 in 6 per 1000 births in developed countries, (in developing countries the incidence of HIE is reportedly higher), with neonatal encephalopathy occurring 2-6 per 1000 births and hypoxic

ischemia occurring 1-8 per 1000 live term births (Volpe 2001a). Estimates from the WHO indicate HIE is the fifth largest cause of death in children under the age of five years (Bryce et al. 2005) with 80% of infants who survive severe HIE develop complications in later neurodevelopment.

Population based studies have studied the incidence of asphyxia at birth leading consequently to HIE from the late 1970's (Hull and Dodd 1992) through to present day (Kurinczuk et al. 2010). While standards in clinical practice have improved over time, reduced incidence rates are offset by variations in case identification due to imprecise clinical criteria. More stringent methodologies over the past few years for case identification from clearly defined populations (Badawi et al. 1998; Evans 2001; Tagin et al. 2012) have provided more accurate indicators of HIE incidence, management and associated risk factors.

Identifying key risk factors in HIE is an essential guide to clinical management and optimal treatment plans. Understanding the pathophysiological pathways are vital, as evidence suggests the condition has a small time-window prior to permanent brain injury (Morley 2005). Some of the risk factors for HIE during pregnancy include a combination of maternal age, family history of neurological disorders (including and excluding seizures), alcohol consumption, birth weight and growth, thyroid disease and gestational age (reported by Badawi et al (1998)). During the peripartum period (leading up to birth and directly after), other risk factors are associated with the onset of HIE including presentation (position of birth), mode of delivery (vaginal, breech or emergency caesarean), maternal fever during labour and general anesthesia effects (Badawi et al. 1998). Asphyxia leading to HIE is further complicated by multifactorial risk factors which result in an acute brain injury. Early intensive care monitoring thus relies on characterization of cardiorespiratory and brain responses to provide clinically qualitative and quantitative biomarkers that may help predict short and long-term outcomes. These biomarkers, in combination with risk factors, provide a critical understanding of newborn pathophysiology.

1.2.2 PRETERM BRAIN INJURY: RISK FACTORS AND INCIDENCE

Preterm birth is typically defined as birth prior to 37 weeks gestation (Beck et al. 2010). There are three sub-categories of preterm birth – those born extremely preterm (<28 weeks), very preterm (28 to 32 weeks) and moderate to late preterm (<37 weeks) (WHO 2013). The premature birth of an infant is the leading cause of neonatal death within the first four weeks of life and poses a significant risk to morbidity and mortality.

Preterm birth leads to a multitude of physiological disturbances, which can be primarily characterized into: (1) cardiorespiratory (2) systemic (i.e. metabolic, coagulopathy) and (3)

neurological sequelae. Its significant prevalence worldwide is due to a combination of maternal, fetal, genetic and environmental risk factors (Beck et al. 2010).

Neurodevelopmental outcomes at 18 months of age for preterm birth survivors potentially include:

- Cerebral Palsy,
- Sensory deficits,
- Learning disabilities,
- Respiratory illnesses.

Based on recent reports of neonatal births worldwide, the incidence of preterm birth is estimated to be 11% of all livebirths (Blencowe et al. 2012) with increasing rates of preterm delivery reported. Statistics from about 184 countries show that preterm birth occurs for between 5% and 18% of births (WHO 2013). This is largely due to increases in multiple births, risk of maternal infection, greater use of reproductive techniques in developed countries and variable socioeconomic factors in developing countries (Callaghan et al. 2006). Complications arising from preterm birth account for over a million deaths each year, and contribute to over 50% of all neonatal deaths (Blencowe et al. 2012). In addition, it is the second leading cause of death for children under five years of age behind pneumonia (WHO 2013).

The incidence of preterm birth has been the subject of many population based studies, with investigations primarily into causal factors and long-term clinical monitoring of the neonate through to early childhood (Goldenberg et al. 2008). Factors which cause birth prematurity include intrauterine infection (e.g. urinary tract, bacterial vaginosis), lifestyle factors (e.g. smoking, alcohol), maternal history (i.e. congenital conditions) and environment (e.g. malnutrition). Moreover, preterm birth is further identified as being either spontaneous or via *clinically initiated* labour (either through elective caesarean or induced labour) (Blencowe et al. 2012). After birth a preterm infant is exposed to a multitude of physiological disturbances, with a high risk of brain injury in the first few days of life (e.g. periventricular and intraventricular hemorrhage) (Ballabh 2014). The combination of causal risk factors leading to preterm birth, the gestational age of the infant and the development of acute conditions after birth influence mortality and long-term outcome.

In short, the cause and incidence of preterm birth has a significant impact onto the development of children worldwide. In particular the risk factors in combination with early gestational age greatly affect the neurodevelopment of a newborn, with problems persisting into later childhood and adulthood. Thus, early identification of acute brain injury in the preterm and potential prediction of long-term outcome is critical to ensure optimal recovery. Table 1.1 highlights the

key epidemiological factors commonly identified leading to two different types of neonatal birth.

	Full-term HIE	**Preterm infants**	**Both populations**
Incidence	1 in 6 per 1000 births hypoxic ischemia occurring 1-8 per 1000 live term births	Mean of 11% of live births - between 5% and 18% of births	-
Risk factors	Presentation at birth Mode of delivery Fetal blood factors	Intrauterine enrvironment Infection (maternal, fetal) Fertility treatment	Maternal age Family history Lifestyle factors Ethnicity

Table 1.1 – Common associated risk factors and incidence for full-term HIE and preterm infants

1.3 COMMON MEASURES IN NEONATAL BRAIN MONITORING

Advancements in neonatal intensive care have vastly improved infant survival, following preterm birth or full-term asphyxia. In modern day neonatal intensive care units (NICU) clinical management provides basic support for cardiorespiratory and systemic stabilization, along with screening for neurological sequlae (Ballabh 2010; McCrea and Ment 2008). Importantly, neuroprotective care for infants is a critical to post-natal mortality and morbidity. In this section I briefly outline neuroprotective strategies employed for birth asphyxia and preterm birth as well as the diagnostic monitoring involved in identifying and treating newborns.

1.3.1 NEUROPROTECTIVE CARE FOR AT-RISK INFANTS: FULL-TERM HYPOXIA AND PRETERM BIRTH

Neuroprotective care in the modern day NICU is usually complemented by standardized cardiorespiratory monitoring. Term infants with severe HIE and very or extremely preterm infants require respiratory ventilation support to sustain breathing during the first days of life (Sabir et al. 2012). This prevents hypoxia or hyper/hypocapnia (either an increased or decreased amount of carbon dioxide in the blood). In addition, fluid and glucose homeostasis play an important role in preventing hyper/hypoglycaemia (high or low blood glucose levels) because both may accentuate brain damage (Salhab et al. 2004). Both ventilator support and fluid management aim to compensate for intracellular energy failure while stabilizing blood pressure and blood acidosis (Ballabh 2010).

Following premature birth or asphyxiation at full-term birth (HIE), acute brain injuries can lead to serious impairment of neuronal function. For example, one of the most common occurrences in HIE is the event of seizures, which affects neonatal health by compromising major bodily functions (S. Miller et al. 2002). This includes respiratory function, fluid management and cerebral blood pressure. In the preterm neonate, early delivery interrupts crucial neural and homeostatic mechanisms responsible for the regulation of cerebral blood flow, with consequent hypoxic ischemic injury which can also lead to seizures, disturbed blood coagulation factors and hemorrhage (Ballabh 2010; Bolisetty et al. 2014; Volpe 2009).

The clinical management of these at-risk neonates is vital to their long-term prognosis. The level of care is one of the principle factors in determining neurologic outcome (Abend and Licht 2008). The difficulty associated with predicting outcome from term hypoxia is largely due to identification of HIE severity. Furthermore, it has been reported that a majority of case studies (Shewmon 2000) provide little information regarding exact definitions of good or poor outcome or mild, moderate, sever neurological disability associated with HIE. Recently, the use of mild

hypothermia has been utilized as a temporary neuroprotective strategy (Gluckman et al. 2005; Shankaran et al. 2005) to reduce metabolic rate and cell apoptosis. Clinically, hypothermia must be applied within the first six hours of life and maintained for a 48-72 hour period (Shankaran 2002) to provide maximum benefit. An important component of neonate treatment is the administration of anti-epileptic (anticonvulsant) and anaesthetic drugs to control seizure events while aiming to stabilize cerebral function. The most common anaesthetics used include the use of phenobarbital, phenytoin, and benzodiazepines (S. Miller et al. 2002).

A vital monitoring tool that assists neuroprotective care of neonates is the electroencephalogram (EEG), in particular the observation of abnormal background patterns in the electrical activity of the brain (Sinclair et al. 1999). Continuous monitoring of newborns using EEG is discussed in the following section.

1.3.2 CONTINUOUS ELECTROENCEPHALOGRAPHY MONITORING OF NEONATES

Continuous brain monitoring of neonates via the EEG is a well-established measure of the brain's electrical activity, acquired at the scalp via surface electrodes. Its use clinically has been well established, having an unparalleled temporal resolution in non-invasively measuring the brain's electrical activity (Ernst Niedermeyer and da Silva 2005). As a result, its use has improved clinical prediction and treatment of at-risk neonates (André et al. 2010; Lamblin et al. 1999). The prognostic value of an EEG measurement for neonates is reportedly its sensitivity for assessing brain damage (Grigg-Damberger et al. 1989; van Rooij et al. 2005; Watanabe et al. 1999). For example, in hypoxic-ischemic injury, the potential failure of synaptic transmission due to poor metabolism in the brain causes normally fast rhythmic continuous electrical activity to reduce in amplitude, which is subsequently followed by an increase in erratic mixed wave patterns (van Putten and van Putten 2010). These patterns on an EEG are known as burst suppression and are commonly associated with poor developmental prognosis in neonates (Grigg-Damberger et al. 1989).

Clinical outcome of full-term hypoxic and preterm infants depends primarily on assessing the severity of the acute encephalopathy, in addition to clinical management (e.g. therapeutic hypothermia, drug therapies). Continuous monitoring of EEG offers crucial functional markers of abnormality within the first few hours of life after birth (Holmes et al. 1982). For instance, after initial diagnosis of HIE, EEG can provide important prognostic information, even in neonates treated with hypothermia (Hallberg et al. 2010). Further, EEG can reliably monitor for the presence of seizures, a potential pre-cursor to epilepsy, where the risk of poor neurological outcome is distinctly greater, particularly if seizures occur frequently (S. Miller et al. 2002). There is considerable ongoing research that aims to improve the role of post-natal EEG. An

example of such is the automated amplitude integrated EEG trends (aEEG) and limited-channel EEG (channel montages) which has improved short-term assessment and management of preterm and full-term infant groups (Hellström-Westas and Rosén 2005; Olischar et al. 2004; Wikström et al. 2012).

Despite improvements in the use of EEG (qualitative and quantitative), a number of barriers still exist. Expert interpretation of continuous EEG recordings in infants is challenged by interruptions to data continuity and artifacts from NICU environments (Schumacher et al. 2011; Wikström et al. 2012). Background activity from aEEG/EEG in the first 72 hours has predictive value but requires expert selection of epochs to distinguish artifacts from abnormal cortical activity (Wikström et al. 2012). Notwithstanding these challenges and other factors, the EEG still remains the most common and rapid method for assessing post-natal brain function. For time-limited injuries such as HIE and hemorrhage, EEG still remains the most practical solution, despite advances in brain imaging. This thesis seeks to demonstrate the utility of EEG through novel quantification of cortical activity, whilst considering the challenges in which neonatal brain monitoring is encumbered by, to provide a robust and reliable solution for outcome prediction.

1.4 INSIGHTS FROM NEUROSCIENCE

Recent neuroscientific research indicates that criticality has emerged as a leading dynamical candidate for healthy and pathological neuronal activity. Criticality occurs in systems which border on the cusp of stability and disorder, transitioning between these two extremes via temporary system instability (Bak et al. 1987; Beggs and Timme 2012; Sethna et al. 2001). It is a phenomena that is commonly observed in physical systems (Bak and Tang 1989; Papanikolaou et al. 2011; Sethna et al. 2001; Zapperi et al. 2005) and provides potentially novel insights into human brain dynamics.

A growing body of evidence now contends that cortical networks operate near criticality (Beggs and Plenz 2003; Haldeman and Beggs 2005; Kinouchi and Copelli 2006; Meisel et al. 2012; J. A. Roberts et al. 2014; Shew et al. 2009). The study of criticality can be dichotomized into two classes: those systems which "self-organize" and those tuned to operate at critical points. Within these two classes of criticality, terminology such as "scale-free activity", "avalanches" and "crackling noise" are commonly used to characterize highly specific spatiotemporal dynamics that occur within a system. Critical systems typically exhibit scale-free activity, i.e. measured statistics that have no characteristic time or length scale. These scale-free statistics measured at spatial scales are expressed as avalanches, whereas in the temporal domain they are characterized as the fluctuations of crackling noise.

In this thesis I seek to provide a background into concepts such as criticality, crackling noise and the scale-free nature of temporal fluctuations present in neonatal EEG to present an alternative hypothesis to understanding early brain development. These concepts found in natural phenomena and neurobiological models, offer evidence of complex temporal structures that transition between balance and imbalance (Beggs and Plenz 2003; Biyu J. He et al. 2010). In this thesis I explore how criticality plays a fundamental role in the temporal dynamics of the neonate cortex. These processes may further facilitate understanding of neurobiology in the compromised full-term or immature preterm brain. Notably, I contend that the study of these phenomena can provide novel, predictive markers of early brain activity that advances current clinical assessment of neonate EEG.

1.5 RESEARCH AIMS AND HYPOTHESES

This thesis develops novel methods for predicting clinical outcome from neonatal brain activity recordings drawing on concepts of criticality. The overarching theme of this study is to test whether neonatal brain activity has unique scale invariant features, soon after birth, which may reflect a complex, yet universal set of dynamics found elsewhere in nature. These features, when statistically characterized and robustly extracted may yield important temporal signatures of cortical behaviour which have direct clinical and neurodevelopmental relevance.

The aims and objectives of this thesis are thus summarized below:

- To identify stochastic processes present in neonatal brain activity following full-term hypoxia through a detailed statistical characterization;
- To objectively extract signatures of cortical bursts measured via the neonatal electroencephalogram (EEG) in full-term hypoxic and preterm neonates;
- To combine detailed statistical characterization and signatures of cortical bursts to predict clinical outcome in neonates.

Significantly, this thesis hypothesizes that:

- Neonatal brain activity exhibits inherently scale-free processes;
- Scale-free behavior in the neonate brain is indicative of criticality and a complex form of stochastic behavior known as crackling noise ;
- Properties of crackling noise in the neonate brain are inextricably linked with neurobiological processes, such as metabolic constraints and the development of cortical pathways;
- Characterizing early neonate brain activity through the analysis of scale-free and crackling noise dynamics yields highly predictive properties of neurodevelopmental outcomes.

1.6 ORGANIZATION OF THESIS CHAPTERS

This thesis aims to guide the reader toward the application of a clinical outcome prediction metric. Here, I present an application of novel methods based on bedside recordings of brain activity to predict outcome of at-risk neonatal populations. The organization of the following chapters is as follows:

In Chapter 2, I review selected literature pertaining to the methods and analyses for this thesis. In the first half of this chapter I focus on characterizing pathophysiological mechanisms relevant to abnormal electrical activity patterns common to full-term hypoxia and preterm infants. For each of these neonatal populations, I explore previously developed quantitative measures, with a focus on summarizing properties of EEG burst activity used to determine outcome. In the following half of chapter 2, I provide background into criticality and scale-free networks, both in physical systems and in neuroscience, before concluding with a consideration and reasoning for characterizing scale-free processes, criticality and crackling noise in the neonate brain.

In Chapter 3, I present original research on the empirical nature of neonate brain activity following post-natal hypoxia. This chapter presents an alternative viewpoint on current clinical interpretations of data by characterizing the underlying statistical behavior present in neonatal EEG. Through detailed validation, I present and discuss results of a full-term hypoxic cohort. Notably, this chapter introduces a method for analyzing cortical activity patterns in the neonate EEG. Here, temporal properties of EEG bursts are characterized by principles of crackling noise via an analysis of average burst shapes across a hierarchy of time scales. These average bursts are further quantified for their change in symmetry and sharpness over time. The application of a phenomenological model is used to demonstrate how cortical bursts can change in symmetry and sharpness. Results of both neonate data and a simple model are compared to draw further discussion and insight into bursting behavior and metabolic constraint models. This chapter forms two peer-reviewed publications: (doi: 10.1523/JNEUROSCI.4701-13.2014, doi: 10.3389/fnsys.2014.00154).

In Chapter 4, I utilize methods from the previous chapter to study the application of empirical distribution functions in predicting clinical outcome of full-term hypoxic neonates. In sum, prediction of outcome at 2 years of age is achieved from analysis of statistical distributions in full-term hypoxic neonates undergoing hypothermia treatment hours after birth. Significantly, I report that the characterization of statistical distributions in neonate burst suppression offer predictors of outcome that are temporally precedent to later clinical findings, i.e. brain imaging (MRI). This chapter forms a full peer-reviewed publication (Iyer et al. 2014, Annals of Clinical and Translational Neurology).

In Chapter 5, I apply the methods developed in Chapter 3 to predict long-term outcome for a cohort of extremely preterm infants. Using outcome measures of preterm infants (gestational age 23 – 28 weeks) at first week of life and at 2 years of age I demonstrate that early preterm brain activity is characterized by scale-free dynamics which carry developmental significance. The use of the EEG burst metric provides rapid and early clinical prediction of neurodevelopmental outcomes whilst taking into account the gestational age of the preterm infant. This chapter forms a full (standalone) peer-reviewed manuscript (Iyer et al. 2015, http://dx.doi.org/10.1093/brain/awv129).

Chapter 6 utilizes average burst shape analysis to predict acute brain injury of preterm infants (gestational age 23 – 28 weeks), namely the risk of developing intraventricular haemorrhage (IVH). Specifically, I report upon the efficacy of average burst shape analysis in predicting the onset of IVH. Notably, I contrast findings from cranial ultrasound with an assessment of average burst shape to reveal features of burst sharpness and symmetry which significantly co-vary with the occurrence of IVH (pre and post injury). The use of average burst shape analysis reveals the first novel indication of preterm hemorrhage injury through bedside assessment of EEG prior to screening via a cranial ultrasound. This chapter forms an entire (standalone) peer-reviewed manuscript (Iyer et al. 2015, in press).

In Chapter 7, I summarize and conclude upon the main findings of this body of work, discussing the major limitations, contributions of this thesis and consider directions for future work.

2.0 REVIEW OF SELECTED LITERATURE

ABSTRACT

Significant research over the past 60 years in neurology, neonatology and neuroscience has contributed to our understanding of causes and consequences of birth asphyxia and premature birth. These works have defined, examined and hypothesized upon the pathophysiological mechanisms after birth leading to the types of electrical activity phenomena observed in the clinic. This chapter aims to distil key literature highlights from research into full-term hypoxia, preterm birth and their associated pathophysiological and neurological abnormalities. Specifically, this chapter focuses on the features of electrical activity in the neonate brain, contrasting pathological patterns such as burst suppression with physiologically generated activity patterns in the preterm. It also formally introduces the study of criticality, scale-free networks and crackling noise in physical systems and how they relate to human brain dynamics. The utilization of such higher order statistics and stochastic models has yielded new insights into the field of neuroscience and provides an important background into the implementation of the methods and analyses presented in this thesis. The chapter concludes with a consideration for the use of scale-free dynamics in the prediction of clinical outcome in neonates.

2.1 FULL-TERM HYPOXIA AND BURST SUPPRESSION

Asphyxia at birth is the most common trigger for a hypoxic-ischemic injury in a newborn. The occurrence of maternal hypovolemic shock or cord prolapse (Morley 2005) significantly contributes to brain injury. Findings from MRI studies have found that HIE may continue to develop without significant hypoxia beyond the initial insult (Alderliesten et al. 2013; Cowan et al. 2003). In developed countries, newborns with hypoxia that are routinely oxygenated after birth are candidates for rapid diagnosis and treatment. However, prolonged asphyxiation during birth leads to multiple pathophysiological effects. Here, I review pathophysiological mechanisms of neonatal asphyxia that lead to abnormal electrical activity patterns in the brain. Furthermore, I summarize quantitative methods in the field in order to inform the methods designed in this body of work.

2.1.1 PATHOPHYSIOLOGY OF HIE

Neonatal asphyxia results in a cortex that is severely compromised by the deprivation of oxygen. Oxygen deprivation, or hypoxia, has a damaging multi-organ effect on the brain, heart and pulmonary system (Volpe 2008). The onset of HIE is sudden and unfolds as a two part cascading physiological process, where the result of hypoxic and ischaemic effects sequentially cause brain damage. The two major neurological events of HIE are:

- Primary neuronal damage: Inhibition of energy-producing molecular processes due to an asphyxia related event, leading to compromised cellular integrity
- Secondary neuronal damage: a delayed phase where inflammatory response leads to cell necrosis or apoptosis 72 hours or more after the insult

Factors such as compromised cellular integrity and the inhibition of energy producing cells are largely dependent on the severity and duration of the initial insult. The first stage of hypoxic-ischaemic insult relates to the function of normal cerebral auto-regulation, which maintains blood supply throughout the brain. This compensatory system is disturbed during an event of asphyxia causing a fall in cerebral blood flow and reducing the capability of blood to perfuse with oxygen (Morley 2005). As blood flow to the brain reduces, blood pressure falls leading to a failure to replenish intracellular energy-rich metabolites (Volpe 2001a).

Significant biochemical processes contribute to the failure to produce energy at a cellular level. Initially an impaired uptake of glutamate, a major excitatory neurotransmitter, results in over-activation of amino acids, such as N-methyl-D-asparate (NMDA) (Levene et al. 1995). The presence of this amino acid increases the level of glutamate production causing an accumulation

of sodium (Na^+) and intracellular calcium (Ca^{2+}), which in turn, activates the production of lipases (fatty acids) and nitric oxide (Fellman and Raivio 1997). The combination of these activated enzymes results in structural damage to the cell and a production of free radicals. A build-up of sodium, mainly due to a reduction in adenosine triphosphate (ATP) production (the key energy source for all cellular respiration processes), results in a deregulation of Na^+/ K^+ (potassium) channel pumps. Free radical production, along with an accumulation of Na^+ acts as one of the pre-cursors to cell apoptosis as the brain undergoes reperfusion.

The combination of free radicals and a decrease in ATP production activates cell apoptosis, the secondary delayed phase of neuronal damage. As the neonate immune system is underdeveloped and exposed to inflammatory pathogens, the oxidative nature of free radicals advances the necrosis of brain tissue (Fellman and Raivio 1997). The presence of cell death becomes evident mainly in areas of otherwise high metabolic activity, namely, the basal ganglia and the cerebral cortex, which can affect later neurodevelopment. As the brain injury progresses, neural activity slows down and the cascade of cell apoptosis begins over a 72 hour period (Morley 2005).

2.1.2 COMMON EEG FEATURES IN BURST SUPPRESSION

Under normal conditions, a conventional burst of electrical activity in an EEG recording of the infant brain, is described as a "phasic synaptic depolarizing intracellular potential" which occurs at the cortical level (Amzica 2009). In a normal full term infant, electrical activity is typically continuous and rhythmic with well-defined burst cycles. A burst suppression pattern is distinctly different to this normal burst activity across the cerebral cortex.

Burst suppression (BS) is characterized by alternating periods of erratic mixed waves (slow or fast) of high amplitude followed by periods of flat EEG (M Steriade et al. 1994). The most common occurrence of BS is immediately after birth asphyxia where it frequently occurs during the first few minutes of life and then resolves within 12-24 hours (Holmes et al. 1982). Other occurrences of BS include during the administration of general anaesthetic drugs or, less frequently, during an event of hypothermia, where the brain undergoes a form of inactivation (Lukatch et al. 2005). The nervous system of the newborn is immature in its cortical connections. One contention is that incomplete myelination of nerve fibres predisposes the neonatal cortex to effective deafferentation between cortical areas (the elimination or interruption of afferent nerve impulses) (Grigg-Damberger et al. 1989). The persistence of BS patterns in the newborn post-hypoxia results in poor clinical outcomes such as infantile death or compromised neurodevelopmental, e.g. cerebral palsy.

The electrical behavior in the brain during BS has been hypothesized as being in a constant state of hyper-excitability over a range of cortical neurons (M Steriade et al. 1994). The global nature of BS indicates that severe disturbances of cerebral function involving both cerebral hemispheres exist. Basic features on BS phenomena, extending to anaesthetic burst suppression, have been well established in terms of its characteristics and timing (Brenner et al. 1975).

Characteristic features that are present during BS include:

- Synchrony of burst onset: the generation of burst periods are simultaneous across the cortex, indicating spatial homogeneity (Grigg-Damberger et al. 1989). While less common, asynchronous burst activity can also occur. It is suggested that this arises due to further cortical deafferentation (Lazar et al. 1999).
- Parametric sensitivity: BS patterns are continually changing in response to underlying biophysical processes such as the level of anesthesia administered, or intensity of hypoxia and/or hypothermia. An example of this is exhibited by general anesthesia which lengthens suppression time (Ching et al. 2012)
- Heterogeneity in neural activity timescales: the timescales between BS and normal neural activity significantly differ as the brain enters a mode of inactivation. Delta oscillations of the brain commonly observed during sleep and general anesthesia range from 0.5-2 Hz and have an associated periodicity. However, BS occurs on a much slower and broader spectrum of timescales (Fig. 2.1)

Thus, burst suppression commonly occurs as a "global" spatial phenomenon where large slow wave fluctuations are followed by periods of cerebral silence at most locations across the cortex. The distribution of bursting activity across the cortex is time limited due to a depletion of extracellular calcium (Ca^{2+}), where levels are so low that it becomes incompatible with synaptic transmission (Amzica 2009). During suppression periods, synaptic silence allows neuronal pumps to restore interstitial Ca^{2+} toward normal levels.

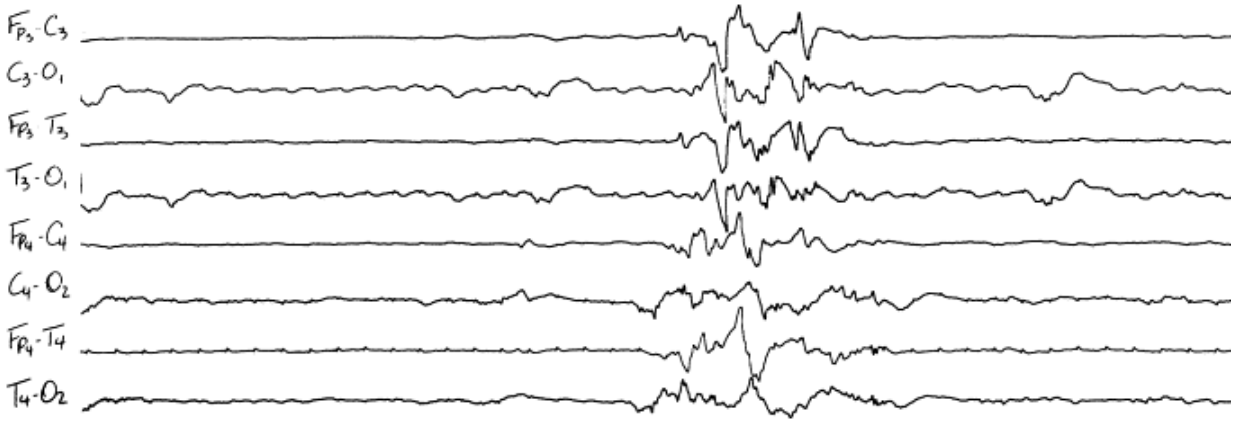

Figure 2.1 – From Sinclair (1999): a sample EEG trace demonstrating a burst suppression pattern in a neonate with term hypoxia (HF 70 Hz, LF 1 Hz, 5 μ v/mm).

BS patterns range from acute onset, pathological, drug induced to recovery based BS leading to a transition to continuous EEG. Acute BS is the earliest onset of slow wave large amplitude activity (within first 3 hours of birth) (Grigg-Damberger et al. 1989). The transition from acute onset to pathological BS corresponds to typically abnormal (discontinuous EEG) patterns (Lamblin et al. 1999) in electrical activity. The use of drugs (Lazar et al. 1999; S. Miller et al. 2002), (such as barbiturates), can also be used to induce burst suppression across the cortex, while recovery based BS is an early indicator that the electrical activity is transitioning towards a more continuous EEG pattern (Spitzmiller et al. 2007; Ter Horst et al. 2004).

While studies into BS have revealed a characteristic presence for globally occurring large amplitude fluctuations of electrical activity, recent research in newborns (Fransson et al. 2013) has focused on the spatial distribution and frequency of these bursts in the neonatal cortical network. It has been hypothesized that a complex network of brain cells which alternates between periods of quiescence and periods of sudden fluctuations may reflect a state of criticality in the brain (Ter Horst et al. 2004). This concept may provide vital links to BS activity and neonatal HIE clinical outcome.

Research has aimed to identify burst suppression patterns in background term hypoxic EEG, either under hypothermia or without hypothermia treatment. A recent review (Walsh et al. 2011) summarizes the conventional use of EEG in identifying abnormal patterns such as BS with reference to the types of clinical criteria used to assess infants and the typical features of background activity present in EEG.

2.1.3 QUANTIFICATION OF EEG FEATURES FROM NEONATAL BURST SUPPRESSION

The detection of bursting content in neonatal EEG is an increasing focus of clinical research. A focus of this thesis is the detection and characterization of cortical burst signatures in the hypoxic neonate to derive a clinical outcome prediction metric. Below I present a summary of previous metrics developed toward this goal (search period up until September 2014). Though methods vary between datasets, there is commonality in their feature extraction, analysis constraints and methods for optimization. A summary of selected works (Table 2.1) indicates the use of automated techniques in neonates and their associated methodologies. Here, I focus the literature search on reports of automated analysis of full-term neonate BS EEG. In particular, I highlight the types of constraints applied to pre-processing EEG recordings, features extracted from BS data and the classification methods employed to determine outcomes.

Author	GA (wks)	Feature selection			Summary	
		Filtering & Channels	Thresholding & constraint	Target	Output	Optimization (OP) & Validation (V)
(Thordstein et al. 2004)	39-40 wks	0.5–70 Hz 50 Hz notch filter and detrend (baseline removal) 8 channels, 0–20 system at positions F7, F3, T5, P3, F8, F4, P4 and T6	SACS epoch export program for burst periods Power spectra limited to 0–30 Hz; zero padding for episodes shorter than 1024 points	burst periods manually selected from epoch Mean relative power LFA 0-4Hz, HFA 4-30Hz	segments in each cluster of absolute and relative spectral powers in two frequency bands and spectral edge frequency (SEF95)= the frequency below which 95% of the power resides	OP: empirical (mimicking visual analysis) V: matched controls, though small number (9 versus 9)
(Witte et al. 2004)	38 -41 wks	No specific preprocessing 8 channels, Fp1, Fp2, C3, C4, T3, T4, O1, O2;	95% confidence threshold is $2/\sqrt{M}$, where M is the number of EEG patterns used for the bichorence estimation 1–1.5 Hz to 3.5–4.5 Hz frequencies	Gabor expansion, a FFT biamplitude, bicoherence and phase-bicoherence time courses of both burst and interburst patterns	Quadratic phase coupling (peaks of bispectra analyzed) characteristics between both patterns within the time period from 0.75 to 1.5 s after the pattern onset at electrode Fp1	OP: t-test paired samples of bispectral parameters in local pairs and global pairs V: segmentation of burst and interburst patterns by physician
(Wang and Agarwal 2007)	Neonates	0.5-35 Hz 8 channels	fixed (but adjustable): e.g. < 9 µV duration: suppression 1-60s, burst >0.5s	suppression in burst-suppression pattern instantaneous amplitude across channels smoothed by calculating moving average in 0.5s window	burst-suppression event count in 60s window, mean duration of suppression in each burst-suppression cycle in 60s window	OP: Event wise comparison of detection results with manually marked data from 4 neonates, using different thresholds. V: none

(Löfhede et al. 2008)	~36-40 wks	0.5-20 Hz 8 channels, F7, F3, T5, P3, F8, F4, P4 and T6	SACS epoch export program for burst periods Sliding window with a length of 1 s, corresponding to 200 samples, used, with overlap of 0.75 s	5 features for classifier -spectral edge frequency - 3hz power (1Hz-3Hz) - median absolute value - Variance - Shannon entropy	Feature signals normalized by fitting their distributions between the first and 99th percentile into the interval 0 to 1 to construct classifier ROC curves	OP: 3 classifiers used Artificial neural network, Fisher discriminant and support vector machine V: leave-one-out training to build ROC curves on 6 neonates
Vairavan (Vairavan et al. 2009) (MEG study)	38-45 wks	1-25 Hz 5 channels,	Median of the feature is calculated channel wise from time windows Mean across channels is the threshold. duration: burst: >1s	bursts (and IBI) in segments of discontinuous MEG Detection via full-wave rectified data signal content above the baseline is investigated for the calculation of the burst durations	3 outputs for burst duration and IBIs - spectral ratio, - Hilbert phase - discrete wave transform Values used in each to construct ROC curves using sensitivity and specificity of based on each output as a range of thresholds according to discontinuity	OP: Area under curve (AUC) of ROC curves is maximized using data from 14 neonatal EEGs with manual scoring by two reviewers. V: none, though ROC curves for spectral ratio, Hilbert phase and discrete wave transform are compared as an overall assessment of performance
(Löfhede et al. 2010)	~36-40 wks	1.6 – 44Hz Notch at 50Hz 8 channels, F7, F3, T5, P3, F8, F4, P4 and T6	SACS epoch export program for burst periods Sliding window with a length of 1 s, corresponding to 200 samples, used, with overlap of 0.75 s	22 features including -spectral edge frequency - 3hz power - median Shannon entropy -zero crossings - variance - spectral centroid (Continued in	Performance was measured in terms of the probability of error calculated as Perr = P(class 1)P(class 2|class 1) + P(class 2)P(class 1|class 2) Formula gives a weighted sum of 2 misclassification probabilities, where the weights are the proportions of the two classes in data	OP: manually pre-classified training and validation sets Classifier, Fisher discriminant V: leave-one-out training to build ROC curves, 20 healthy and 6 sick neonates

				Table 1 of paper)		
(Bhattacharyya et al. 2011)	37- 42 wks	0.5–35 Hz 6 bipolar channels T4-P4, P4-C4, C4-T4, T3-P3, P3-C3, and C3-T3	FIR filter of Kaiser window Manual marking segments of single channel labeled EEG extracted, maximum limit as 10 s for bursting	Burst or normal segment, preceded by 3 s and followed by 2 s of background EEG 15 features extracted (Table 2 of paper)	Classifier output is binary 0=normal, 1 =burst segments radial-basis function (RBF) kernel function provides indices of data to model fitting, which is used for sensitivity and specificity analysis	OP: Support vector machine used for feature selection and training V: Visual marking by three clinicians, event marked epochs for burst and normal segments
(Flisberg et al. 2011)	>36 wks	1.6 and 44 Hz 8 channels F7, F3, T5, P3, F8, F4, P4 and T6	SACS epoch export program for burst periods Detrended via median value of epochs	10-min epochs of burst suppression classified epochs, target to quantify suppression time 22 Features extracted using a genetic algorithm	Results of classifier and segmentation used for calculating suppression time according to epoch length (1hr) based on 22 feature signals	OP: Fisher linear discriminant, segments where no burst suppression activity was detected, zero suppression length was inserted V: training was performed using a small set of manually classified data from patients of the same age and type

Table 2.1 – Quantification methods and analyses in studies in neonatal burst suppression. Table legend: Interburst interval (IBI), Gestational Age (GA) where wks = weeks. SACS refers to a brain monitor device. "Constraint" is information provided by the authors for any specifications or limitations placed on automatic detection. "Output" refers to the features which are selected for analysis and subsequent results. "Optimization" refers to any specific adjustments, correlations or classification algorithms. "Validation" refers to confirmed absence or presence of normality or abnormality.

These selected articles suggest two approaches for quantification of burst suppression patterns. One approach focuses on burst epochs, and their associated spectra with an empirically driven method for classification and prediction. Other methods utilize many features, (time, frequency and higher order computations) in a methods-driven exercise to generate feature based classification. Such studies and others (adult anaesthetised burst suppression and piglet models) have aimed to develop classification schemes to separate burst and suppression content of EEG.

2.2 CORTICAL ACTIVITY IN THE EARLY PRETERM

Cortical activity patterns in the immature preterm brain are inherently different from that of compromised full-term neonates. The preterm brain is an immature neuronal network of cortical connections that is highly dependent on its ability to generate and sustain rhythmic electrical synapses. The disruption to neuronal growth and propagation of synaptic connections that normally transpire in-utero (Eeg-Olofsson 1980; Lagercrantz et al. 2010) causes system instability and results in a high risk of neurological morbidity (Van Baar et al. 2005). Thus, it is vital that critical care of these premature neonates revolves around providing the environment and treatment to stabilize their systemic responses and neurological well-being (Olischar et al. 2004). In the following section, I review pathophysiological mechanisms that are relevant to types of preterm cortical activity patterns. Moreover, I summarize previous quantitative methods which explore both normal and abnormal types of cortical activity in preterm populations.

2.2.1 PATHOPHYSIOLOGICAL MECHANISMS POST PRETERM BIRTH

Immediately following preterm birth, there is a high risk for several pathophysiological mechanisms that occur either through maternal intrauterine environment or at birth. These mechanisms have acute and severe impacts on the preterm brain and its overall function. Conditions such as damage to white matter through hypoxic-ischemia, haemorrhagic lesions and perinatal inflammation are some of the most commonly occurring that have a potential for severe effect.

One of the most common acute forms of injury in the preterm brain is the development of an intraventricular hemorrhage (IVH) within the first few days following birth. Common mechanisms that lead to intraventricular hemorrhage (IVH) include failure of cerebral autoregulation or cerebral blood flow (CBF) (Milligan 1980; Watkins et al. 1989), hypoxic ischemic insult and sepsis (Volpe 2009). An inability to maintain constant CBF is compounded by the fragility of the germinal matrix and coagulation disorders present in the blood (Ballabh 2010). The increasing severity in which the haemorrhagic injury is defined includes mild IVH (grade 1) where brain bleeding is confined to the subependymal germinal matrix, moderate (grade 2) hemorrhage into the lateral ventricles, severe (grade 3) where there is enlarged bleeding of the ventricles and very severe (grade 4) bleeding into surrounding brain tissue parenchyma (Papile et al. 1978).

In the preterm, dysfunctional function and regulation of CBF leads to two variations in blood flow to the cortex: pressure-passive CBF regulation and alternations to functional hyperaemia (increase in cerebral blood flow due to metabolic demand). Pressure passivity, a term used to describe the inability to maintain constant CBF, differs from normal autoregulation mechanisms where smooth muscle cells relax or constrict (myogenic response) to compensate for CBF variations (Ballabh

2010). Through this myogenic response, there is an elevation of intracellular Ca^{2+} and opening of ionic channels resulting in depolarization and contraction, a process which is dysfunctional during pressure-passive CBF (Ballabh 2010). Conversely, functional hyperaemia is a response to metabolic demand, largely postulated as a result of an activation of glutamate receptors resulting in a post-synpatic increase in calcium (Iadecola and Nedergaard 2007) leading to an increase in vasoactive agents such as CO_2, nitric oxide and other metabolites. Whilst the latter is less understood at a molecular level, dysfunctions in these mechanisms contribute to a high risk of haemorrhage and cerebral ischemia.

The most common form of injury in the preterm brain is damage to cerebral white matter. It is associated with a high risk for neurodevelopmental impairment stemming from injuries such as IVH, leading to a more adverse injury - periventricular leukomalacia (PVL) (Larroque et al. 2003). PVL is a two-fold injury that combines focal necrosis in white matter with the loss of pre-myelinating oligodendrocytes (pre-cursor to myelin producing cells) (Volpe 2003). Factors for PVL in the preterm are primarily maturation-dependant where initiating factors such as cerebral ischemia, infection (maternal or fetal) or systemic inflammation are key pathogenic factors (Larroque et al. 2003). White matter injury in the preterm manifests through upstream and downstream mechanisms. Upstream mechanisms result primarily through preterm development and involve cerebral ischemia, due to pressure-passivity, hypertension, or inflammation (caused by infection) (Larroque et al. 2003). Downstream mechanisms are brought upon by insults such as hypoxic-ischemia and infection as well, resulting in free radical attack and excitotoxicity – an effect of the vulnerability in pre-myelinating oligodendrocytes (Larroque et al. 2003). Further cascading effects including Ca^{2+} influx and generation of reactive oxygen species also become apparent as the severity of white matter damage increases.

Other pathological factors such as perinatal inflammation and variations in carbon dioxide and glucose levels also predispose a preterm towards acute brain injury. Moreover, inflammation is involved in the upstream pathway of PVL injury where it results in the up-regulation of inflammatory cytokines and activation of microglia contributing further to white matter damage (Volpe 2001b). Carbon dioxide levels as well play a role in brain injury. High CO_2 levels contribute to hemorrhage (vasodilation in CBF) and low CO_2 levels are associated with ischemic injury (vasoconstriction in CBF) (Gorm Greisen and Børch 2001; Kaiser et al. 2006). These pathophysiological mechanisms described are multi-factorial, and without proper treatment or recovery, result in impaired neurodevelopment.

2.2.2 COMMON TEMPORAL FEATURES IN PRETERM EEG

Continuous monitoring in the neonatal intensive care unit (NICU) of the preterm provides insight into underlying neurological pathology (Hellström-Westas and Rosén 2005; Olischar et al. 2004; Watanabe et al. 1999; Wikström et al. 2012). During this monitoring window, brain activity is predominantly discontinuous, whereby periods of high amplitude electrical bursts are interrupted by low-voltage periods known as interburst intervals (André et al. 2010; Hellström-Westas and Rosén 2005; Vanhatalo and Kaila 2006). Notably, this type of electrical activity has similarities to burst suppression following full-term hypoxia. However, discontinuous activity patterns in the preterm brain tend to reflect maturing thalamocortical networks (André et al. 2010; Vanhatalo and Lauronen 2006). These discontinuous periods of activity vary in their temporal evolution and spatial synchronicity across the cortex and are typically observed in preterm ages of 24-30 weeks. Further, preterm gestational age plays an important role in the progressive activation of circuits from the brain stem to the cortex (Eeg-Olofsson 1980). The presence of discontinuous activity can be delineated into two categories: normal and abnormal background patterns. Characteristic features in normal preterm EEG include:

- Periods of bursts punctuated by sharp transients, of mixed frequency content, with accompanying inter-burst (IBI) periods (André et al. 2010).
- Spectral analysis for infants less than 32 weeks gestation shows that delta wave activity dominates (<1Hz region).
- Nearing term age, theta and alpha activity is more easily recognized
- IBIs become shorter and burst become frequent (Bell et al. 1991; Tolonen et al. 2007)
- Fast activity bursts are superimposed on slower wave amplitudes (spontaneous activity transients, SATs) (Vanhatalo and Kaila 2006)
- Emerging and established cyclical variations in EEG patterns become apparent
- Changes to behavioral state (respiration, eye movements) and sleep-wake cyclicity (SWC) reflect hypothalamic connectivity (Fuller et al. 2006)

Characteristic features in abnormal preterm EEG include:

- Acute or chronic stage abnormalities which may present in EEG as attenuation of fast frequencies, longer IBI periods and a loss of sleep-wake cyclicity (Watanabe et al. 1999)
- Lowered amplitude fluctuations, which correlate with the above features to reflect disorganized patterns of brain activity, with the emergence of abnormal waveforms such as positive rolandic sharp waves (Marret et al. 1997)

Whilst these features are most commonly associated with normal and abnormal EEG patterns in the preterm, several studies have aimed to highlight typical EEG background patterns during the presence of brain injury. For instance, IVH has been associated with a depression in amplitudes (Aso et al. 1993; Clancy et al. 1984; Hellström-Westas et al. 2001) and infant mortality has been associated with the numbers of bursts (Hellström-Westas et al. 2001). Abrupt abnormal EEG patterns such as status epilepticus have also been correlated with haemorrhagic lesions in amplitude-integrated EEG (aEEG) (G Greisen et al. 1987; Hellström-Westas et al. 1991). Other abnormal features include the absence of regular sleep wake cycling and potential white matter damage indicated by chronic abnormalities such as positive rolandic sharp waves (PRSW) (Akihisa Okumura et al. 2002). Despite the identification of these features in background patterns and burst-specific features in the preterm EEG, there is still a need for further characterization of how bursts are related to short-term and long-term outcome. Moreover, the temporal patterns of cortical bursting in the preterm are maturation-dependant and strongly influenced by the development of cortical pathways.

2.2.3 AUTOMATED DETECTION OF EEG FEATURES IN PRETERM EEG RECORDINGS

Preterm EEG has also been the subject of method and data driven quantifiers. Here, I focus on literature works that utilize automated analysis techniques to EEG recordings to predict outcome in preterm populations (search period up until December 2014). Specifically, I summarize the types of constraints applied to pre-processing EEG recordings, features extracted from preterm data and the classification methods employed to determine outcomes (Table 2.2).

Author	GA (weeks)	Feature selection			Summary	
		Filtering & Channels	Thresholding & constraint	Target	Output	Optimization (OP) & Validation (V)
(Wertheim et al. 1991)	24-32 wks	0.5-11 Hz 1 (F4-P4 and F3-P3 positions)	Amplitude threshold with time constraint fixed: <25 uV and duration > 6s	Low amplitude intervals (amount of discontinuity)	Number of low amplitude intervals in 1 min analysis epoch - mean of the square amplitude in 1 min analysis epoch	OP: Empirical V: proportion of visually identified discontinuous epochs correlated with mean proportion of automatically detected low amplitude intervals
(Arnold et	27-31	Adapted FIR	Neural	Spike patterns	High instantaneous	OP: Automatic

al. 1996)	wks	filter 8 (Fp1, Fp2, T3, T4, C3, C4, O1, O2)	network with adaptive pre-processing unit	detected via Hilbert-transformer	power values for spike patterns	(neural network) V: Visual
(Vanhatalo et al. 2005)	32-36 wks (preterm subset)	0.5 Hz 2 only (C3, P3, C4 and P4)	fixed: number of frequency bands:>=4. adaptive: normalized amplitude envelope: 1.5SD	normalized amplitude envelope in 10 frequency bands, number of frequency bands above the amplitude threshold	Multiband activity transients (MBAT)	OP: empirical, e.g thresholds V: Rate of occurrence MBATs in real data was compared with detection of MBATs in 200 realizations of randomly shifted surrogate data.
(West et al. 2006)	<32 wks	1-50 Hz 2 only (C3, P3, C4 and P4)	No constraint fixed: > 50 uV	Amplitude range median values of 4 s segments	Continuity (proportion of high amplitude epochs in 1 min analysis epoch)	OP: Thresholds 10, 25, 50 and 100 uV were tried out. 50 uV was the optimal threshold
Niemarkt et al (2010)	29±0.3 wks	0.5 – 8 Hz 1 channel derivation (C3–C4)	Adaptive: > 20th percentile Fixed: 40 μV^2 (power)	bursts, inter-burst-intervals	proportion of discontinuous activity (inter-burst ratios)	OP: Correlation analysis with post menstrual age V: none
Palmu et al (2010)	23-30 wks	0.1-8 Hz (EEG band), 47-49 Hz (artefact band) 1 channel	fixed: > 300 µV^2 (burst), < 40 µV^2 (IBI), both in EEG band. > 10000 µV^2 (artifact) duration (burst > 1-2 s, IBI > 2s)	burst, IBI, (continuous EEG/artifact)	smoothed NLEO output in two different frequency bands	OP: performance measured against a gold standard of unanimous markings by 3 clinicians
Jennekens et al (2011)	29-34 wks	0.5-32 Hz + 50 Hz notch 18 channels	fixed: 30 µV (below: IBI, above burst/continuous activity) duration (burst: <20s, continuous activity >20s,	bursts, inter-burst-intervals and continuous patterns	Burst, IBI and continuous pattern envelopes	OP: Thresholds based partly on literature, but partly on comparison of sensitivity values against manual notations by two experts.

			IBI > 1s), number of channels with high-/lowamplitude activity (burst/continuous activity: 4, IBI: 18).			V: Validation done on different data than optimization.
(O'Reilly et al. 2012)	<29 wks	2 only (C3, P3, C4 and P4)	No threshold Amplitude bands with boundaries 0-10μV,10-25 μV, 25–50 μV, 50–100 μV and above 100 μV	Peak-to-peak values in raw EEG 2 s segments Where rEEG is the upper estimate of peak to peak EEG values	8 indices were calculated to characterize the distribution of values in 1 min epochs aEEG, rEEG, half wave decomposition, root mean square	OP: Spearman rank correlation and bland altman test each measure V: Linear mixed models for all indices including aEEG, rEEG, half wave decomposition, root mean square \
Hartley (2012)	23-30 wks	0.5-70 Hz + 50 Hz notch 9 or 11 (F3, F4, C3, C4, P3, P4, T3, T4, O1, O2 and Cz P3, P4)	fixed: >0.8, duration > 4/22 s, consecutive events within 0.5 s were counted as one	bursts of nested oscillations (BNO)	inter-event-intervals (IEI) further studied for long range temporal correlations	OP: threshold based partly on experiments, partly on intended confidence level V: detection validated visually by 4 researchers
Mitchell et al (2013)	27-29 wks	0.1 Hz highpass 2 channels	delta waves that were at least 100 μV in amplitude and between 0.5 Hz and 1.5 Hz Interburst intevals; amplitude remained under 10 μV and exceeded 5 s.	based on wave morphology utilizing Bayesian probability theory of delta waves and inter-burst intervals	posterior probability of each pattern based on template matching	OP: 2 of 14 recordings were used for pattern optimization V: 12 of 14 recordings (=separate test set) was used to evaluate the performance. Validation method: confusion matrixes with algorithm and one of the readers compared to the other reader.
Koolen et al (2014)	26-34 wks	1-20 Hz	adaptive: > 0.85*mean of line length feature in 150s	bursts (and inter-bursts)	Median IBI duration, maximum IBI, burst percentage and	OP: Line length threshold: Evaluation of ROC curves generated

		9 electrodes	epoch difference in amplitude between a successive non-detected and detected point and vice versa should be > 0.4 * SD of median line lengths in 150s segment	median of normalized line lengths in each channel	median deviation	with manual markings by two experts as gold standard. Additional constraint was defined heuristically. V: Separate test set. Detection results were compared with manual markings by two experts and reported as confusion matrixes.

Table 2.2 – Quantification methods and analyses in studies in preterm EEG, (with content modified from (Palmu 2015)). Table legend: Interburst interval (IBI), Gestational Age (GA) where wks = weeks, "Constraint" is information provided by the authors for any limitations placed on automatic detection. "Output" refers to the features which are selected for analysis and subsequent results. "Optimization" refers to any specific adjustments, correlations or classification algorithms. "Validation" refers to confirmed absence or presence of normality or abnormality.

These studies employ a multitude of analysis paradigms which aim to automatically quantify preterm EEG features and derive prognostic features. Quantified methods within preterm EEG research vary in use of classifiers and data constraints. There appear three different approaches for quantifying preterm EEG patterns. One that is qualitatively driven by fixed thresholds and selected features, where maximum, minimum limits are set. Secondly, multiple quantitative methods are employed to extract an array of features which are used for prediction via a machine learning classifier. Third, spectral methods are used to analyze changes in different cortical bursting and suppression periods across preterm development ages.

The use of these methods in preterm and full-term populations informs us about the range of methodologies employed to extract prognostic information from neonate EEG recordings. In particular, the research presented in Table 2.1 and Table 2.2 suggests common analysis challenges such as: 1) accounting for data variability, e.g. electrical noise, neonate movements; 2) objective threshold estimation, 3) robust statistical characterization of empirical distributions in data and 4) rapid extraction of cortical signatures from infant brain activity. In this thesis, I focus on mitigating these challenges in designing an analysis paradigm for neonate EEG that offers predictive markers of clinical outcome. Prior to commencing empirical chapters, I first review the concepts I bring to this question, namely criticality, scale-free statistics and crackling noise.

2.3 PRINCIPLES OF CRITICALITY AND SCALE-FREE NETWORKS

Theories of universality in nature and the ubiquity of "1/f" noise fluctuations in physics and biology have been areas of immense scientific discovery (Bak et al. 1987; Schuster et al. 2014). In the context of complex fluctuating behaviour, there are tremendous amounts of energy that dissipate and transform across a range of temporal scales. These fluctuations in nature represent behavior of systems which are fundamentally complex and have a propensity to transform into a critical state. Concepts such as self-organized criticality, scale-free dynamics and crackling noise offer quantitative insights into systems which exhibit stochastic behavior across a broad range of sizes.

The exploration of these concepts, in physics and nature, has yielded tremendous insights into how large scale systems maintain and transform energy processes that exist in complex fluctuating behavior. As described in section 2.1 and 2.2, the temporal characteristics of a newborn's EEG, particularly following brain injury or premature birth, contains uniquely ubiquitous cortical bursts – an aspect of neurophysiology that may lend itself to previously detailed studies of critical phenomena. Neonatal EEG has yet to be investigated using principles of criticality, a concept which has provided significant insights in characterizing the dynamics of healthy and pathological neuronal activity (Beggs and Plenz 2003; Haldeman and Beggs 2005; Kinouchi and Copelli 2006; Meisel et al. 2012; J. A. Roberts et al. 2014; Shew et al. 2009). The following sections aim to discuss the evolution of criticality in physics and neuroscience. In particular, through detailing the literature of criticality, I seek to strengthen the reasoning for the study and presence of critical phenomena in newborn EEG.

2.3.1 CRITICALITY, SCALE INVARIANCE & CRACKLING NOISE IN PHYSICAL SYSTEMS

Criticality occurs through complex, stochastic processes arising in systems close to the point of chaotic instability or occurring to compensate for spontaneous changes to a system. Models of criticality in physical systems demarcate two classes of dynamics: systems which display criticality through "self-organizing" mechanisms or exhibiting critical dynamics via an external tuning parameter. Systems which are self-organizing re-establish the order in a system when a critical point of instability is reached (Bak et al. 1987). An exemplar of self-organizing, uniform dynamics is the 'sand pile' model which has no specific hierarchical organization. As the sand pile grows, a point of criticality is reached and the pile collapses, partially before building back up. Here, energy dissipates from the system without being driven by any external tuning parameter. Systems that self-organize do not need to be tightly tuned to show spontaneous instability, but rather organize to this state by amplifying internal fluctuations. This occurs as the system passes through instability

and rearranges to a more stable state. The term commonly used in systems which encounter these fluctuations near critical points are called "avalanches" (Bak et al. 1987). Avalanche behavior is observed in a wide variety of physical systems, including earthquakes (Gutenberg and Richter 1945; Pisarenko and Sornette 2003), snow avalanches (Birkeland and Landry 2002) and forest fires (Malamud et al. 1998) where a fluctuation above a critical threshold results in a characteristic cascade of events. These events propagate throughout the system. The spatial and temporal distributions of avalanche events are uniformly distributed across scales.

In complex systems, avalanche type events have unique statistical properties which yield insight into the scaling behavior with relation to size, area and duration of an event (Frette et al. 1996; Laurson and Alava 2006). The presence of an external or internal driving force coupled with an underlying hierarchy of characteristic scales provides better understanding of complex scaling exponents which influence system spontaneity (Sornette and Cont 1997). This introduces the concept of scale invariance and the presence of heavy tailed distributions in physical systems, such as the power-law (Pareto) distribution.

A system that is scale invariant indicates that fluctuations range very broadly across event size (i.e. existence of small avalanches to large avalanches). A characteristic of a power-law distribution is that the occurrences of events vary over the system, i.e. larger avalanches are less frequent, more often expected by chance, than smaller avalanches (Kadanoff et al. 1989; Sethna et al. 2001). Within a power-law distribution a mathematical ratio is maintained across the system. In particular, the log of the likelihood of an event occurring co-varies linearly with the log of the size of that event. For example, an earthquake which is lower on the Richter scale occurs more frequently than larger scale earthquakes thus maintaining a common ratio across the system. Power-law scaling and other heavy tailed distributions (Levy, Cauchy, Weibull) capture the empirical statistical distributions present in avalanche type events in natural world phenomena (Clauset et al. 2009). Moreover, power-laws are evident in systems which self-organize.

Scaling laws such as a power-law regime offer a quantitative insight into the mathematical function of system behavior, particularly if the quantities of avalanches in a system are not well captured by their average and standard deviation. Within a power-law scaled system the vast spectrum between small and large cascading avalanche events is often followed or preceded by periods of quiescence. These aperiodic intervals contain informative ‘noise’ interactions - termed “crackling noise” - where a system is in a critical balance between amplification and dissipation (Sethna et al. 2001). Further, crackling noise exemplifies characteristics of universality because it arises through varied mechanisms in diverse phenomena yet exhibits stereotypical scale-free properties. In physical systems, crackling noise has been observed during the occurrence of avalanches in ferromagnets responding to changes in the external magnetic field (Zapperi et al. 2005). The transition between

these changes indicates the various time scales at which events occur, the range in event sizes and the critical points of a system.

The study of crackling noise phenomena provides informative insights into the mechanisms of self-similarity and state-dependent effects present during stochastic fluctuations in a system. Systems which are at a critical balance reflect a transformation in energy, whether it is subcritical (small internal fluctuations) or supercritical (large fluctuations superimposed upon a power-law regime). Here the study of average fluctuation shapes elucidate upon energy expenditure within a scale-free system, where fluctuations at a range of sizes converge towards a universal set of dynamics and scaling functions (Baldassarri et al. 2003). A classic example of average shapes collapsing towards scale-invariance is the erratic, bursty Barkhausen noise pulses of ferromagnets (Mehta et al. 2002; Perković et al. 1995; Zapperi et al. 2005). These pulses, which exhibit a power-law regime during changes in an external magnetic field, are an example of crackling noise across a hierarchy of time scales (Papanikolaou et al. 2011; Spasojević et al. 1996; Zapperi et al. 2005). Moreover, stochastic models developed to replicate the behavior of these pulses have yielded additional insights into how scale-free systems utilize their resources. For example, the uncorrelated unbiased Gaussian random walk has an entirely symmetric, scale-invariant morphology in terms of average burst shapes with robust power-law regimes (Baldassarri et al. 2003). The asymmetry of average burst shapes, discovered in Zapperi's work on domain wall velocities in magnetic materials (2005), successfully elucidated upon scale-dependent effects at long time scales. These data experiments and models provide critical insights into a subtle set of dynamics which are embedded within scale-free systems.

2.3.2 SCALE-FREE NEURONAL NETWORKS

Concepts of self-organized criticality and crackling noise in physical systems present a significant premise for the study of criticality in the human brain (Beggs and Plenz 2003; Chialvo 2010; Schuster et al. 2014). Characterizing the scaling laws present in network level neuron interactions and temporal cortical activity may provide crucial insight into healthy brain states. Patterns in neonate brain recordings consisting of burst suppression during hypoxia and discontinuous patterns of the immature preterm cortex are similar to avalanche type events, i.e. there is a broad range of fluctuation sizes occurring at different time scales. Studies over the past decade have shown that self-organizing networks in neurobiological models display scale invariance through avalanches and crackling noise (Beggs and Plenz 2003; de Arcangelis et al. 2006; K. J. Miller et al. 2009; Rubinov et al. 2011). These models have shown that scale invariant systems are inherently stochastic, fluctuating on a continuum between ordered information processing to unstable signalling randomness.

The study of criticality in the brain over the past decade has progressed substantially from cortical level research (Beggs and Plenz 2003), to modeling the spatial distribution of avalanches (Chialvo 2010) and its application at a functional level (Eguiluz et al. 2005; Haimovici et al. 2013; Biyu J. He et al. 2010). In Beggs and Plenz's (2003) seminal experiments using small grids of electrodes, critical branching processes were observed through the spiking patterns in a multi-electrode array in cortical slices of the rat, where 'neuronal avalanches' operated at a point of network stability and instability. These neuronal avalanches constituted activity bursts which conformed to a classical power-law distribution with respect to event sizes and occurrence of small and large bursting patterns. Further, this experiment and similar studies (Haldeman and Beggs 2005; Mazzoni et al. 2007; Shew et al. 2009; Steyn-Ross et al. 1999) frequently observe scale-free distribution of avalanches in neuronal populations, with a power-law exponent close to -3/2 for event sizes. These studies observed criticality when externally driven by a tuning parameter, e.g. tuning to a threshold, rather than those that spontaneously propagate avalanche events through self-organization.

Recent studies have expanded upon in vitro and in vivo experiments to demonstrate criticality via computational models and explore the presence of self-organizing mechanisms in neuronal systems. These mechanisms, which are largely unknown at a neurophysiological level, hypothesize on the timing of burst spikes (Meisel and Gross 2009; Pasquale et al. 2008; Rubinov et al. 2011) and the strength of activity through synaptic plasticity (de Arcangelis et al. 2006; Levina et al. 2007; Tetzlaff et al. 2010). The basis for these models is that the parameters which drive a system towards criticality adhere to self-organizing principles such as increased activity dependence or a slow build-up of energy before fast dissipation and relaxation.

Measurements of criticality in the brain have been captured through long range correlations across cortical systems. The use of neural field modeling focuses on the spatial mechanisms driving avalanche behavior rather than features of criticality (Aburn et al. 2012; Benayoun et al. 2010; Robinson et al. 2010). In the human brain, study of local field potentials, EEG and MEG derived data have demonstrated different signatures of subcritical, critical and supercritical behavior in cortical networks (Linkenkaer-Hansen et al. 2001; Palva et al. 2013; Priesemann et al. 2013; Shriki et al. 2013). These large scale analyses along with earlier cortical level experiments have contributed greatly to the understanding of the human brain and the mechanisms in which critical behavior is observed.

2.4 HYPOTHESIS DEVELOPMENT FROM THE LITERATURE

In this thesis I test hypotheses which further explore the mechanisms of scale-free activity, criticality and crackling noise in the human neonate brain. Using neonatal brain activity recordings I contend that cortical activity early after birth is inherently scale-free, a process which is a

ubiquitous signature of complex natural systems. Significantly, I disambiguate an important point – that systems which yield scale-free power-laws do not necessarily display criticality (Beggs and Timme 2012). This follows in testing whether scale-free behavior in the brain is consistent with criticality or whether it speaks to other complex scale dependent processes. Here, I investigate event duration and size statistics present in neonatal EEG and the correct scaling estimation and model likelihood fitting required to differentiate between critical power-laws and scale-free distributions exhibiting a different set of dynamics (Biyu J He 2014).

Following on from criticality experiments in physics, such as bursts of Barkhausen noise in microscopic ferromagnetic domains (Sethna et al. 2001), I further explore hypotheses that the stochastic nature of cortical bursts in the brain can be elucidated via principles of crackling noise. Recent analytic approaches to neurophysiological signals have focused on temporal dynamics of cortical bursts, characterizing features of bursting content to assess underlying brain states as opposed to conventional interburst interval analysis (Lewis et al. 2013; Westover et al. 2015; Vanhatalo and Kaila 2006; Benders et al. 2014). The characterization of bursts in hypoxia, induced burst suppression or preterm trace alternant activity may yield important insights into how neuronal constraints, e.g. metabolism, and cortical networks are bounded by a finite resource pool. Given that these types of cortical bursting patterns are (predominantly) spatially homogenous, I investigate the temporal properties of the bursts to reveal new markers of brain activity, with a view to explicate the link between neuronal activity and its neurophysiological underpinnings.

The first half of this chapter focused on pathophysiological mechanisms of full-term hypoxia and preterm populations. Specifically, abnormal cortical activity patterns, such as burst suppression and discontinuous EEG, are seemingly indicative of systems which are poised between system stability and instability. These types of abnormal patterns in the brain are fundamentally stochastic, particularly in a neonate cortex, and may reflect the constraint of metabolic nutrients or the excitability of cortical networks. Importantly, utilizing features of scale-free analysis from neonatal electroencephalography towards an outcome prediction metric will provide an enriched understanding of neurodevelopmental outcome and potentially, an effective tool for bedside identification of at-risk neonates.

3.0 SCALE-FREE CORTICAL BURSTS FOLLOWING HYPOXIA AT BIRTH

ABSTRACT

The cortex of the human brain is susceptible to oxygen deprivation at any age, but never more so than at birth. Following perinatal hypoxia, cortical activity exhibits a stereotypical recovery pattern that includes a period of highly irregular electrical fluctuations known as burst suppression. A healthy outcome requires the rapid resolution of bursts and the resumption of continuous cortical activity. In this chapter, we describe methods for statistically characterizing and analyzing routinely monitored EEG bursts, following hypoxia, to highlight the potential clinical relevance of scale-free fluctuations. Analysis of empirical distributions of burst durations and their sizes demonstrate that bursts are a fractal phenomenon with power-law scaling up to five orders of magnitude. Through an analysis of average shapes, cortical bursts converge toward a simple scaling function which, in most infants, shows a leftward asymmetry at long time scales. Significantly, the resumption of normal electrical activity corresponds to the loss of leftward asymmetry and the re-organization of other key scaling relationships. Burst suppression, an important clinical phenomenon, hence belongs to a very broad class of physical processes known as crackling noise. These findings reveal novel neurophysiological mechanisms and hold promise for new ways to monitor recovery from cortical hypoxia in the newborn.

3.1 INTRODUCTION

The hypoxic neonate brain represents a highly compromised cortex where metabolic supply is limited and pathological states of cortical activity, such as burst suppression commonly exist (Amzica 2009; Kostović and Judaš 2010). In Chapter 2, section 2.2.3 we highlighted key issues for variability in automated measures of EEG to predict outcomes. Notably, we identified the need for objective data analysis paradigms that circumvent the use of applying arbitrary choices (e.g. threshold, filtering constraints). This chapter motivates the use of statistical characterization to identify key features of neonate EEG. In particular, we study a dataset of full-term hypoxic neonates and extract robust statistical properties to differentiate between abnormal and healthy cortical activity states.

In this study we employ a method for analyzing burst durations and burst sizes to characterize their respective scaling relationships during hypoxia induced burst suppression. Many prior qualitative methods rely upon perceiving burst suppression as a uniform entity, deriving standard statistics such as the mean burst intervals and inter-burst periods to predict acute and long-term outcome (Walsh et al. 2011). These temporal 'snapshots' of data in neonates are typically used to derive indication of outcomes, requiring further stipulation of statistical normality or non-normality, resulting in possible estimation errors and conclusions. We pursue an alternative approach to classification and correlational analyses that assume underlying normality, opting for a data driven approach by characterizing probability distributions of bursts during burst suppression in post-hypoxic infants. Probability distributions in data, such as population growth, economic models and biological signals, rarely conform to a Gaussian normal distribution (McKelvey and Andriani 2005). The idea of scalability, or 'fractal geometry', draws upon the concept that self-similarity of the smallest features in complex phenomena correlate strongly with features at larger scales (Mandelbrot and Hudson 2004). In recent decades, the analysis of heavy-tailed distributions has revealed subtle, yet complex mechanisms of model likelihood and consequent prediction. As described in Chapter 2, there is growing body of literature that demonstrates signatures of self-organization, crackling noise and criticality in both physical and biological systems. In these studies, characterizing scale-free distributions in data provides a critical interpretation of heavy-tailed phenomena in revealing the underlying statistical mechanisms within a system.

This study draws upon concepts of criticality, self-organizing mechanisms and crackling noise to test the hypothesis that burst suppression arising in the hypoxic neonate conforms to a complex heavy-tailed empirical distribution function known as a power-law. Moreover, statistics of bursts, such as burst durations and burst sizes are contrasted with theoretical power-law models to contend

that power-law scaling is a signature of the neonatal hypoxic brain soon after asphyxic insult, and that these features are not only scale-free but consistent with criticality.

We also introduce a novel analysis method for analyzing burst content during burst suppression. This chapter aims to further understand scale-specific shapes of cortical bursts, and their inter-scale relationships to differentiate between subcritical, critical and supercritical processes (Papanikolaou et al. 2011; Zapperi et al. 2005). These scale-specific shapes, hereafter referred to as average burst shapes, provide a deeper understanding of the temporal dynamics of burst fluctuations. Moreover, the stochastic nature of cortical bursting patterns also suggests state transitions between burst suppression and continuous activity, reflecting a reorganization of neuronal resources. We seek to understand the reorganization of these cortical activity patterns through quantifying the changes to burst shape across a hierarchy of burst durations.

Our findings motivate the use of computational models which have demonstrated scale-invariance, i.e. an undamped stochastic process equivalent to a Brownian walk (Baldassarri et al. 2003; Colaiori et al. 2004), and modeled state-dependant effects such as damping and asymmetry at longer time scales (Papanikolaou et al. 2011; Sethna et al. 2001; Zapperi et al. 2005). Through model simulations of scale-invariance, activity-dependent damping and asymmetry, mechanisms of energy expenditure are reconciled with trends in burst symmetry and sharpness found in the post-hypoxic neonatal brain. This study tests the hypothesis that cortical activity in hypoxic neonates have characteristic average burst shapes which arise from initial insult. These burst shapes are posited to yield signatures of recovery soon after burst suppression patterns resolve as a response to metabolic replenishment.

3.2 MATERIALS AND METHODS

The dataset comprised thirteen consecutively admitted infants (gestational age 39±2 weeks) with birth asphyxia leading to hypoxic ischemic encephalopathy (HIE) in the tertiary level neonatal intensive care unit of Helsinki University Central Hospital. Use of these archived, de-identified EEG recordings was approved by the Ethics Committee of the Hospital for Children and Adolescents, Helsinki University Central Hospital.

3.2.1 NEONATAL COHORT

Infant EEG recordings were collected over a 30 month period from November 2009 to April 2012. Further, these infants underwent whole-body hypothermia treatment during long-term EEG monitoring in the first week of life.

Inclusion criteria for this study involved high-quality EEG epoch selection from a trained neurologist. Periods of initial burst suppression occurred within 18 hours of birth. EEG epochs were relatively artifact-free, ranging between 40-330 minutes in length. Recordings were available over the first 72 hours after birth. 10 of 13 neonates resolved from burst suppression to continuous activity patterns.

Exclusion criteria for this analysis included the presence of epileptic seizures or non-neuronal artifacts such as those due to physical movements or respiration. Clinical details regarding delivery, drug treatments, complications immediately following birth (i.e. infection), and Apgar scores 1, 5 and 10 min after birth were also collected. Infants comprised of 13 neonates (9 male) having presented with either asphyxia at birth (n=12) or a sudden cardiorespiratory collapse with severe asphyxia immediately following birth (n=1).

Table 3.1 summarizes the details of the cohort studied

Infant	Sex	Recording (min)	pH at Birth	GA (weeks±days)	Apgar (1/5/10 min)
1*	m	75	6.71	34 + 5	0/0/6
2*	m	120	6.76	40 + 1	2/4/4
3*	m	90	7.10	40 + 3	0/0/1
4*	f	120	6.89	41 + 4	2/3/5
5*	f	180	6.86	40 + 1	1/1/1
6*	f	60	6.80	41 + 3	2/2/5
7*	m	100	7.30	36 + 1	1/4/5
8*	m	330	7.02	40 + 0	2/3/5
9*	m	40	6.84	38 + 1	1/4/5
10*	m	70	7.30	36 + 1	1/4/5
11	m	60	6.90	41 + 0	5/6/6*
12	m	60	7.15	39 + 3	1/1/1
13	f	160	6.68	36 + 4	0/2/3

Table 3.1 - Gestational age refers to the number of full weeks plus the number of days. Apgar scores refer to the short standard clinical test done immediately after birth that examines breathing effort, heart rate, muscle tone, reflexes, and skin color. pH at birth was measured from umbilical cord blood sample. m, Male; f, female. *Infant 11 has normal Apgar values at birth, because he presented with sudden cardiovascular collapse and ensuing asphyxia at 33 min of age. Asterisked values indicate those infants that resolved to continuous EEG.

3.2.2 DATA ACQUISITION AND PRE-PROCESSING

Data were recorded via two EEG amplifiers – the NicOne (Nicolet Biomedical) and the Olympic (Natus) monitor – at sampling rates of 250 and 500 Hz or 256 Hz, respectively, and stored offline for later analysis. Further exporting of data involved either European Data Format (for NicOne) or ASCII format (Olympic monitor). Pre-processing of data (in MATLAB) was conducted to standardize the sampling rate of all data to 250 Hz, i.e., 500 Hz recordings were downsampled (n=6) by discarding every second point, and the 256 Hz recording was resampled (n=1) by using an anti-aliasing (low-pass) filter. Channel selection for this data only included the single biparietal derivation (P3–P4). This is the most common recording configuration in use in the neonatal intensive care setting. Moreover, as highlighted in Chapter 2 although analysis of the spatial

properties of post-hypoxic burst suppression would likely be informative, this analysis focuses here on characterizing the temporal signatures of the term hypoxic brain.

Temporal analysis of EEG epochs involved initial pre-processing for optimizing cortical burst selection. Firstly, we obtain amplitude envelopes of data using the magnitude of the Hilbert transform. The Hilbert transform is an effective signal processing tool for this type of data as it preserves the temporal properties of a signal whilst detecting slow time variations without the incursion of small, rapid oscillations (Thrane et al. 1995). Burst suppression patterns in full-term hypoxic infants involve large, slow duration burst fluctuations (> 1 s). These fluctuating bursts can be often compounded by small, rapid oscillations either arising from respiratory, physical movement or heart-rate variability. Extracting the signal envelope via the Hilbert transform, captures burst events and preserves temporal resolution for further analysis.

The second step we employ in pre-processing the data is signal filtering. The data is squared to obtain the instantaneous power and then smoothed via a 10th-order Savitzky-Golay filter (19 Hz cutoff) to reduce noise on short timescales. This also assists with the convergence of average burst shapes (Papanikolaou et al. 2011). This filtering technique allows smoothing of high frequency noise whilst maintaining the shape and peak of a waveform using least-squares polynomial estimate (Savitzky and Golay 1964; Schafer 2011).

Analyses of multiple filter settings for both the raw data and power fluctuations were studied as a quality check for robustness in terms of pre-processed signal and post-hoc analysis for scale-free distributions and average shape analysis of bursts. In this chapter, this testing of filter settings extended to the robustness of burst distribution statistics and further the effect of these filters on average burst shapes. Examples (Fig. 3.1) illustrate the use of the Hilbert transform on the EEG, filtering of the signal and the power fluctuations present in a windowed epoch of data.

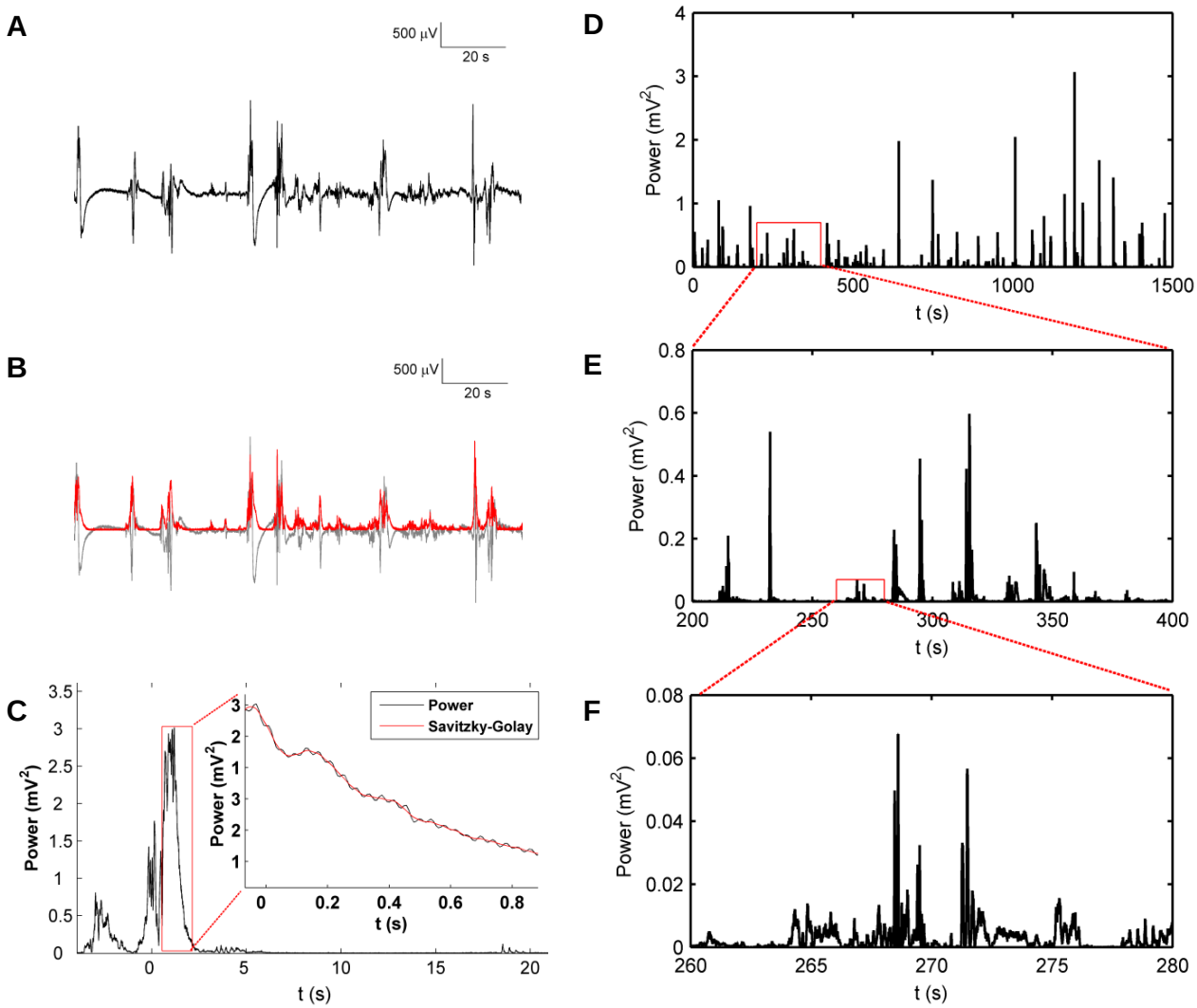

Figure 3.1 – Extracting bursts from the envelope of BS EEG from the biparietal electrode montage P3-P4. (A) A small snippet of a BS epoch (B) the magnitude of the Hilbert transform of the signal (red overlay), (C) Instantaneous power with the Savitzky-Golay filter smoothing high frequency noise, (D) – (F) Self-similar bursts in the power epoch of the BS EEG give an indication of scale-invariance.

3.3 STATISTICAL CHARACTERIZATION OF CORTICAL BURSTS

Following pre-processing, data epochs were analyzed via the following steps: (1) threshold estimation; (2) burst extraction; (3) calculation of burst areas and durations; (4) fitting burst distributions (5) empirical validation (6) calculation of average shapes at different time scales; and (7) quantification of variations in shapes by calculating asymmetry and flattening. These steps are further described.

3.3.1 THRESHOLD ESTIMATION AND BURST EXTRACTION

As outlined in Chapter 2, Table 2.1 and Table 2.2, quantitative and qualitative methods for feature detection employed for burst and inactive periods depend upon subjective choices for threshold values. Hence, it was crucial that the application of a heuristic method such as data thresholding could be applied to all datasets. In this work we focus on the detection of burst events, and further characterizing the size, duration and shape statistics in a robust and objective manner. Using this method, we obtain a threshold by maximizing the number of identified bursts and hence avoid manual marking of each EEG epoch. Visual inspection of a sample EEG epoch from an infant with burst suppression (Figure 3.1A) consists of typically inactive periods with intermittent low level bursts (<5 μV) followed by much larger amplitude bursts. Applying a threshold to account for inactive suppression periods and low level bursts thus becomes an important starting point for any threshold estimation. Threshold values below noise level yield very few bursts. As a threshold value rises above the noise floor, suprathreshold bursts emerge, although for small thresholds, many of these will be artificially merged. High thresholds fail to identify small bursts and, in the extreme, fail to identify any bursts at all. Hence the number of bursts is a simple unimodal function of threshold with a single maximum (Fig. 3.2A). This maximum threshold value — unique to each dataset— can be used as the choice of threshold.

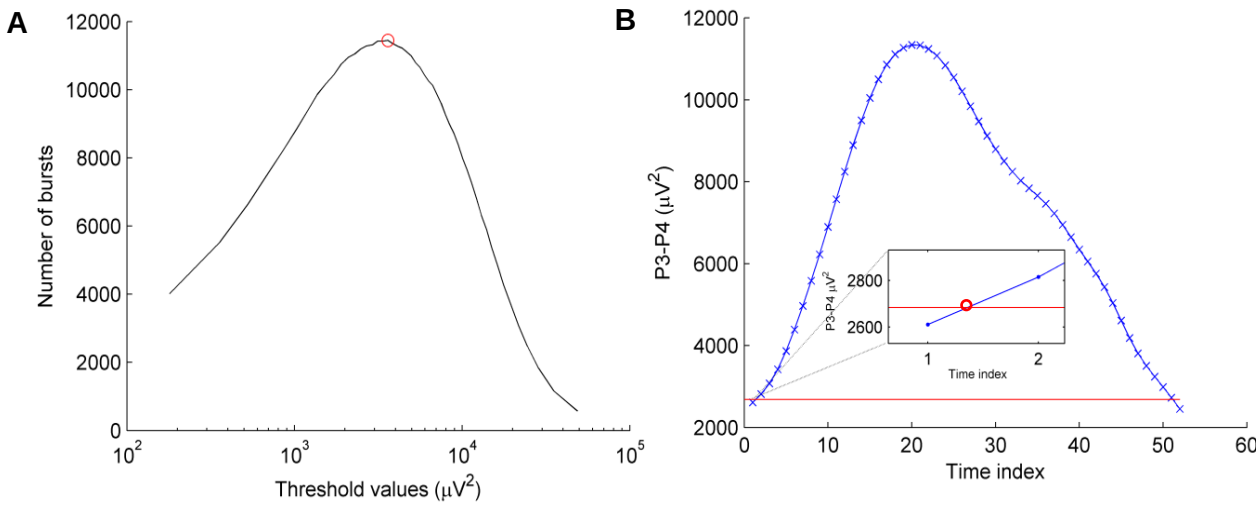

Figure 3.2- Threshold estimation and burst extraction. (A) Example of threshold values versus number of bursts found in an EEG epoch with BS where the maximum (red circle) indicates the threshold at which the most number of bursts events are detected. (B) Using the threshold value, a burst can be extracted based on points supra-threshold; inset (red circle) shows an approximation of a data crossing derived via linear interpolation.

Due to coarse sampling it is typical that a threshold crosses data between two samples rather than on the exact threshold value. To improve temporal precision of endpoints we used linear interpolation to find an approximation at which the threshold crosses (Fig. 3.2B, inset) with respect to below threshold and supra-threshold points. This method ensures that each burst begins and ends

at the exact threshold value. In this analysis, a burst event is defined as all successive supra-threshold data points, beginning when the signal crosses the threshold from below and ceasing when the signal next crosses the threshold from above. Using this method suppression periods or inter-burst intervals can also be extracted. To reduce computation time, we restrict the set of thresholds tested to 50 quantiles of the data as results are insensitive to the precise number as the relationship between threshold and number of bursts is relatively smooth in all our datasets. Moreover, we tested the sensitivity of our results to the precise choice of threshold.

3.3.2 EMPIRICAL DISTRIBUTION FUNCTIONS PRESENT IN BURST SUPPRESSION

Following thresholding and identifying discrete bursts, two features of bursts were analyzed for their statistical distributions. Specifically, burst size (supra-threshold burst area under the curve) and burst duration (time between successive threshold crossings), as illustrated in Figure 3.3, were identified using the threshold value. In this study, bursts of duration less than 40 ms were excluded as these are coarsely sampled (10 samples) at 250 Hz.

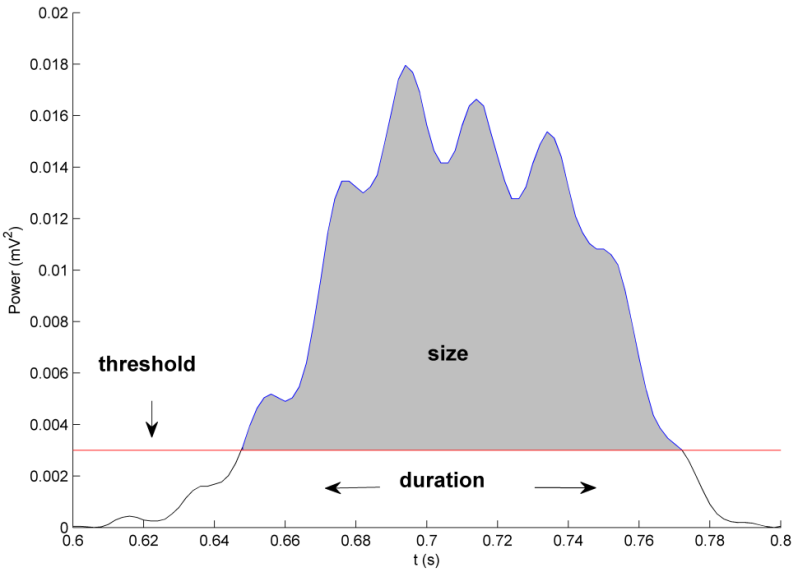

Figure 3.3 - Schematic burst with its duration (time above threshold) and size (area under the curve above threshold, shaded).

After extracting burst durations and burst sizes, (referred interchangeably as *areas*), cumulative distribution functions were then examined. For each epoch, extracting burst durations greater than 40 ms yielded each infant's unique set of fluctuation statistics. These fluctuations were used to construct an upper cumulative distribution function (i.e. 1-P(X > x)). To examine the empirical characteristics of each cumulative distribution, heavy tailed candidate fits were fitted via the method of maximum likelihood. This analysis employed five heavy tailed distributions commonly present in natural phenomena: power-law (Pareto distribution), power-law with exponential cutoff, log-normal, stretched exponential (Weibull distribution), and exponential distribution (Fig. 3.4A).

We also analyze the scaling relationship between burst durations and burst areas, given the temporal self-similarity of bursts at range of sizes and durations. Here, bursts were binned by duration into logarithmically spaced bins and we calculated within each the median duration and median area. Estimation of the scaling exponent (slope of the linear relationship in log-log coordinates) was performed using a linear least-squares fit. Figure 3.4B shows a sample plot of the scaling relationship present between burst duration and burst areas.

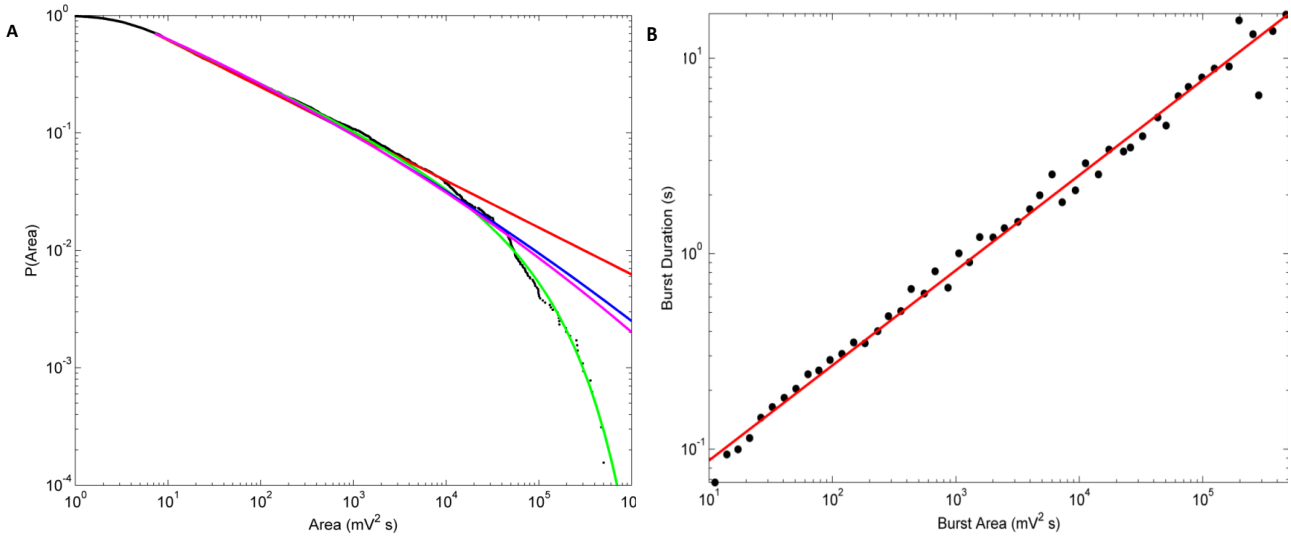

Figure 3.4 – Statistical distributions of burst duration and burst area. (A) Upper cumulative distribution of burst area (solid circles) showing lengthy power-law regime. Solid lines show best-fitting candidate long-tailed distributions: power-law (red), Weibull (blue), log-normal (magenta), and exponentially truncated power-law (green) (B) An example of the scaling relationship of median burst size and burst duration in double-logarithmic coordinates.

3.3.3 *ESTIMATING MODEL LIKELIHOODS IN EMPIRICAL DATA*

Using established techniques, each theoretical distribution was fitted to the right-hand side of the empirical cumulative distribution function (CDF), above a lower bound that minimizes the Kolmogorov–Smirnov goodness-of-fit statistic between the power-law model and the data (Clauset et al. 2009). This method of determining the range of the fit strikes a balance between fitting too wide a range (i.e. outside the power-law regime) and too narrow a range (i.e. unnecessarily throwing away data), thus maximizing the fitting range for a power-law. The same fitting range for all five candidate distributions were used in each data epoch. An estimated p-value was calculated for each fitted power-law by comparing 2500 synthetic datasets drawn from a true power law. This p-value provided an estimate of the likely deviation between the data and the fitted power law. A significance level greater than 0.1 indicated the likelihood of power-law behavior, otherwise power-law behavior cannot be considered plausible (Clauset et al. 2009).

Contrasts of candidate distribution functions were tested via a hierarchical approach that balances model likelihood with model complexity (Clauset et al., 2009). Here, fitted power-law distributions are compared with alternative distribution fits using likelihood ratio tests. We compared power-law distributions with functions of lower complexity, such as the exponential distribution, and three heavy tailed distributions: a power law with exponential cutoff, log-normal, and stretched exponential (or Weibull) distributions (Figs. 3.4A). Likelihood ratio tests further discriminate one data models' preference over another (Clauset et al. 2009). This test, in isolation, is not completely definitive in deciding which fit is more favourable as data is also prone to "chance" fluctuations which can significantly influence one model distribution over the other. Thus, significant deviation of the likelihood ratio from zero was tested using Vuong's methods (Vuong 1989). The combination of the likelihood ratio test with Vuong's estimate provides further evidence for model favourability.

Statistical comparison of log model evidences allows differentiation of which candidate fits are favoured within the dataset. This comparison draws upon Bayesian Model Selection (Stephan et al. 2009), which tests which distribution scaling process is most significant in our data based on log model evidences. Using Bayesian inferences, the posterior expectation of log evidences in five candidate fits gives the likelihood that the model (r) explains observed data events (y). The model with the highest posterior expectation indicates the most favoured distribution function present in the dataset.

Another form of power-law distribution is the strictly-truncated power law, which is restricted to a range of data between both lower and upper cut-offs – a narrower range than the tail distributions fitted above (Deluca and Corral 2013). Verification of power-law fits were further tested via the use

of strictly truncated power-laws fitted to burst distributions (Deluca and Corral, 2013). These fits were used to identify self-consistent ranges of power-law scaling in areas and durations. The strictly truncated power-law is essentially the Pareto distribution restricted to a finite range of data bounded by lower and upper cutoffs (cf. the Clauset et al., 2009 method that fits the entire tail above a lower cutoff). We estimated cutoffs from the data by examining a 100-by-100 grid of logarithmically spaced ranges. For each candidate range, the strictly truncated power-law was fitted using maximum likelihood estimates, and used to generate 50 synthetic datasets. Following the method of Deluca and Corral (2013), the fitted range that was the widest was chosen (maximizing the ratio of upper and lower cutoffs) that yielded a plausible fit, defined as requiring at least 20% of the synthetic datasets to deviate from the fit by at least as much as the data.

3.3.4 ANALYSIS OF AVERAGE BURST SHAPES

For each epoch of data, all bursts of duration greater than a minimum duration bin (in this case 40 ms) are extracted and further pooled into specific duration lengths. This binning involves analyzing bursts in a hierarchy of time scales, partitioning burst fluctuations into fixed duration bins. In this data cohort, bins were logarithmically spaced with edges at durations of 160 ms, 320 ms, 640 ms, 1.28 s, 2.56 s, and 5.12 s. The first step in calculating average bursts was to interpolate all bursts in each fixed bin to the lowest respective bin edge. For example a burst of duration 178 ms would be resampled and interpolated to have a duration of 160 ms within the duration bin of 160 ms to 320 ms. Using this process, we can assign all bursts into each duration bin (and all other respective bin sizes). This step obtains all bursts during an epoch at their specified duration bin lengths leading to the next step of rescaling and normalization. A key step for this analysis is being able to compare and contrast the change in burst shapes over a range of time scales. Rescaling burst durations to have a unit area and unit duration achieves this goal (Colaiori et al. 2004). We can calculate unit time based on values between start and end points for each burst (Fig. 3.5A). Here, unit time is derived from the ratio of each coordinate of a burst subtracted by the first suprathreshold point (Fig. 3.5A, inset) divided by the difference between the start and end points of a burst. Each burst is then re-interpolated over unit time. The magnitude of these bursts are then rescaled to have unit area (Fig. 3.5B). The process is repeated for all bursts at each duration bin edge. The average shape of the burst is the average of all unit areas over unit time for each duration bin (Fig. 3.5C).

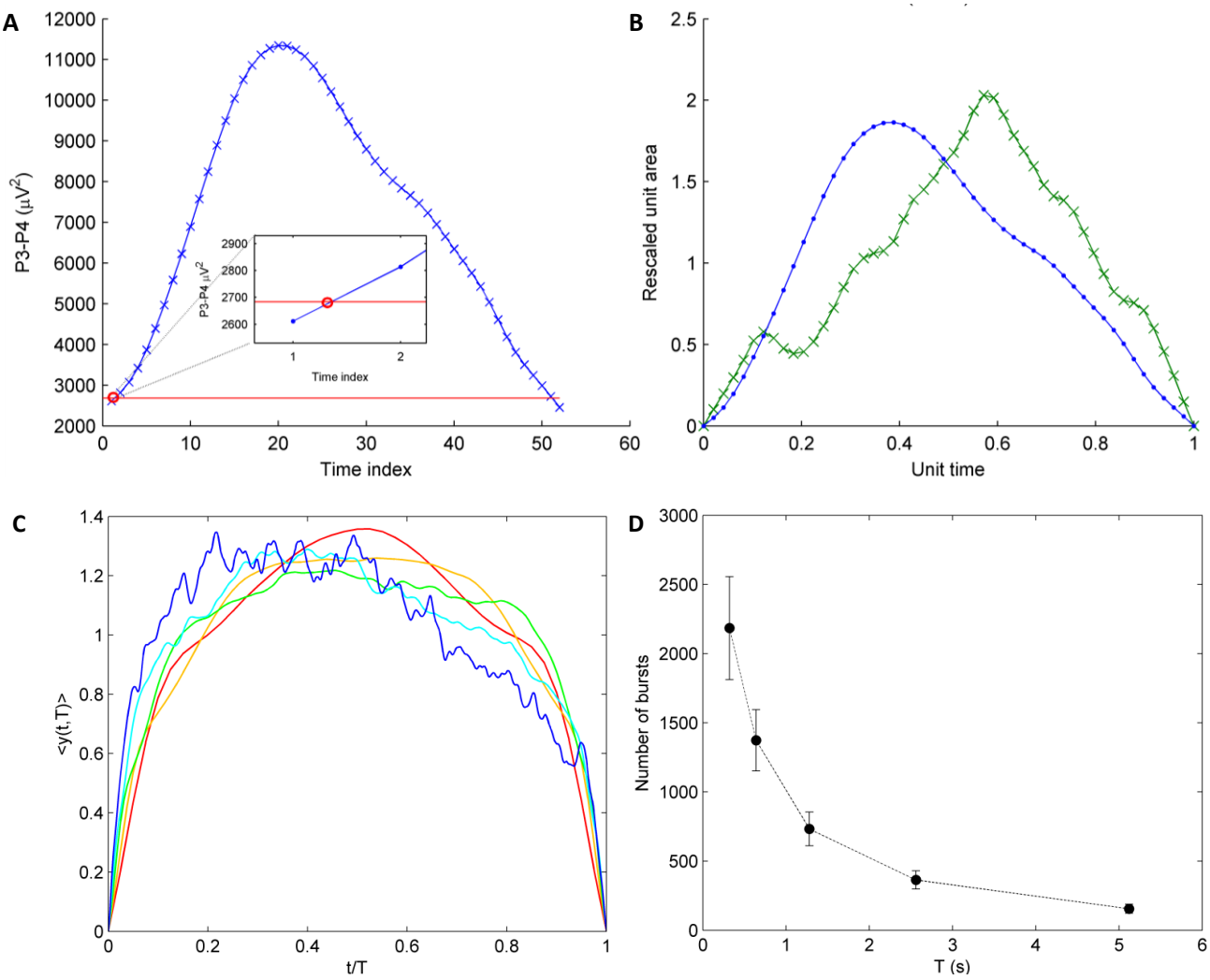

Figure 3.5 – Rescaling bursts to unit time and unit area and the average burst shape. (A) An example burst with supra-threshold points above a threshold. (B) The same burst (blue) rescaled to have unit time and area compared with a burst of different duration (green) with the same data axes. (C) Average burst shape <y(t,T)> during burst suppression across a hierarchy of time scales. Colors correspond to successive durations T (red=160 ms, yellow=320 ms, green=640 ms, cyan=1.28 s, blue=2.56 s). (D) Burst numbers across burst duration bins ±SEM. Here, short duration bins (< 1.28 s) have more bursts than and longer duration bins (> 1.28 s).

3.3.5 QUANTIFIERS OF BURST SHAPE: SKEWNESS AND KURTOSIS

Average burst shapes vary in their symmetry and flattening across time scales. To quantify asymmetry and flattening of the average shapes, estimates of skewness and kurtosis were calculated, respectively, as a function of duration (Eq. 3.1-3.3). This quantification served as an extension of work by Zapperi (2005), where skewness was calculated on the average shape of fluctuations in ferromagnetic material (Barkhausen-noise). Further, these measures are not to be confused with the skewness and kurtosis (i.e., 3rd and 4th standardized moments) of the time series itself.

Skewness Σ is given by

$$\Sigma(T) = \frac{\frac{1}{T}\int_0^T dt\langle y(t,T)\rangle (t-\bar{t})^3}{\left[\frac{1}{T}\int_0^T dt\langle y(t,T)\rangle (t-\bar{t})^2\right]^{3/2}} \tag{3.1}$$

and kurtosis *K* is given by

$$K(T) = \frac{\frac{1}{T}\int_0^T dt\langle y(t,T)\rangle (t-\bar{t})^4}{\left[\frac{1}{T}\int_0^T dt\langle y(t,T)\rangle (t-\bar{t})^2\right]^{2}} - 3 \tag{3.2}$$

where <y(t,T)> denotes the average shape over duration T.

$$\bar{t} = (1/T)\int_0^T dt\langle y(t,T)\rangle t \tag{3.3}$$

The integrals in all equations were evaluated using the trapezoidal rule. The above expressions are the same as those for the theoretical skewness and kurtosis of a probability density function given by <y(t,T)>. Figure 3.6 demonstrates how the average burst shape template (Fig. 3.6A) is quantified by skewness and kurtosis. To estimate skewness (Fig. 3.6B) and kurtosis trends (Fig. 3.6C), average shapes were calculated on a finer partition of durations rather than being used for displaying the average shapes. The linear trends, in this dataset, as a function of duration were estimated by ordinary least squares.

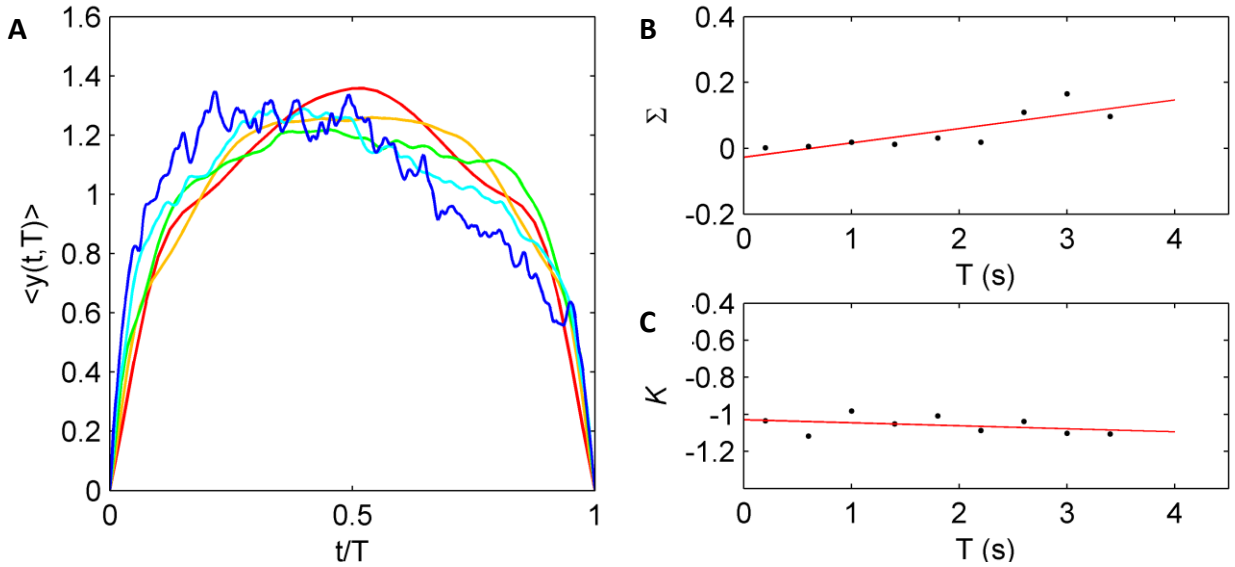

Figure 3.6 – Quantifiers of burst symmetry (skewness, Σ) and sharpness (kurtosis, *K*). (A) Average burst shape example of burst suppression. (B) Trend in skewness (Σ). Finer partition of duration bins indicate that the skewness trend is positive, corresponding to an increasingly leftward asymmetry in average burst shape over burst duration. (C) Kurtosis (*K*) over the same partition of bins remains constant. Lines (in red) are linear least-squares fits.

3.4 RESULTS

EEG epochs in the full-term hypoxic neonate revealed classical temporal sequences of BS (Fig. 3.7). During recovery from asphyxic insult, these neonates typically experienced periods of complete inactivity in which the EEG contains only non-neuronal noise (Fig. 3.7A), followed by burst suppression (Fig. 3.7B, C) before the resumption of continuous activity (Fig. 3.7D). Periods of BS exhibit highly variable electrical bursts erratically punctuating a low amplitude, "suppressed" EEG trace (Fig. 3.7B, C). Whereas the periods of suppression contain low-voltage amplifier noise and non-neuronal artifacts, the bursts reflect intermittent, spontaneous activity in large pools of neurons (Niedermeyer et al., 1999).

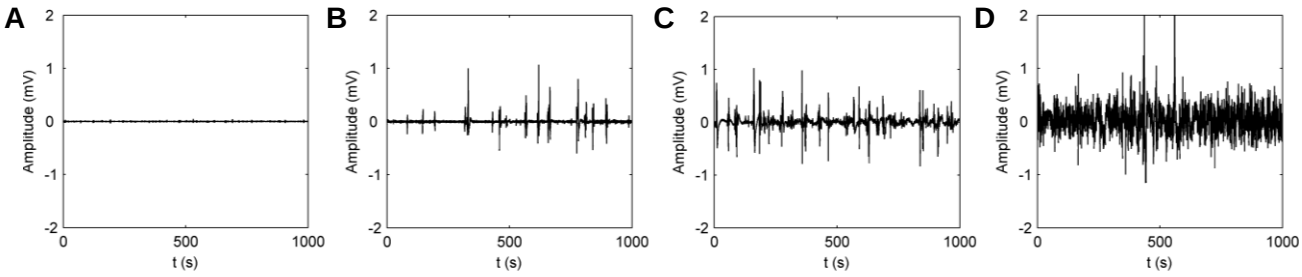

Figure 3.7 – From burst suppression to continuous cortical activity in the asphyxic newborn. (A) Cortical inactivity immediately after birth asphyxia. (B) Sparse occurrences of burst suppression activity. (C) Dense burst suppression activity. (D) Transition toward normal continuous cortical activity.

3.4.1 SCALE-FREE BURSTS FOLLOWING HYPOXIA

The striking self-similarity in burst sizes (3.1D-F) was a feature of 13 neonates with BS in this dataset. Notably, the upper CDF was typically heavy-tailed, with broad power-law scaling regimes spanning between 2 and 5 orders of magnitude before exponential truncation at their far right tails (Appendix A, Section 1). Four infants exhibited a "knee" before the truncation (denoted by asterisks). Burst duration CDFs also follow truncated power laws, albeit over a more restricted 1–2 orders of magnitude (Appendix A, Section 2).

The likelihoods of all four heavy-tailed distributions easily exceeded that of the exponential distribution. Among the heavy-tailed candidates, model likelihood was highest for the exponentially truncated power-law distribution in 12 of 13 recordings (Table 3.2). Using log model evidences, Bayesian model selection confirms the power-law with exponential distribution as the dominant candidate fit (see Fig. 3.8C). In the remaining case, the likelihood of the stretched exponential was marginally higher than the truncated power law, but model comparison showed this difference to not be significant. However, when penalized for extra complexity, the simple power-law distribution was more likely than the truncated power-law in three of the datasets (Table 3.2).

Infant	Power	Power law with cut-		Log-normal		Stretched		Distribution
	p	LLR	*p*	LLR	*p*	LLR	*p*	
1	0	-56.2	$1.89x10^{-5}$	-24.2	$1.6x10^{-6}$	-28.6	$5.0x10^{-7}$	Power law with cut-off
2	0.16	-0.157	0.57	-0.112	0.79	-0.0282	0.97	Power law with cut-off
3	0	-24.3	$3.2x10^{-12}$	-19.5	$6.8x10^{-5}$	-21.6	$3.5 x10^{-5}$	Power law with cut-off
4	0	-31.8	$1.4 x10^{-15}$	-29.4	$5.1x10^{-12}$	-31.9	$1.8x10^{-7}$	Power law with cut-off
5	0.8	$-6.34x10^{-3}$	0.91	-0.746	0.11	-0.207	0.5	Power law with cut-off
6	0.03	-9.05	$2.1x10^{-5}$	-0.183	0.68	1.25	0.49	Power law with cut-off
7	0	-288	0	-201	$2.2x10^{-39}$	-219	$1.2x10^{-42}$	Power law with cut-off
8	0.034	-23.4	$8.2x10^{-12}$	-4.28	0.035	-4.81	0.039	Power law
9	0.6	$-6.48x10^{-3}$	0.91	-0.393	0.18	0.262	0.44	Power law
10	0.028	-18.6	$1.0x10^{-9}$	-3.49	0.049	-3.96	0.048	Power law with cut-off
11	0	-65.9	0	-26.1	$7.8x10^{-7}$	-29.5	$3.8 x10^{-7}$	Power law with cut-off
12	0	-45.7	0	-16.8	$2.7x10^{-5}$	-19.5	$1.4x 10^{-5}$	Power law with cut-off
13	0.035	-15.6	$2.4x10^{-8}$	-6.04	0.016	-6.73	0.014	Power law

Table 3.2 – Model likelihood tests for cumulative distributions of burst size. Negative log-likelihood ratio (LLR) values favour that specific column's distribution compared with a power-law distribution fit; e.g., for subject 1, an LLR of -56.2 favours a power law with exponential cut-off. For the power law column, p-value is for the hypothesis that the power-law distribution is a plausible fit. For the other distribution columns, p-value is for the hypothesis that the corresponding LLR is zero. For subject 4, both power-law with exponential cut-off and stretched exponential are favoured, with the hypothesis test unable to decide between these.

From the burst size CDF fits, scaling exponents for the power-law with exponential cutoff ranged between -2.32 and -1.18 (mean, -1.59; SE, 0.11; 95% CI, -1.38 to -1.81; see Table 3), Exponents for the fitted duration distributions ranged from -3.32 to -1.35 (mean: -1.97; SE, 0.16; 95% CI: -2.28 to -1.66). Plotting probability distributions functions showed similar fitted ranges spanning between 3 orders of magnitude for burst duration and 7 orders of magnitude for burst area (Fig. 3.8A). These fits provide additional support for the existence of power-law distributions in the dataset. Table 3.3 summarizes the scaling exponents and fitted ranges for burst duration and burst size.

Infant	Distribution exponent (BA)	Fitted range of BA (min, max) (mV^2 s)	Distribution exponent (BD)	Fitted range of BD (min, max) (s)	BA vs BD exponent
1	1.29	$3.9 x 10^2$, $3.7 x10^5$	1.35	$3.91 x 10^2$, $1.8 x 10^6$	0.49
2	2.21	$8.5 x 10^3$, $5.5 x10^5$	1.91	$8.5 x 10^3$, $9.1 x 10^5$	0.60
3	1.66	3.6 x 103, $1.1 x 10^5$	1.8	$3.6 x 10^3$, $1.1 x 10^5$	0.61
4	1.18	$1.4 x 10^2$, $1.5 x 10^9$	2.51	$1.4 x 10^2$, $1.5 x 10^9$	0.56
5	2.32	$2.0 x10^5$, $1.0 x10^7$	2.81	$2.0 x 10^5$, $1.0 x 10^7$	0.54
6	1.47	$5.3 x 10^0$, $1.8 x10^6$	1.75	$5.3 x 10^0$, $1.8 x 10^6$	0.56
7	1.32	$2.2 x 10^0$, $2.7x 10^5$	1.62	$2.2 x 10^0$, $2.7 x 10^5$	0.49
8	1.39	$3.6 x 10^2$, $1.0 x10^7$	1.61	$3.6 x 10^2$, $1.0 x 10^7$	0.53
9	2.28	$2.8 x 10^4$, $2.4 x10^6$	3.32	$2.8 x 10^4$, $2.4 x 10^6$	0.54
10	1.43	$3.9 x 10^2$, $2.4 x10^6$	1.8	$3.9 x 10^2$, $2.4 x 10^6$	0.48
11	1.36	$6.4 x 10^0$, $5.0 x10^5$	1.56	$6.4 x 10^0$, $5.0 x 10^5$	0.51
12	1.30	$2.5 x 10^2$, $6.9 x10^6$	1.48	$2.5 x 10^2$, $6.9 x 10^6$	0.51
13	1.53	$1.4 x 10^3$, $3.6 x10^6$	2.10	$1.4 x 1^{0\,3}$, $3.6 x 10^6$	0.52

Table 3.3 - Burst area (BA) CDF exponent estimated from the fit to an exponentially truncated power law. BD, Burst duration.

The relationship between median burst size and burst duration also exhibited a striking power law in all neonates, showing a linear regime in double-logarithmic coordinates that in most cases spanned over 4 orders of magnitude of burst size (see insets, Fig. 3.8 B, D & F and Appendix A, Section 1). Notably, the power-law scaling relationship between size and duration extended to very large scales without truncation in all neonates. The availability of uninterrupted EEG recordings over the first 72 hours after birth asphyxia in this dataset enabled the study of continuous cortical activity patterns (Fig. 3.8D) following the resolution of burst suppression. Here, 10 of 13 neonates successfully transitioned from burst suppression to continuous (CTS) activity. Similar statistical trends in CTS activity were found, such as the model likelihood of truncated power-law distributions. However, the slope of the scaling relationship between burst size and burst duration showed a significant increase following the transition to continuous EEG (Fig. 3.8E, $p=0.017$, $df=9$, $t=3.1$, paired t-test). Hence, power law regimes during continuous activity are heavily truncated which is reflected in the scaling relationships between burst duration and burst area during the resumption of continuous cortical activity. Thus, it is plausible to contend that scale-free activity persists within continuous EEG in a hypoxic newborn (immediately following burst suppression). Figure 3.8 summarizes key observations in this dataset.

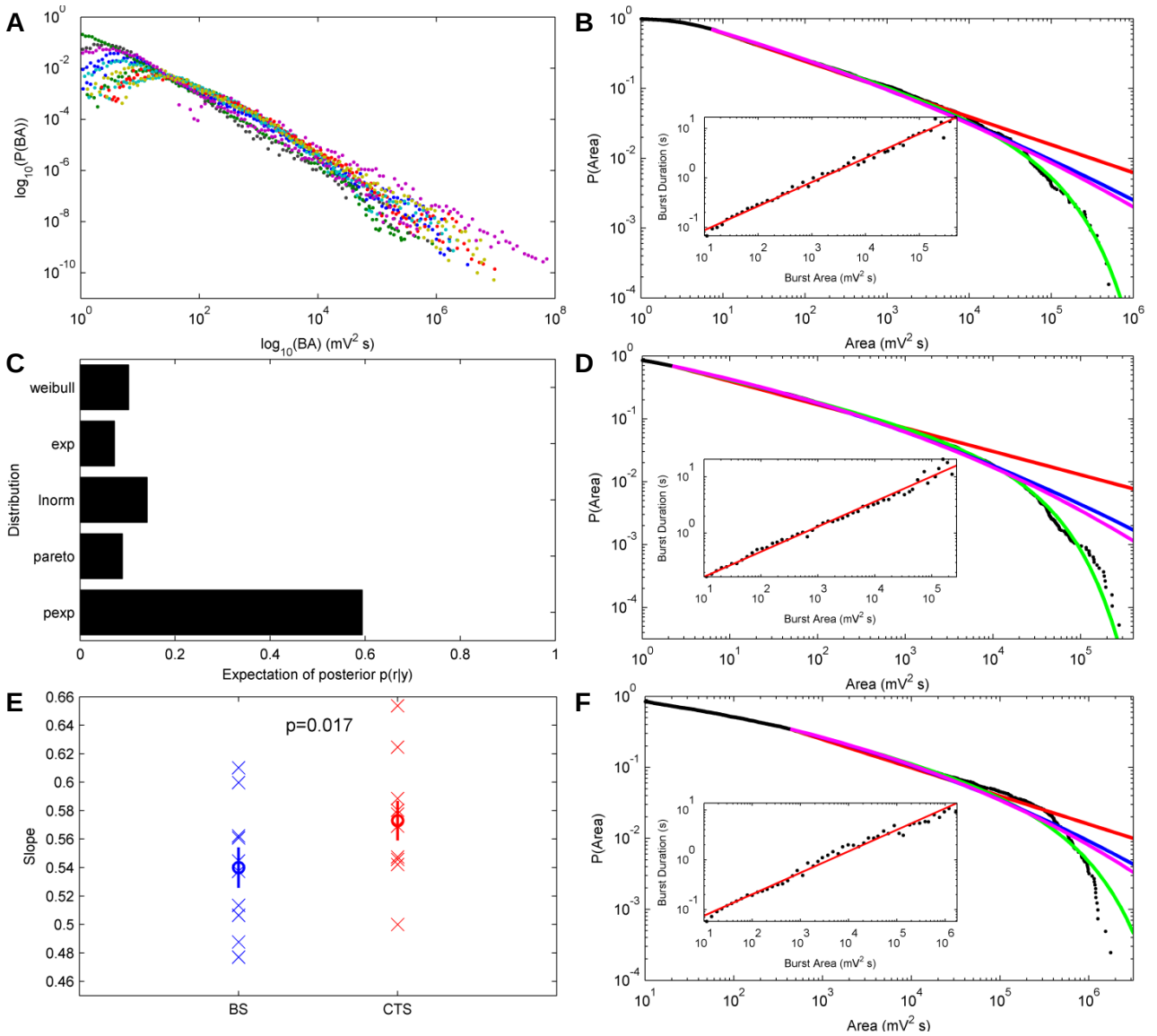

Figure 3.8 - Empirical distributions and scaling relationships in burst suppression data. (A) Overlay of probability distribution functions for all hypoxic neonates showing a predominant right tail. (B), (D), (F) Exemplar upper cumulative distributions of burst area (solid circles) showing lengthy power-law regimes. Solid lines show best-fitting candidate long-tailed distributions: power-law (red), Weibull (blue), log-normal (magenta), and exponentially truncated power-law (green). Insets show scaling relationship between median burst size and burst duration in double-logarithmic coordinates. (C) Bayesian model selection of log-model evidences, where p(*r*|*y*)=0.6 indicates the power-law with exponential cut-off as the dominant candidate fit in this dataset. (E) Scaling relationship between burst area and burst duration for burst suppression (BS, blue) and after the resumption of continuous cortical activity (CTS, red). Crosses denote data points, circles denote means, lines denote ±SEMs.

To ensure robustness of distribution functions, a range of thresholds and filter settings were tested. Significantly, slight changes in threshold value do not have a great effect on later quantitative analyses. For moderate changes in threshold of ±10%, the exponent of the exponentially-truncated power-law revealed a <1% change in exponent for 11 out of 13 infants with BS (20% range in threshold), showing that empirical results were robust to choice of threshold. Of the remaining 2 out 13 infants, the exponent changes by 7% and 20% respectively – in both cases this was due to the threshold falling near a jump in the lower cut-off as determined by the Clauset et al. algorithm. Note that these two cases both exhibit large bursts above the background trend. For large changes in

threshold by a factor of 2, the overall shape of the distributions remains largely unchanged, with only slight effects on the smallest bursts (Fig. 3.9A). Lengthy scaling regimes in particular are insensitive to the particular choice of threshold. Similarly, varying the filter cut-off frequency has little effect on the distributions (Fig. 3.9B). More stringent filtering (lower cut-off frequencies) primarily eliminates the smallest bursts causing no net change to empirical distribution functions (Fig. 3.9B).

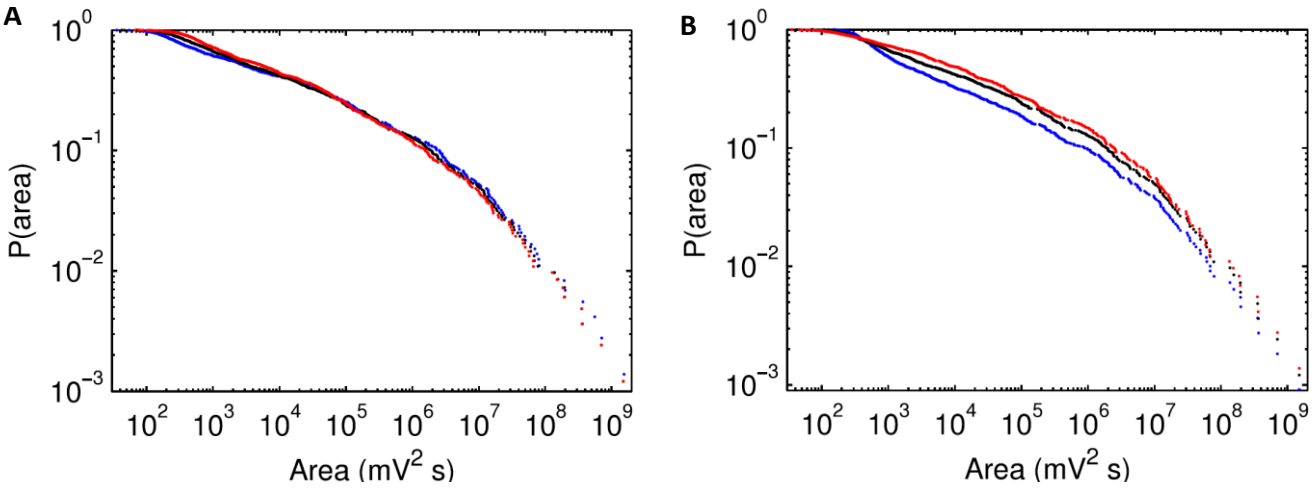

Figure 3.9 - Robustness of burst distributions to variations in thresholds and filter settings. (A) Burst area CDFs for half (blue) and double (red) the chosen threshold (black). (B) Burst area CDFs for smoothing filters with cutoffs at 12 Hz (red), 19 Hz (black), and 37 Hz (blue).

3.4.2 AVERAGE BURST SHAPES IN HYPOXIC INFANTS

Average burst shapes in all burst suppression data showed clear leftward asymmetry, increasing in extent towards longer time scales. The grand average of all 10 neonates with burst suppression shows a symmetrical, inverted parabolic shape at the shortest time scale (0.16-0.32 s) (Fig. 3.10A). Thereafter, at successively longer time scales, the average shapes skew progressively to the left (Fig. 3.10B). In contrast, shape kurtosis was approximately scale-invariant (Fig. 3.10C). At longer time scales the smaller number of bursts results in noisier average burst shape. Using the grand average burst shape, we observe the difference between burst suppression and continuous activity recordings. Inspection of average burst shapes following the resumption of continuous activity (Fig. 3.10D) suggested a marked reduction in leftward asymmetry (Fig. 3.10E) and constant kurtosis trends.

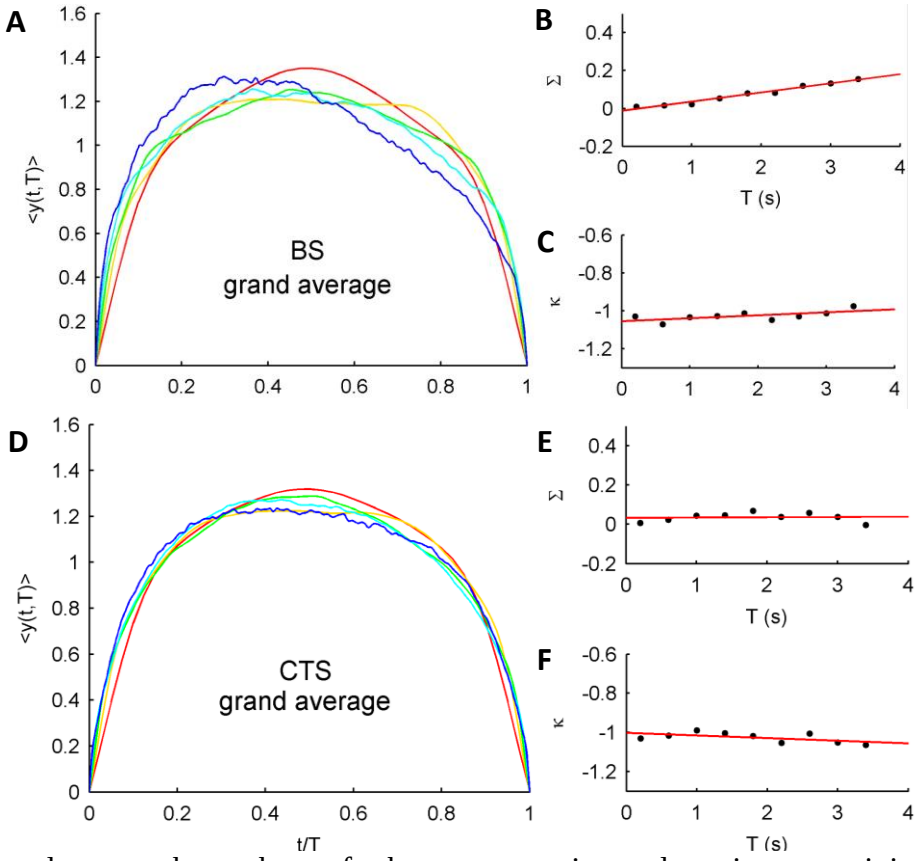

Figure 3.10 – Grand average burst shapes for burst suppression and continuous activity recordings. (A) Average burst shape for burst suppression with (B) skewness increasing in leftward asymmetry and (C) constant kurtosis. (D) Average burst shape for continuous activity patterns converged to a more symmetric burst shape where (E)-(F) skewness and kurtosis remained constant. Color legend for average shapes: red=160 ms, yellow=320 ms, green=640 ms, cyan=1.28 s, blue=2.56 s.

Trends of skewness and kurtosis were calculated from the slope of the linear least-squares fit to skewness (and kurtosis, respectively) versus duration (Table 3.4). This method of fitting was preferred over maximum likelihood estimation methods as the duration bins are clearly bound between 200 ms and 6 s, allowing an simple method of estimation and analysis. Using these slope values, a paired (repeated measures) comparison of this burst shape asymmetry effect in the 10 neonates with burst suppression and continuous EEG, revealed a significant difference in skewness (Fig. 3.11A, $p<0.007$, t=3.37, df=9, paired t-test). Due to the pooling of data – and hence the increase in the number of bursts – the average shapes were smoother in appearance in these grand averages than in shapes derived from individual subjects.

It was further found that the numbers of bursts were comparable in both types of activity patterns and yielded no significant differences at each burst duration bin (Fig. 3.11B). Furthermore, Fig. 3.11B indicates that average burst shapes can be reliably characterized if in a given infant EEG epoch burst numbers have a minimum of 2000 bursts (or a 20 minute recording of EEG).

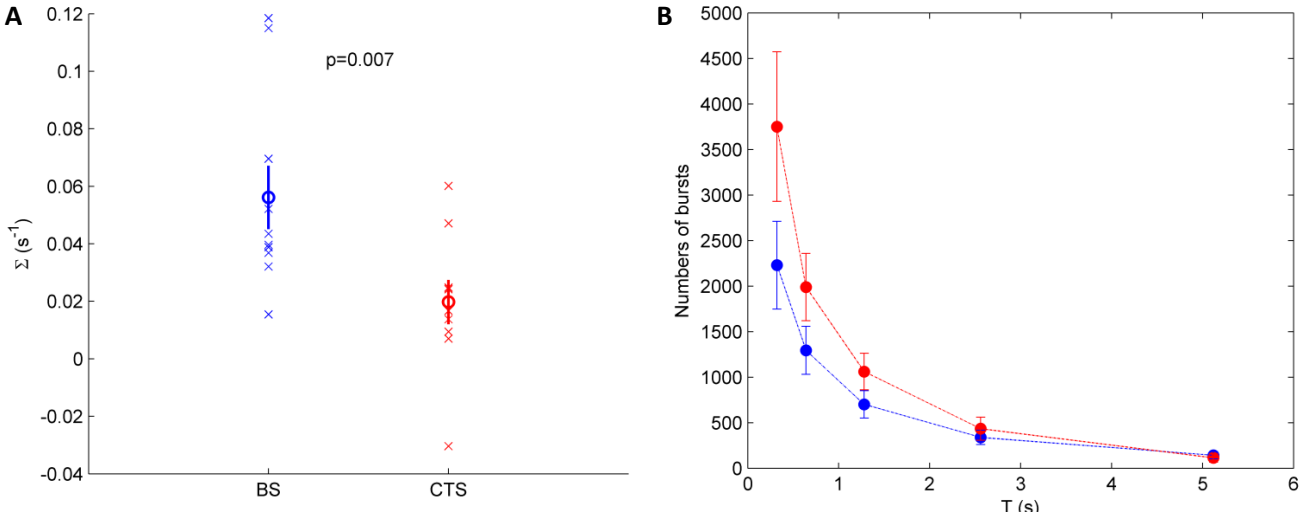

Figure 3.11 – Comparisons of skewness and numbers of bursts in burst suppression (blue) and continuous EEG patterns (red). (A) The slope of skewness (Σ (s^{-1})) is significantly different (p=0.007, df=9, paired t-test) in burst suppression when compared with continuous EEG. (B) Numbers of bursts in both activity patterns have no significant differences (paired t-test) across all burst durations.

Infant	**Skewness slope (Σ(s^{-1}))**	**Kurtosis slope (K(s^{-1}))**
1	0.09	0.03
2	0.04	-0.016
3	0.12	0.06
4	0.015	-0.03
5	0.04	-0.009
6	0.03	0.03
7	0.04	0.024
8	0.006	-0.03
9	0.12	0.12
10	0.05	0.05
11	0.07	0.04
12	0.04	0.03
13	0.05	-0.06

Table 3.4 - Skewness Σ(s^{-1}) and kurtosis K(s^{-1}) slope values calculated by the least-squares fit across burst durations.

3.4.3 Scaling interrelations

In critical systems, the various scaling exponents are often interrelated (Sethna et al., 2001; Friedman et al., 2012). We sought to identify a scaling relationship between the exponents for area distributions (a), duration distributions (d), and the duration versus area exponent (c). Theory predicts that if the distribution of burst areas scales as $\sim s^{-a}$, the distribution of durations scales as $\sim T^{-d}$, and the average size scales with duration as $\sim s(T) \sim T^{1/c}$, then the exponents obey the relationship c=(a-1)/(d-1). To test whether this relationship holds in our data, we estimated the three exponents over self-consistent ranges of the data identified using the Deluca and Corral (2013) method. Specifically, we used the fitted range of areas to identify the corresponding range of durations, then fitted the duration distribution and duration versus area relationship to obtain a set of three exponents for each recording. Beyond exponent interrelations an important feature to test for criticality is the existence of a scaling function that relates the duration versus area exponent to the average burst shape (Sethna et al. 2001, Friedman et al. 2012). In testing this relationship, it is expected that $\langle y(t,T\} \rangle \sim T^{(1/c-1)} F(t/T)$, where $F(t/T)$ is the scaling function describing the average shape independent of scale. In comparing the predicted and measured scaling exponents in statistical distributions of data we find good agreement within the uncertainties of estimates (Fig. 3.12). Specifically, scaling exponents of burst area and burst duration obey the relationship with the duration versus area exponent: c=(a-1)/(d-1). Furthermore, we find that the duration versus area exponents do relate to the average burst shape. The analysis of average burst shapes does reveal heterogeneity in the dataset, where not every recording collapses with this method over the same range of durations. Figure 3.12 summarizes the scaling interrelations found in the data.

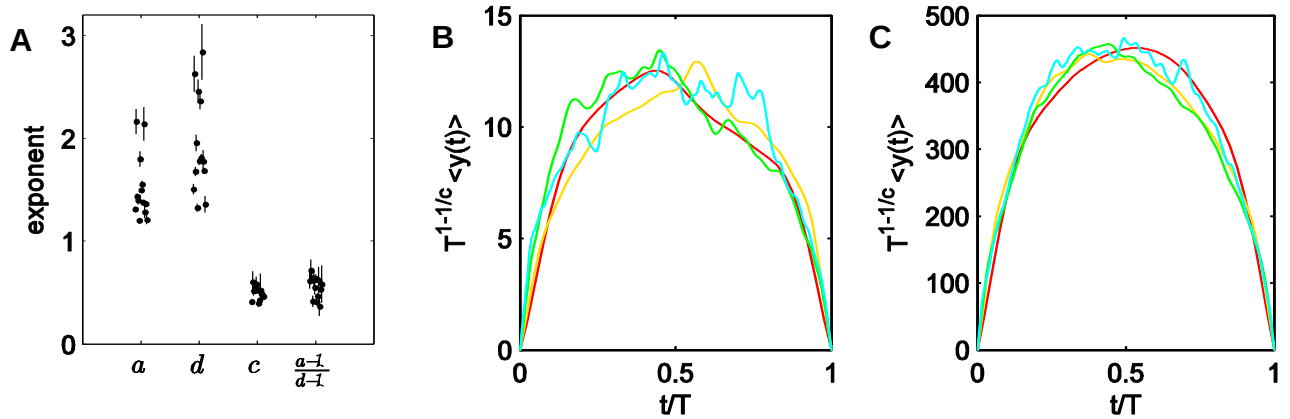

Figure 3.12 - Scaling interrelations. A, Scaling exponents for area (a), duration (d), duration versus area (c), and the predicted relationship (a-1)/(d-1). Uncertainties are 95% confidence intervals derived for a and d from the SD of the maximum likelihood estimator (Deluca and Corral, 2013), for c from the least-squares fit, and for (a-1)/(d-1) by propagating the uncertainties from a and d. Points are plotted with small horizontal offsets for clarity. B, C, Collapse of average shapes after rescaling raw averages by a function of duration and the duration versus area exponent, T 1_1/c, for exemplar burst suppression (BS; B) and continuous (CTS; C) subjects. Colors correspond to those in Figure 9, and we estimated c by fitting over all bursts used in the averages (i.e., 0.16 –2.56 s).

3.5 SIMULATING BURST SUPPRESSION THROUGH STOCHASTIC MODELS

The processes underlying bursting phenomena have been successfully elucidated in numerous physical systems through the use of stochastic models (Colaiori 2008). This thesis extends upon theoretical work in simulating several candidate stochastic models to elucidate the basic mechanisms underlying the average burst shapes in hypoxic EEG data. The changes to burst shape symmetry from burst suppression to continuous EEG activity (Fig. 3.10), suggests that following hypoxia, cortical activity directly reflects a period of metabolic recovery. Thus it is reasonable to assume that following post-hypoxic insult, neuronal metabolites such as extracellular calcium (Amzica 2009; Ching et al. 2012; Volpe 2008), deplete rapidly during the course of a burst and replenish during the subsequent quiescent phase of burst suppression. Here, we describe three models of burst generation and analyze their average shapes. Further, we interpret the mechanisms of burst generation that cause symmetry, flattening and asymmetry over long time scales.

3.5.1 PHENOMENOLOGICAL MODELS OF BURST GENERATION

In simple phenomenological models, the activity of the cortex is summarized by a single scalar term, *x*, which is subject to random fluctuations. The simplest continuous stochastic process models fluctuations in *x* that are subject to uncorrelated random perturbations, given by

$$\dot{x} = \xi, \tag{3.4}$$

where ξ is an uncorrelated zero-mean Gaussian process (the "Wiener process"). Equation (3.4) models a perfectly-balanced critical process, where the probability of incremental growth of a burst equals the probability of incremental decay. While Eq. (3.4) has traditionally been used to study the motion of particles subject to random perturbations — that is, Brownian motion — in the present setting, the value of *x* corresponds to the voltage measured at the scalp, and the fluctuations represent the sum total of excitatory and inhibitory influences at any given moment. Such a critical process is consistent with a balance of excitatory and inhibitory processes in underlying cortex (Shu et al. 2003). Sample solutions of this stochastic model were generated by numerical integration using the Heun algorithm (Rümelin 1982). Analysis of the displacement squared of these sample walks recapitulated the well-known result (Colaiori 2008) that fluctuations generated by a Brownian walk exhibit a power-law distribution in size (Fig. 3.13A). These distributions are truncated at the far right tail in our simulations by an upper bound imposed by the finite sample length.

While this simple random walk captures the power-law scaling seen in our data, none of the empirical burst suppression recordings showed scale-invariant burst shapes. Hence a more complex

phenomenological model was considered. In the following model the Brownian walk generalizes to an Ornstein–Uhlenbeck (mean-reverting) process through the introduction of a linear restoring force,

$$\dot{x} = -\lambda x + \xi\,, \tag{3.5}$$

where λ is a constant. The addition of a small, negative restoring force corresponds to a weakly damped, near-critical system, and is a classic model for the motion of a particle within a harmonic potential of concavity λ. In the present setting, this term embodies a weak constant bias towards greater inhibition than excitation within neuronal populations, albeit not of sufficient strength to prevent the triggering of burst activity. This damping term leads to an exponential truncation of the right-hand tail of the fluctuation size distribution (Fig. 3.13B),

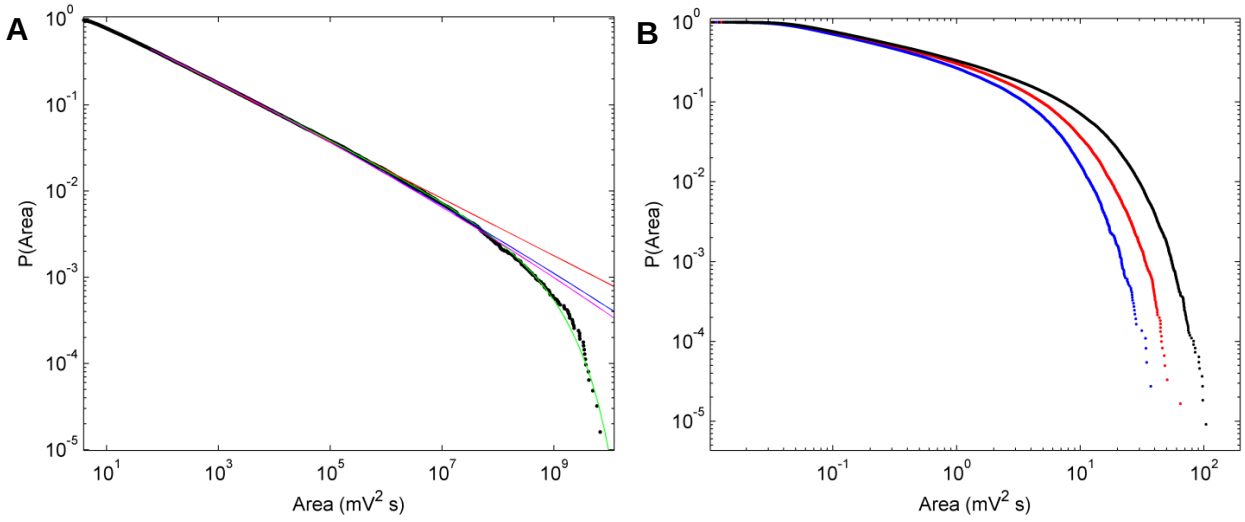

Figure 3.13 – Cumulative distribution functions of burst areas in stochastic models. (A) Upper CDF arising in a Wiener process. (B) Effect of sample damping values λ (black=0.05, red=0.075, blue=0.1) on the upper cumulative distributions of burst area

Neuronal resource depletion is also implicated in mechanisms of self-limiting disinhibited activity (Staley et al. 1998; Tabak et al. 2006). If history-dependent effects increase the inhibitory bias, it could be captured by modifying the damping term λ to vary according to recent burst activity. We thus modified the damping term to depend upon the recent energy expended by the system,

$$\lambda(t) = \alpha_2 \int_{-\infty}^{t} e^{-\alpha_1 (t-\tau)} x(\tau)^2 \, d\tau\,, \tag{3.6}$$

This history-dependent damping term has an exponentially-decaying memory with time constant α_1 and thus relaxes back to zero in the absence of bursting activity. Equation (3.6) can be re-cast as a first-order differential equation,

$$\lambda(t) = -\alpha_1 \lambda + \alpha_2 x^2, \tag{3.7}$$

to be coupled with Eq. (3.7). The time scale constant α_2 determines how quickly burst energy, x^2, drives up the damping, whereas α_1 captures the relaxation of the damping back to zero during suppression.

3.5.2 AVERAGE BURST SHAPES OF STOCHASTIC MODELS

From Eq. (3.4) average shape fluctuations in the model converged at all scales towards a single scaling function, namely an inverted parabola (Fig. 3.14A), without skewing (Fig. 3.14B) or flattening (Fig. 3.14C). Average burst shapes simulated through Eq. (2), exhibited flattening at successively longer time scales (Fig. 3.14F). However, bursts at all scales remain symmetric (Fig. 3.14E). Using Eq. (2) and (4), setting $\alpha_1 = 0.1$ and $\alpha_2 = 30$, quantitatively recaptures the trend of positive skewness at longer time scales observed in burst suppression data (Fig. 3.14H). Fluctuations arising from this process show leftward asymmetry, increasing at longer time scales (Fig. 3.14G) which is consistent with a fast-out/slow-return effect of activity-dependent damping.

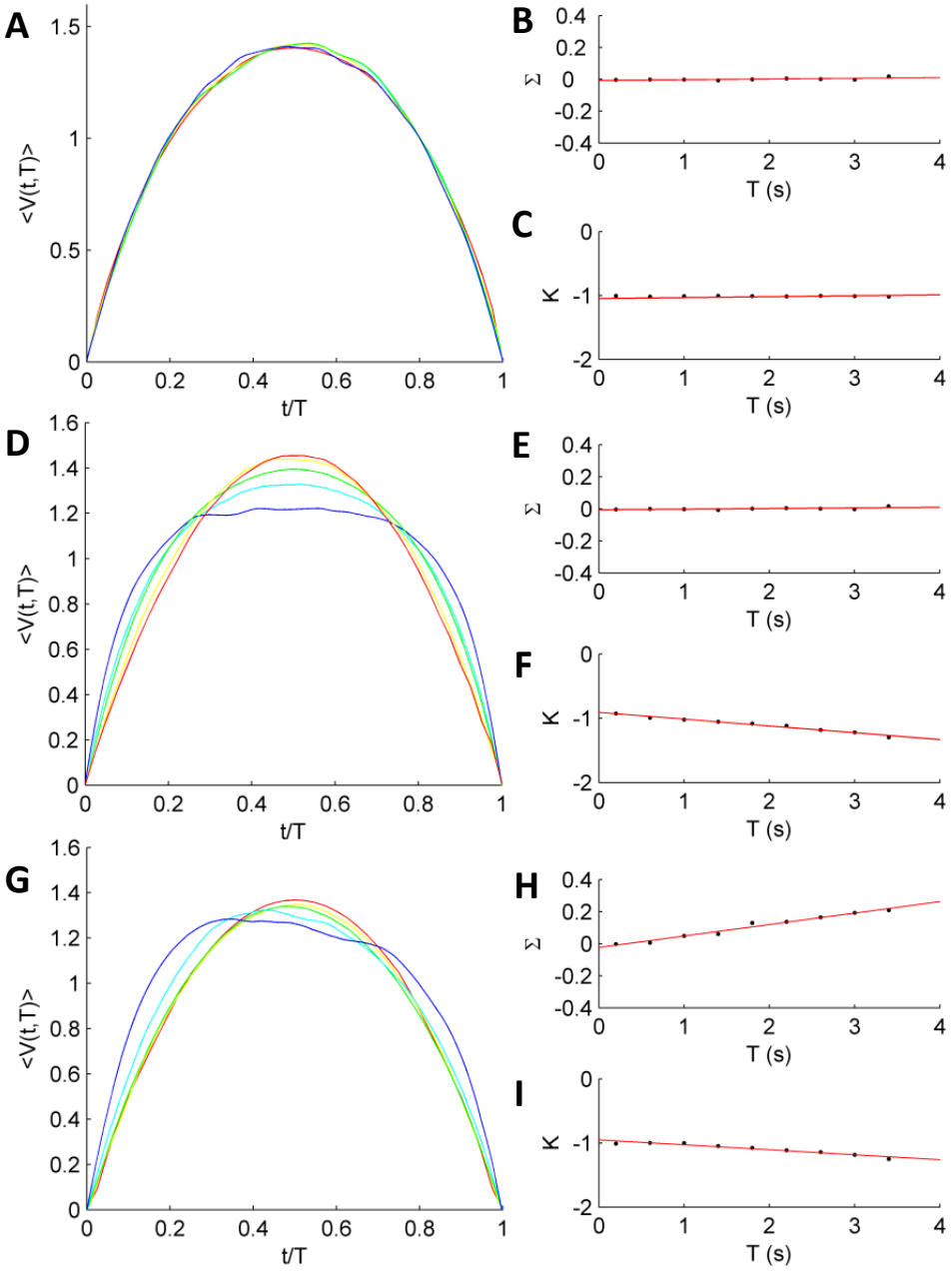

Figure 3.14 - Model average shapes of bursts and their skewness and kurtosis. (A)-(C) Symmetrical average burst shape given by model of Eq. (1). (D)–(F) Symmetrical but successively flattened shapes given by model of Eq. (2). (G)–(I) Leftward asymmetric shapes without flattening given by model of Eq. (2) and Eq. (3). Colors correspond to successive durations T (red=160 ms, yellow=320 ms, green=640 ms, cyan=1.28 s, blue=2.56 s). Simulations used a time step of 0.04 ms, with ξ having SD 0.1 (in the same arbitrary units as x), and initial conditions x(0)=0 and $\lambda(0)=0$.

3.6 DISCUSSION

In this chapter we characterize burst suppression in thirteen hypoxic neonates, using statistics of burst durations and their sizes, and analyze their empirical distribution functions following asphyxic insult. Furthermore, the average shapes of cortical bursts in ten neonates whom resolved to continuous EEG were processed and calculated. The symmetry and sharpness of these shapes over a range of burst durations were also derived. The method employed to study these bursts are objective, data driven and robust to filtering settings and insensitive to minor changes in chosen threshold values. The results in this cohort of full-term hypoxic neonates suggest that features of critical systems commonly found in nature are present in burst suppression patterns. Moreover, average burst shapes reveal scale specific effects across time scales. Here, these features of bursts demonstrate the transitions involved in critical systems as they undergo a transition from burst suppression to continuous activity patterns.

3.6.1 SCALE-FREE DISTRIBUTIONS IN THE HYPOXIC NEONATE

Using a dataset of thirteen term hypoxic neonates it was found that epochs of burst suppression are typically scale-free with broad power-law regimes up to five orders of magnitude. These power-laws are typically truncated by an exponential cut-off, a hallmark of natural systems where energy and size is bounded. The match between empirical and theoretical distribution functions provides significant evidence of scale-free mechanisms present early in the term hypoxic brain. Moreover, the relationship between median burst size and burst duration is strikingly linear in logarithmic coordinates, suggesting a robust scaling relationship. This slope value generally increased upon resumption of continuous patterns of cortical activity.

Whilst reports of scale-free statistics in complex systems have become quite frequent, power-law regimes in data and close theoretical matches to power-law models are relatively uncommon in nature (Stumpf and Porter 2012). In our results, the scaling exponent range in the data coupled with the range in which these power-laws extend over is characteristic of a system displaying criticality. We here posit that burst activity arising from a state of complete quiescence to a pathological activity pattern such as burst suppression indicate a system at a critical balance – a key feature of avalanche type behavior (Bak et al. 1987). Moreover, in a few cases, scale-free distributions had a characteristic "knee" suggesting a slightly supercritical system indicative of fluctuations that are larger and more numerous than the background trend. We validate the presence of a critical system by using the Deluca and Corral (2013) method of exponent interrelations. Here, exponentially truncated power-law scaling exponents are related to the slope of the relationship between burst duration and burst size. Thus, the interrelation of exponents satisfies the hypothesis that the hypoxic neonate brain operates near criticality.

Empirical distributions observed in this dataset also carry significance regarding the hypothesis of excitation or inhibition imbalances present in the full-term hypoxic brain. Following deprivation of oxygen, we can further postulate that patterns such as burst suppression reflect a system that is constrained by a slow build-up of energy and fast energy dissipation when a critical point is reached, resulting in a transient burst. The study of neuronal avalanches in cultured tissues (Beggs and Plenz 2003; Friedman et al. 2012) suggests that crackling noise is highly likely to arise in systems in which excitation and dissipation are tightly coupled. These studies, along with the analyses presented offer further insight into a neonate that is metabolically constrained resulting in a pathologically abnormal burst suppression pattern.

3.6.2 MECHANISMS OF BURST SUPPRESSION VIA AVERAGE BURST SHAPES

The findings in ten term hypoxic neonates whom progressed to continuous activity indicate that in epochs of burst suppression, average burst shapes are typically asymmetric, with a pronounced trend in leftward skew as burst duration increased. On the other hand, continuous activity bursts tend to have a more symmetric form independent of burst duration, indicative of a more scale invariant distribution. Theoretical simulations of stochastic models enable a deeper interpretation of possible effects of energy expenditure in an asphyxiated cortex. The use of these models along with the quantification of symmetry and sharpness, suggest that neurophysiological mechanisms such as state-dependent metabolic depletion and excitation, inhibition imbalances strongly influence patterns such as burst suppression.

As demonstrated, properties of scale-free bursts vary across recovery periods where empirical distribution functions have long power-law regimes during the burst-suppression phase, exhibiting stronger truncation upon the resumption of healthy activity. Here, limitations of simple probability fits and estimation of scaling exponents overlook the change in dynamic mechanisms which drive burst generation and overall burst morphology. The use of average burst shapes serves as a means to differentiate between abnormal patterns such as burst suppression from continuous activity. This is a critical extension of fitting probability functions to empirical data particularly since multiple models can exhibit the same exponents whilst having different mechanisms and avalanche shapes (Sethna et al. 2001). Further, average burst shapes reveal a clear difference in symmetry and sharpness trends during burst suppression when compared with continuous activity, a type of pattern which is inherently linked with the recovery of the hypoxic neonate. This dynamic transition in burst shape builds upon prior use of average shapes in physical systems, where subtleties of scaling laws in critical systems are further explicated (Friedman et al. 2012; Papanikolaou et al. 2011; Zapperi et al. 2005). Average burst shapes thus provide stronger, more robust evidence of scale-free dynamics, leading to hypotheses for the fundamental reorganization of neuronal activity under metabolic resource constraints.

The manipulation of a simple stochastic model exhibiting criticality through perfect scale invariance, to a model exhibiting state-dependant effects, is a valuable means to postulate neurobiological mechanisms which are involved in the reorganization of neuronal activity. Extending upon Zapperi's (2005) ferromagnetic experiments, asymmetry in average burst shape in hypoxic neonates may arise from activity-dependant damping – a feature captured by a fast acceleration with a slow return. Further, the strength of damping in the stochastic model correlates with burst suppression data where this term determines the bias towards inhibition rather than excitation. A constant damping term is indicative of a subcritical process. In the presence of dynamic state dependent damping effects, however, burst fluctuations continue to propagate which contributes to the notion that history-dependent effects arising through metabolic depletion leads to feedback via an inhibitory bias loop. These stochastic models hence provide a understanding of burst phenomenology and potential neurophysiological effects involved following perinatal asphyxia.

The evidence for criticality in an abnormal neuropathology such as burst suppression provides a new avenue for understanding how healthy brain states are optimized during recovery. In a highly complex system like the brain, we can contend that there may be a number of distinct critical points which occur in both healthy states and neurological disorders – a reflection of energy replenishment, e.g. metabolic, or brain maturation. For example, it may be plausible that the neonate brain undergoes a critical transition early in the burst suppression period, during which cortical silent periods evolve towards sparse cortical bursting patterns. Whether this is a mechanism of optimized energy transfer (Kinouchi and Copelli 2006) or representative of balanced brain states (Shew et al. 2011) requires further investigation. Scale-free exponents and average shapes analyses provide a theoretical basis for genuine critical phase transition upon recovery, leading to fully continuous EEG. In this regard, the study of critical behaviour in the brain and its link to pathogenic mechanisms would likely provide new insights into cellular and synaptic determinants supporting the emergence of dynamics that meet criteria for criticality (Massobrio et al. 2015). Though we can only speculate the idea of multiple critical points, further data analyses at these points of recovery (fully continuous EEG) are required in conjunction with a unified computational model to understand the parameters of criticality and its associated neurobiological mechanisms.

Recent neurobiological studies in animals, both *in vitro* and *in vivo*, have focused on how oxygen availability, and its deprivation, affect metabolism in the mammalian cortex (Herculano-Houzel 2011; Ivanov and Zilberter 2011; Zilberter et al. 2010). These studies experimentally observed the acute imbalances towards inhibition arising from energy expenditure of ATP and glucose levels. As a cascade of biochemical processes are involved during and after perinatal asphyxiation, there is evidence to suggest that compensatory mechanisms are primarily involved in driving feedback

loops. For example, reduced cerebral blood flow results in release of inhibitory neurotransmitter GABA, leading to loss of cellular integrity, metabolic imbalance and consequent neuronal death (Lagercrantz et al. 2010; Lauritzen et al. 2012; Morley 2005). As described in Chapter 2, the pathophysiological mechanisms involved in hypoxic-ischemic injury evolve through primary damage (reconciled here via metabolic imbalances) and secondary neuronal damage, which typically occurs in the following 72 hours post-hypoxia. This form of damage predisposes a hypoxic infant to poor neurodevelopmental outcomes limiting overall recovery towards continuous cortical activity. In this analysis, burst shapes reveal an important neurophysiological insight into subcritical processes (leftward skewed burst shapes; metabolic depletion arising from initial hypoxic insult) and critical scale invariance (symmetric shape collapse; recovery to continuous EEG). The presence of supercritical bursts (truncated powerlaw with a knee) in a few infants with burst suppression indicates a system that is not perfectly able to regulate bursting activity throughout the cortex and may provide clues into the extent of hypoxic insult.

Hence, the study of state-dependent changes in burst shapes in this dataset provides deeper insight into the scale-free statistical distributions found in burst suppression data. From these findings we can assert that transitions in burst symmetry and sharpness across increasing burst durations in the neonatal brain are seemingly affected by resource constraints to metabolic nutrients.

3.6.3 GENERAL CONCLUSIONS

The analyses presented in this chapter hence diverges from studies in the field, demonstrating that inherently stochastic processes present in burst suppression yield scale-free processes in which robust metrics can be calculated and validated. The use of such methods is strengthened further by calculating burst statistics present in electroencephalographic data and fitting these statistical distributions to theoretical heavy-tailed models.

An important aspect of this analysis method was the estimation of scaling parameters and validation of model likelihood. Empirical methods, such as quantitative assessments of burst suppression (Brandon Westover et al. 2013; Löfhede et al. 2008; Löfhede et al. 2010), focus on segmentation of epoch windows and human-computer classification of activity patterns. These methods steer away from statistical characterization and distribution functions, focusing more on a methodologically driven heuristic. As noted by Clauset et al. (2009), method driven heuristics along with correlative analyses (which employ least square fits and data regressions) often miscalculate the scaling parameters present in heavy-tailed distributions (Clauset et al. 2009). In this analysis using a maximum likelihood estimate offers a much more stringent test of data cut-offs - in terms of minimum and maximum data ranges – providing a closer approximation of data distribution parameters. Further testing for model likelihood against theoretical candidate distributions enables

better validation of underlying statistical distributions. This is confirmed in this dataset as model likelihood overwhelmingly confirms the significance of a power-law with exponentially truncated regime.

This analysis has hence established a new paradigm in which neonatal burst suppression, and indeed analysis of cortical activity is effectively characterized. The empirical distribution functions present in single stream epochs of EEG data yield closer approximations of bursting activity hours after birth asphyxia. The current findings suggest a novel means of monitoring recovery from neonatal term hypoxia in the clinical setting, while also yielding key quantitative predictions of system balance and/or imbalance. Further understanding the mechanisms of burst suppression could be tested with combined neurophysiological and metabolic recordings in a nonclinical, experimental setting.

The method of average burst shapes provides an objective test for analyzing the burst content in a single stream EEG epoch. Typically, the study of burst suppression has focused on background changes associated with large, slow amplitude excursions and long suppressed periods. In particular, the utility of suppression periods to guide clinical classification has provided some indication of clinical outcome, yet realistically provides limited understanding into cortical mechanisms and neurobiological processes at play (Amzica 2009; Grigg-Damberger et al. 1989; E Niedermeyer et al. 1999). This chapter has presented an alternative hypothesis that bursts yield important features of neuronal damage caused by perinatal asphyxia. The heterogeneity in burst durations in hypoxic neonates has been further characterized by the change in burst shape – a significant step towards understanding the mechanisms involved in metabolic depletion.

The focus of the remaining chapters is the application of methods described in this chapter and the use of scaling parameters in empirical distributions to predict clinical outcome. These outcomes range from acute complications within the first week of life or long-term neurodevelopmental disabilities. The combination of these novel methods henceforth provides a robust and reliable metric for the analysis of electroencephalographic recordings in the clinical setting.

4.0 NOVEL FEATURES OF BURST SUPPRESSION PREDICT OUTCOME

ABSTRACT

Burst suppression patterns in the neonatal electroencephalogram are a reliable marker of recent severe brain insult. The introduction of hypothermia treatment in neonates with burst suppression has compromised the utility for outcome prediction and clear prognostic markers. In this study, we utilize methods from the previous chapter to study the application of statistical characterization of bursts in predicting clinical outcome in full-term hypoxic neonates. Specifically, we extract the scaling exponents of statistical distribution functions in twenty electroencephalographic recordings acquired from hypothermic asphyxic newborns in the hours immediately following birth. Distributions of burst area and duration are benchmarked with conventional analyses of inter-bursts and the coefficient of variation in burst durations. Significantly, statistical characterization is possible from analyzing neonate burst suppression hours after birth. These measures are hence temporally precedent to later outcomes, i.e. brain imaging (MRI) findings and clinical outcomes at two years of age. The findings in this chapter indicate the first early electroencephalographic metrics that offer outcome prediction in asphyxic neonates undergoing hypothermia treatment.

4.1 INTRODUCTION

Hypoxic ischemic encephalopathy following perinatal asphyxia is the leading cause of acquired, severe neurodevelopmental disability (Bonifacio et al. 2011). The neurodevelopmental outcome of HIE depends on how quickly neuronal function recovers from the asphyxic insult. Continuous electroencephalography (EEG) monitoring has become a widely accepted practice in neonatal intensive care units (NICUs) (Hellström-Westas and Rosén 2006; Nash et al. 2011; van Rooij et al. 2005). A key EEG hallmark of severely injured brain function is a pattern of low amplitude (suppressed) EEG punctuated by irregular high amplitude bursts (Fig. 1A) known as burst suppression (BS) (Holmes et al. 1982). Several studies have shown that the resolution of BS in EEG recordings within 6-12 hours of birth correlates strongly with a favorable neurodevelopmental outcome (Toet et al. 1999; van Rooij et al. 2005). Identification of BS and its recovery time in asphyxic newborns has thus been used as a prognostic indicator of brain function to guide therapeutic decisions. While clinical decisions to commence therapeutic hypothermia after birth asphyxia are often based on observing BS in the early EEG, hypothermia treatment itself was recently found to significantly delay BS recovery, hence compromising the utility of early EEG in outcome prediction (Hallberg et al. 2010; Kessler et al. 2011; Thoresen et al. 2010).

Neurophysiological interpretation of BS conventionally rests upon a dichotomous presence-versus-absence classification. While qualitative assessment of "burst sparseness" – a low overall frequency of bursts – may be taken as an additional sign of severity (Walsh et al. 2011), no properties of the bursts themselves have been shown to provide useful prognostic indicators. In this chapter, we test the hypothesis that the scale-free bursts of burst suppression patterns do contain predictive properties towards eventual neurodevelopmental outcome. Exploiting the advances in complex systems analysis (Beggs and Plenz 2003; Friedman et al. 2012; Sethna et al. 2001; Spasojević et al. 1996), we sought to characterize statistical properties of BS under hypothermia, in particular features related to burst duration and area (i.e., burst size). Features identified in this study demonstrate that the bursts of BS carry novel, clinically-important information not provided by current brain monitoring paradigms or evident by visual inspection of EEG alone. These findings provide a novel approach for predicting outcome, based on identifying information embedded in BS activity early after brain injury, a task that has proven thus far elusive.

4.2 MATERIALS AND METHODS

This dataset continues the study of hypoxic term neonates from Chapter 3, extending the dataset to include more infants and outcome information derived at 2 years of age. Recordings of twenty consecutively-admitted newborns were collated (gestational age 39±2 weeks) monitored due to HIE following perinatal asphyxia at the tertiary level NICU of Helsinki University Central Hospital. HIE was assessed according to conventional criteria (Sarnat and Sarnat 1976), including lethargy, stupor, or coma, with one or more findings of hypotonia, abnormal reflexes or clinical seizures. As per the data in Chapter 2, the EEG was acquired from biparietal electrodes at 250 Hz using a NicOne or Olympic EEG device (Cardinal Healthcare, Nicolet Biomedical, Madison, WI, USA and Natus Medical, CA, USA). Lengthy epochs of BS that were relatively artifact-free (120±90 minutes, range 30-600 minutes) were subject to the same filtering settings as the previous analyses. BS was determined visually as an EEG pattern consisting of activity bursts (mixture of sharp, slow waves) periodically interrupted by multiple episodes of suppressed cortical activity (approximately <10 IV). Although BS somewhat resembles trace alternant and trace discontinue activity patterns, these are distinct phenomena. First, they are part of the pseudo-periodic vigilance state cycling that is absent early after asphyxia (Hellström-Westas and Rosén 2006; Thoresen et al. 2010). Second, they only occur in younger preterm babies (trace discontinue), or their suppression period is insufficiently suppressed for classification as BS (trace alternant). Cooling onset preceded EEG recordings in all babies (see Appendix B, Section 1: Outcomes Table).

Clinical data collated from patient reports included: reports from MRI scans during the first week after birth; birth details; NICU drug treatments; and outcome description from the last visit to routine neonatal outpatient clinic (age 12-39 months). Patients were divided into two categories based on MRI findings (presence/absence of a thalamic lesion), and further into four categories based on clinical outcomes: normal versus mildly, moderately, and severely abnormal (see Appendix B, Section 1: Outcomes Table for full details). Four of the twenty available neonatal data were excluded from further analyses due to the presence of excessive seizure activity (n=1), early administration of sedative drugs that likely affected BS (n=1), or missing reliable clinical or MRI information (n=2). The use of patient data for this study was approved by the Ethics Committee of the Hospital for Children and Adolescents, Helsinki University Central Hospital.

To extract statistical properties of the bursts, we utilize methods established in Chapter 3, as summarized by Figure 4.1. We extract three burst metrics for each infant: i) conventional measures of mean burst duration (BD) and its coefficient of variation (CV), ii) scaling exponent (α) of the cumulative distribution function (CDF) of the burst areas (BA) in each recording (Fig 4.1E) and iii) slope value based on the relationship between BD and BA (Fig 4.1F). Here, the scaling exponent (

α) captures how quickly the number of bursts diminishes as a function of increasing area: A large exponent (α >> 1.5) indicates that most bursts are very small in area, whereas the converse (α ~ 1.5) indicates that larger bursts occur relatively more often. Since the distribution closely follows a truncated power law, there is no single characteristic size but rather a broad "scale-free" regime, limited only by finite brain capacity.

These novel metrics focus on properties of bursts, specifically the heterogeneity of BAs, as well as the relationship between BAs and BDs. In addition, we benchmarked these novel measures against those established in prior research, namely the mean and CV of interburst interval (IBI) durations, (Grigg-Damberger et al. 1989). The IBI was automatically derived from points below burst threshold, where durations less than 40 ms and greater than 8 s were excluded from analysis. The slope values from BA vs. BD plots and BA CDF plots were extracted as described in Fig. 4.1E and Fig 4.1F. Notably, the analysis algorithms did rely on visual EEG interpretation nor clinical data measures, resulting in a purely data driven approach.

Group comparisons were conducted using one-way analysis of variance (ANOVA) and verified with non-parametric Mann-Whitney U tests. Correlations of clinical outcomes to EEG metrics were measured using Spearman’s rank correlation coefficient.

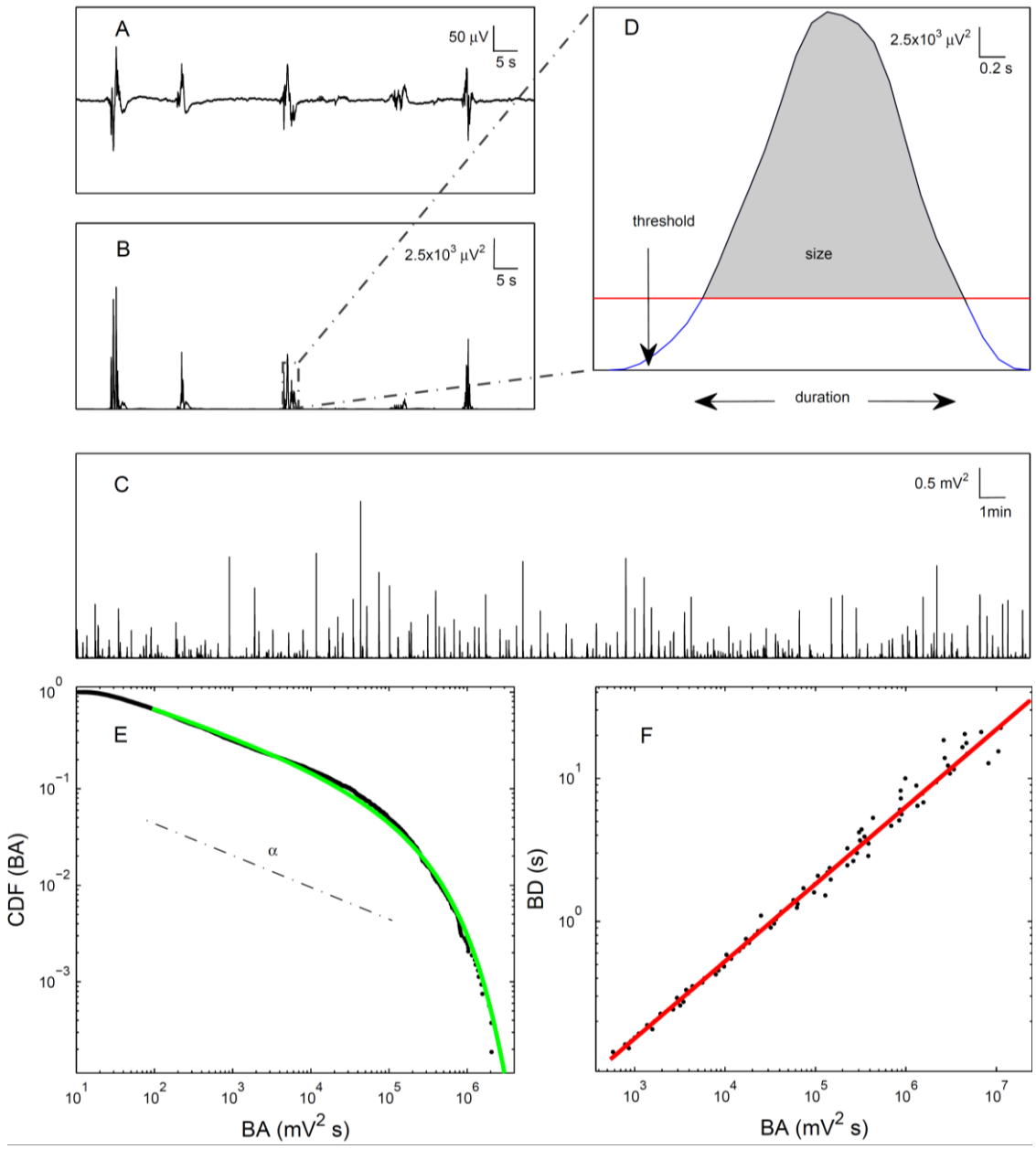

Figure 4.1 – Extraction of burst suppression metrics. (A) Example EEG epoch with burst suppression pattern (P3-P4 derivation). (B) Instantaneous power (amplitude-squared) of the same EEG epoch obtained from the amplitude envelope (via Hilbert transform). (C) Instantaneous power over 80 minutes of a recording to illustrate the variability in the size of bursts over time. (D) Sample burst taken from graph B to illustrate the burst measures. The automated threshold was used for defining the burst area (BA) and the burst duration (BD). (E): Upper cumulative distribution function (CDF) of BA in one infant shows that it follows an exponentially-truncated power law distribution (fit shown in green) over several orders of magnitude. We extracted the scaling exponent (α) of the distribution. Here the dashed line illustrates the corresponding α for the BA as given by the CDF. (F) Relationship between BAs and BDs in one infant, plotted in double logarithmic coordinates. Points are median durations and median areas calculated after dividing the data into 250 quantiles, with the robust linear relationship quantified by the slope of the linear least-squares fit (red line).

4.3 RESULTS

Visual inspection of bursts occurring during post-asphyxic EEG characteristically showed erratic and irregular fluctuations of BS in the amplitude trace (Fig. 4.1A), as well as the corresponding power trace (Fig. 4.1B-C). We hence examined the variability of BA by plotting its CDF (Fig. 4.1E) and the relationship between BA and BD (Fig. 4.1F). We first observed that the CDFs of BA show a robust, power-law relationship over several orders of magnitude (Fig. 4.1E). We also observed a robust linear scaling relationship between log-log coordinates of BA and BD over four orders of magnitude (Fig. 4.1F). Comparison with subsequent MRI findings (Fig. 4.2A and Fig. 4.2B) showed that α was significantly higher ($F_{1, 16} = 5.39$, $p=0.035$; Fig. 4.2A), and the slope between BAs versus BDs was significantly higher ($F_{1, 16} = 7.89$, $p=0.013$; Fig 4.2B) in babies with thalamic lesions. Moreover, both of these metrics showed a significant correlation to neurodevelopmental outcome ($r=0.81$, $p<0.0001$, and $r=0.58$, $p=0.022$, respectively; Fig. 4.2C and 4.2D). Visual comparison of different outcome groups shows considerable variability over time and between records, due to both temporal evolution of BS patterns and physical factors (e.g. subcutaneous swelling). Two extreme cases (normal MRI and outcome versus abnormal MRI and outcome) are shown in Appendix B, Section 2: Supplemental Materials, emphasizing the need for objective, statistically-sound methods for their interpretation.

We then benchmarked these findings against conventional measures of bursts (BDs, BD CVs), and their intervals (IBIs). Statistical analyses revealed that BD CV was significantly higher ($F_{1, 16} = 4.92$, $p=0.042$) in babies with thalamic lesions compared to those with normal MRI findings. However, no difference was found in the mean duration of bursts ($F_{1, 16} = 0.17$, $p=0.68$) or the mean IBIs ($F_{1, 16} = 0.05$, $p=0.81$). In addition, BD CV showed a positive correlation to the developmental outcome ($r=0.37$, $p=0.17$; Fig 4.2E). No correlation was seen between mean burst duration and any measure of IBIs. Additionally, no significant correlations between average burst shapes, i.e. skewness, kurtosis measures were observed in thalamic lesion MRI and neurodevelopmental outcomes.

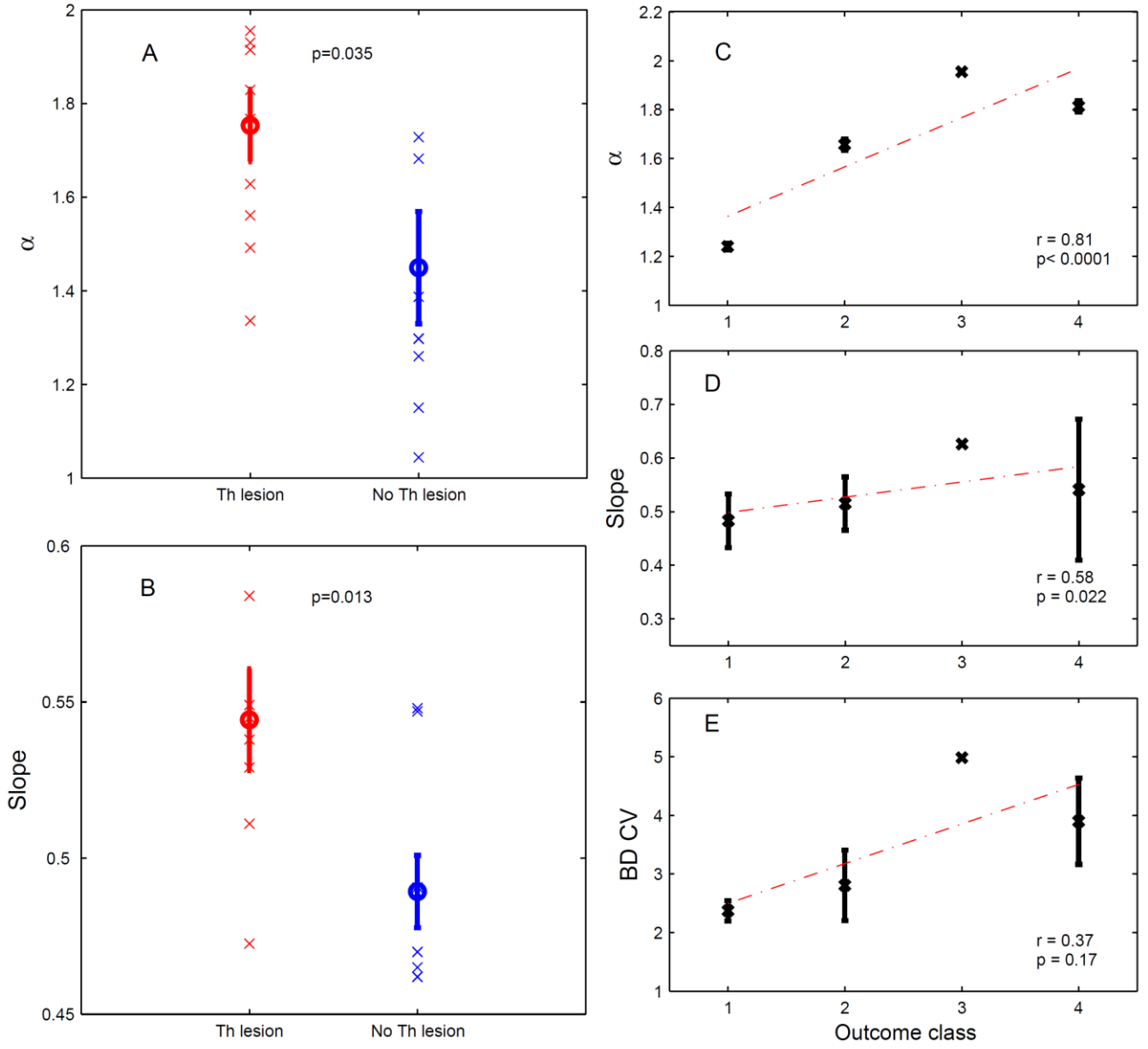

Figure 4.2 - Comparison of burst suppression metrics during first hours after birth to subsequent MRI changes observed several days later. Infants who developed thalamic lesion (Th lesion) apparent in MRI had significantly higher exponents α (A) in the BAs, and a significantly higher slope values (B) in the relationship between BA and BD. The graphs show mean±SEM (circles and lines) and the individual data points (crosses). (C) to (E): Comparison of burst suppression metrics during first hours after birth to clinical outcome categories later in infancy (1=normal; 2=mildly abnormal; 3=moderately abnormal; 4=severely abnormal; see also Appendix B, Section 2: Supplemental Materials). There was a statistically significant correlation between clinical outcome and (C) scaling exponent, α (D) slope and a positive correlation in (E) BD CV. Significant differences were found when dividing outcomes into two categories, good (1&2) and poor (3&4).

4.4 DISCUSSION

This study demonstrates that novel burst statistics derived objectively from EEG, soon after perinatal asphyxia, correlate significantly with MRI findings obtained only several days later, as well as with neurodevelopmental outcomes obtained at two years of age. Utilizing methods described in Chapter 3, we extract measures of burst areas and durations, and their slope relationship, to predict outcome using clinically collated records in cooled asphyxic newborns. We further confirm that traditional measures of mean burst durations and IBIs in hypothermic newborns have insufficient prognostic reliability (Hallberg et al. 2010; Thoresen et al. 2010). The results of this study yield important metrics based on the statistical characterization of bursts during burst suppression. These observations have both theoretical and practical implications.

Theoretically, the presence of robust scale-free statistics is compatible with the notion that a severely compromised brain operates in a critical balance between excitation and inhibition. While such properties of cortical dynamics cannot be assessed using traditional EEG measures, they are rapidly extracted with novel and robust mathematical tools recently developed in computational neuroscience and physics (Papanikolaou et al. 2011; Sethna et al. 2001; Shew et al. 2009) Pragmatically, extracting clinically-informative statistics from a very large number of bursts engenders such metrics insensitive to common noise-related confounders. Moreover, the observations presented in this study significantly challenge the clinical practice of perceiving BS as a uniform entity (Walsh et al. 2011). Rather, these findings are compatible with the alternative notion that functional brain recovery is already ongoing during burst suppression. Thus, in this study we can assess the statistical characteristics of cortical bursts rather than relying on traditionally measured lengths of inactive (IBI) periods.

Importantly, future analyses should consider the integration of scale-free statistics with other measures of hypoxic neonate EEG, such as background abnormality or suppression time. A recent method such as adaptive segmentation in continuous recordings of neonate EEG via IBI extraction has shown high classification accuracy, particularly in the presence of artifacts and seizures (Matic et al. 2014). Whilst a limitation of such analyses is the reliance on laborious visual qualitative assessment and classification of epochs, this analysis allows a clinical comparison with abnormality linked with brain maturation. Significantly, scale-free statistics provide an objective characterization of burst activity in EEG via rigorous tests of model likelihood, distinguishing those epochs that have clinically informative statistics (as evidenced in this chapter). Thus, the calculation of scale-free exponents in conjunction with classification of IBI periods may provide complimentary information regarding hypoxic EEG outcomes and could be integrated through computational machine learning approaches.

Practically, these measures present several clinical advantages. First, because they focus on the bursts only, they avoid a need for uninterrupted recordings. Hence, these measures are robust to intermittent artifacts present in the electrically-noisy NICU environment and challenge traditional analyses of EEG monitoring. Second, the EEG-derived measures provide outcome predictions 4-7 days earlier than MRI findings, possibly enabling early guidance of individually-targeted therapeutic decisions. Third, the analysis paradigm is adaptive and data-driven, reducing inter-individual variability in the overall level of EEG amplitudes caused by technical variations (e.g., inter-electrode distance, constant artifact, or subcutaneous swelling). Amplitude variance caused by artifacts is a serious confounder prevalent in many existing approaches, particularly amplitude-integrated EEG (aEEG, a.k.a. Cerebral Function Monitor (CFM) (Hellström-Westas et al. 2003)). Here, the data-driven algorithm employs burst detection via an adaptive threshold, where scaling properties reported were reliable over a range of thresholds (see Appendix B, Section 2: Supplemental materials). Notably, the EEG measures introduced here are designed for rapid automated prognostication, and thus could be readily implemented as software features in currently-used brain monitoring systems.

While the findings presented in this chapter are encouraging, the dataset studied has limitations, such as a limited sample size and outcome classifications that were retrospectively extracted from clinical archives instead of prospectively-collected standardized neurodevelopmental tests. Significantly, EEG remains the most rapid and continuous real-time monitor of brain function and is hence heavily relied upon by neurophysiologists and neonatal staff. As highlighted in this study, EEG is temporally precedent to brain imaging techniques such as an MRI, where indications of poor outcomes were able to be identified in analysing EEG bursts several days earlier than the MRI based findings. However, it has been it has been highlighted recently that the potential use of more portable imaging modalities such as near infrared spectroscopy (NIRS) and ultrasound with EEG is an important consideration in an diagnostic setting (Sood et al. 2015). Whilst the clinical efficacy is yet to be established the promise of recent studies into oxygen utilization has shown that NIRS and EEG have some level of correlation with brain vulnerability (Tataranno et al. 2015). Further prospective trials in the NICU could benefit from the integration of scale-free methods in parallel with multiple imaging modalities, such as NIRS techniques to monitor critical recovery periods. Future studies on larger patient series with standardized outcome measures are needed to validate the present observations. It will also be important to examine the clinical potential of these measures in differential diagnoses of BS etiologies (e.g., asphyxia, trauma, sedative drugs), a common diagnostic challenge in acute patient care. Finally, it is likely that these same statistical properties of BS are also found in adult neurointensive care, expanding the clinical utility of the metrics employed.

5.0 CORTICAL BURSTS PREDICT LONG-TERM OUTCOME IN PRETERM INFANTS

ABSTRACT

Intermittent bursts of electrical activity are a ubiquitous signature of very early brain activity. Previous studies have largely focused on assessing the amplitudes of these transient cortical bursts or the intervals between them. Recent advances in basic neuroscience have identified the presence of scale-free "avalanche" processes in bursting patterns of cortical activity in other clinical contexts. Here, we hypothesize that cortical bursts in human preterm infants also exhibit scale-free properties, providing new insights into the nature, temporal evolution, and prognostic value of spontaneous brain activity in the days immediately following preterm birth. We examined electroencephalographic (EEG) recordings from 43 extremely preterm infants (gestational age 22-28 weeks) and demonstrated that their cortical bursts exhibit scale-free properties as early as 12 hours after birth. The scaling relationships of cortical bursts correlate significantly with later mental development - particularly within the first 12 hours of life. These findings show that early preterm brain activity is characterized by scale-free dynamics which carry developmental significance, hence offering novel means for rapid and early clinical prediction of neurodevelopmental outcomes**.**

5.1 INTRODUCTION

Early brain development depends upon spontaneously occurring, intermittent electrical activity (Blankenship and Feller 2009; Colonnese and Khazipov 2012; Kilb et al. 2011) that supports neuronal survival and sustains primary growth of brain networks. This electrical activity is highly sensitive to various endogenous and exogenous disturbances, creating clinical challenges in the acute care of preterm infants. Despite advances in neonatal intensive care units (NICU), early preterm birth is still associated with a high risk of adverse neurodevelopment (Aarnoudse-Moens et al. 2009; Back and Miller 2014; Van Baar et al. 2005). A major endeavor in neonatal care is to complement cardiorespiratory support with intensive brain monitoring, a rapidly emerging clinical benchmark. Thus, the goal of continuous preterm brain monitoring is to identify early markers of cortical disturbance which could then guide appropriate clinical interventions.

As described in Chapter 2, the analysis of continuous EEG recordings in preterm infants is challenging due to data interruptions and artifacts from NICU environments (Schumacher et al. 2011; Wikström et al. 2012). The presence of amplifier noise in the NICU is a common issue that arises as a "continuous nonrepetitive artifact" (Walls-Esquivel et al. 2007) during EEG recordings. Existing amplifiers are not immune to mains interference (50 Hz) or higher frequency harmonics (100 Hz, 200 Hz), particularly in a NICU environment where numerous medical devices are routinely used (e.g. incubators, electric syringes, catheters). Consequently, the dominant approach for aEEG/EEG assessment remains a qualitative, subjective appraisal which is vulnerable to confounders arising from technical artifacts and inter-rater variability. Background activity from aEEG/EEG in the first 72 hours has predictive value but requires expert selection of epochs to distinguish artifacts from abnormal cortical activity (Wikström et al. 2012). Recent quantitative analyses of cortical bursting (Palmu et al. 2010; Stevenson et al. 2014) in preterm EEG carries potential for objective, real-time prognostication (Benders et al. 2014; Wikström et al. 2012). Robust characterization and outcome prediction based on the properties of these bursting patterns has proven difficult due to a number of factors, namely the acute presentation in the first few days of life (Smith et al. 2011), the relative shortness of uninterrupted, artifact-free EEG (Olischar et al. 2004), the role of brain activity cycling (Kidokoro et al. 2010; Palmu et al. 2013) and, crucially, the lack of an analytic framework that speaks to the nature of the burst dynamics. Hence, there is an unmet challenge to derive cortical activity signatures of early brain function that are robust, objective, and based on firm statistical evidence.

In this chapter we hypothesize that the preterm brain is also governed by scale-free processes that can be measured using robust statistical metrics. Further, we hypothesize that such properties in early brain activity reflect likely outcome and provide insight into underlying brain development

processes. We thus test the value of characterizing scale-free behavior in preterm infants across gestational ages in predicting long-term outcome, highlighting critical periods immediately after birth

5.2 MATERIALS AND METHODS

Following on from predicting clinical outcome in HIE infants from the statistical distributions of bursts, we apply methods utilized in Chapter 3 to predict long-term outcome from discontinuous bursts of EEG in extremely preterm neonates.

5.2.1 DATA COHORT AND CLINICAL DETAILS

We analyzed EEG recordings of 43 preterm neonates (gestational age (GA) 22-28 weeks) that were monitored in the neonatal intensive care unit (NICU) at Lund University Hospital, Sweden. Other details of this cohort have been previously published (Wikström et al., 2012, Stevenson et al., 2014). Infants were included in the study after informed parental consent. The study was approved by the Regional Ethics Committee at Lund University. The demographics of the cohort and basic details of the data are summarized in Table 5.1. The EEG was acquired from surface EEG electrodes at a sampling rate of 256 Hz using a NicOne amplifier (Cardinal Healthcare, Madison, WI, USA). These data were acquired from the parietal (P3, P4) channels in all babies, and additionally from the frontal (F3, F4) in half of the neonates. However, we focused only on the biparietal P3-P4 derivation and selected relatively artifact-free EEG epochs (average epoch duration of 115 minutes, range 70-120 minutes) at four postnatal ages: 12, 24, 48 and 72 hours. These relatively artifact-free epochs were selected via visual inspection on the basis of two criteria: 1) the presence of an uninterrupted recording of data and 2) the absence of excessive (high amplitude) or prolonged (tens of seconds) artifacts during NICU monitoring. No artifact correction was performed on these data. Each recording was exported to MATLAB (Mathworks, Natick, MA, USA), bandpass filtered (0.2-20 Hz)

All infants underwent standardized neurodevelopmental testing at 2 years corrected age with the Bayley scales of infant development and toddler development, version II (BSID-II). The BSID-II provides developmental scores for cognition (Mental Development Index, MDI) and motor skills (Psychomotor Development Index, PDI). In addition, two dichotomous outcome groupings were used, D1: a composite outcome classification (good versus poor) was created from observing one or more of the adverse outcomes (MDI<70, PDI<70, cerebral palsy, blindness, deafness, or death); and D2: infants considered optimal versus suboptimal based on a cut-off MDI score of 85. This cut-off score is minus 1 standard deviation from a mean MDI of 100.

		Value	Range (min, max)		Unit
Clinical details					
Subjects		43			*n*
Sex, male/female		20/23			*n*
Gestational Age (mean)		25	22	28	weeks
Birth Weight (mean)		820	460	1340	grams
SGA[a]		10			*n*
5 min Apgar score (mean)		7	2	10	
IVH[b] grade 1-2		8			*n*
grade 3-4		5			*n*
Antenatal steroids		all			
Morphine[c]		27			*n*
EEG information					
Recording duration (mean)		69	62	80	hours
Epochs (*n)* at postnatal hours:	*12*	24			*n*
Duration (mean):		119	115	120	minutes
	24	35			*n*
		117	90	120	minutes
	48	39			*n*
		118	90	120	minutes
	72	25			*n*
		112	70	120	minutes
Burst count per epoch		2376	195	4402[d]	*n*
Clinical outcomes					
MDI (mean)		87	50	118	
PDI (mean)		85	50	121	
D1[e,] good/poor		25/18			*n*
D2[e], optimal/suboptimal		21/15			*n*
Died < 2 years		7			*n*

Table 5.1 - Demographics of the preterm dataset with EEG recording information and clinical outcomes. [a] Small for gestational age, defined as birth weight less than 2 standard deviations below the mean for an infant's gestational age, [b] Intraventricular Hemorrhage (IVH) in the first 72 hours after birth, [c] Morphine received within the first 72 hours after birth. [d] No statistically significant relationship between burst count and postnatal hours (p<0.096). [e] D1 refers to composite outcome classification created from observing one or more of the adverse outcomes (MDI<70, PDI<70, cerebral palsy, blindness, deafness, or death); D2 refers to infants considered optimal versus suboptimal based on a cut-off MDI score of 85.

5.2.2 PRE-PROCESSING AND ANALYSIS

Bursts were extracted from all available recordings and their statistical properties were characterized using the pipeline shown in Figure 5.1. Drawing from methods in chapter 3, we quantify two aspects of burst morphology: First, the distribution of burst durations and burst areas are quantified across a wide spectrum of scales, yielding insights into putative scaling properties of early brain function; Second, the average shape of bursts at different time-scales are estimated, which speaks to their underlying dynamical mechanisms (Papanikolaou et al. 2011). To study

scaling relationships present between burst durations and burst areas, we also estimate their linear regression in log-log coordinates (see Figure 5.2D), yielding a regression slope (*S*). Second, the average shape of bursts at different time-scales are estimated, which speaks to their underlying dynamical mechanisms (Papanikolaou et al., 2011, Roberts et al., 2014a). Average burst shapes are quantified by the change in symmetry (Σ) and sharpness (*K*) across burst durations from 200 ms up to 6 s in length.These features of burst duration, area, and shape permit rapid, automated analyses of burst statistics from EEG epochs acquired at each postnatal age across gestational ages which we then correlate against clinical outcome indices. Statistical comparisons were conducted via general linear model fitting (GLM) and one-way analysis of variance (ANOVA). The GLM yields Pearson correlation coefficients (R) of burst statistics against continuous variables (i.e., GA in days; MDI and PDI scores between 50-120), and dichotomic outcome variables (0=good outcome, 1=poor outcome).

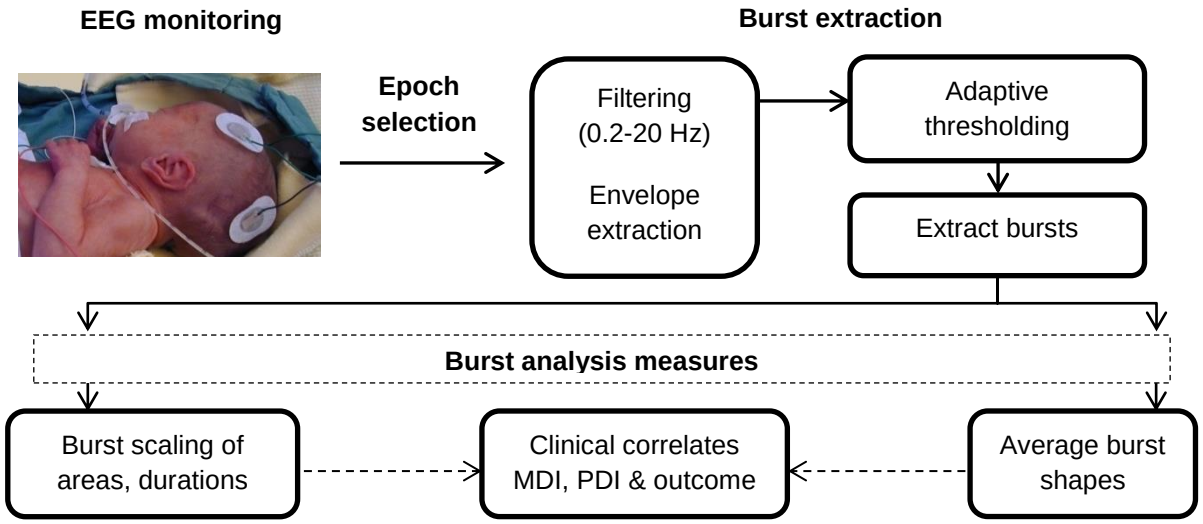

Figure 5.1 - Schematic of cortical burst analysis procedure for preterm EEG recordings.

5.3 RESULTS

Visual inspection of bursts occurring in the EEG of these extremely preterm infants characteristically showed discontinuous, bursting EEG activity at 12 and 72 hours after birth (Fig. 5.2A-B). We first studied burst scaling as captured in the upper cumulative distributions (CDFs) of burst areas (Fig. 5.2C), and the relationship between burst area and burst duration (Fig. 5.2D).

5.3.1 SCALE-FREE BURSTS HOURS AFTER PRETERM BIRTH

Burst areas and burst durations clearly revealed scale-free relationships present across nearly three orders of magnitude. At 12 hours, the upper CDF (Fig. 5.2C) is closely described by an exponentially truncated power law, while the corresponding scaling relationship of burst areas with durations (Fig. 5.2D) exhibited a linear regime in double-logarithmic coordinates. To formally test the validity of scale-free behavior in our data, we examined the empirical shapes of burst area CDFs against four theoretical distributions: power law (pareto), power law with exponential cutoff, log-normal, and exponential (Clauset et al., 2009). We assessed the candidate fits for the data using log model evidence and Bayesian Model Selection (Stephan et al., 2009). This test indicates that the exponentially truncated power law is clearly the best description of the scaling process present in our data (Fig. 5.2E). We also examined the average burst shape at sequential timescales (Fig. 5.2F), observing changes in burst symmetry (a measure of burst skewness, Fig. 5.2G), and sharpness (a measure of burst kurtosis, Fig. 5.2H). A summary of scaling regimes found robust presence of power-law regimes indicative of scale-free processes (Appendix C, Section 1: Statistical distribution summary in preterm EEG data).

Exponent interrelations of the slope of burst size and burst duration (c) were compared with the predicted relationship that indicates a system exhibiting critical features, namely c=a-1/d-1. Whilst there is a reasonable approximation, close inspection suggests a small nut noticeable difference in these sets of values (see Fig. 5.3). Statistical testing shows that the values do differ ($p<0.01$). These relationships hence approximate but do not statistically satisfy these analytic conditions for criticality.

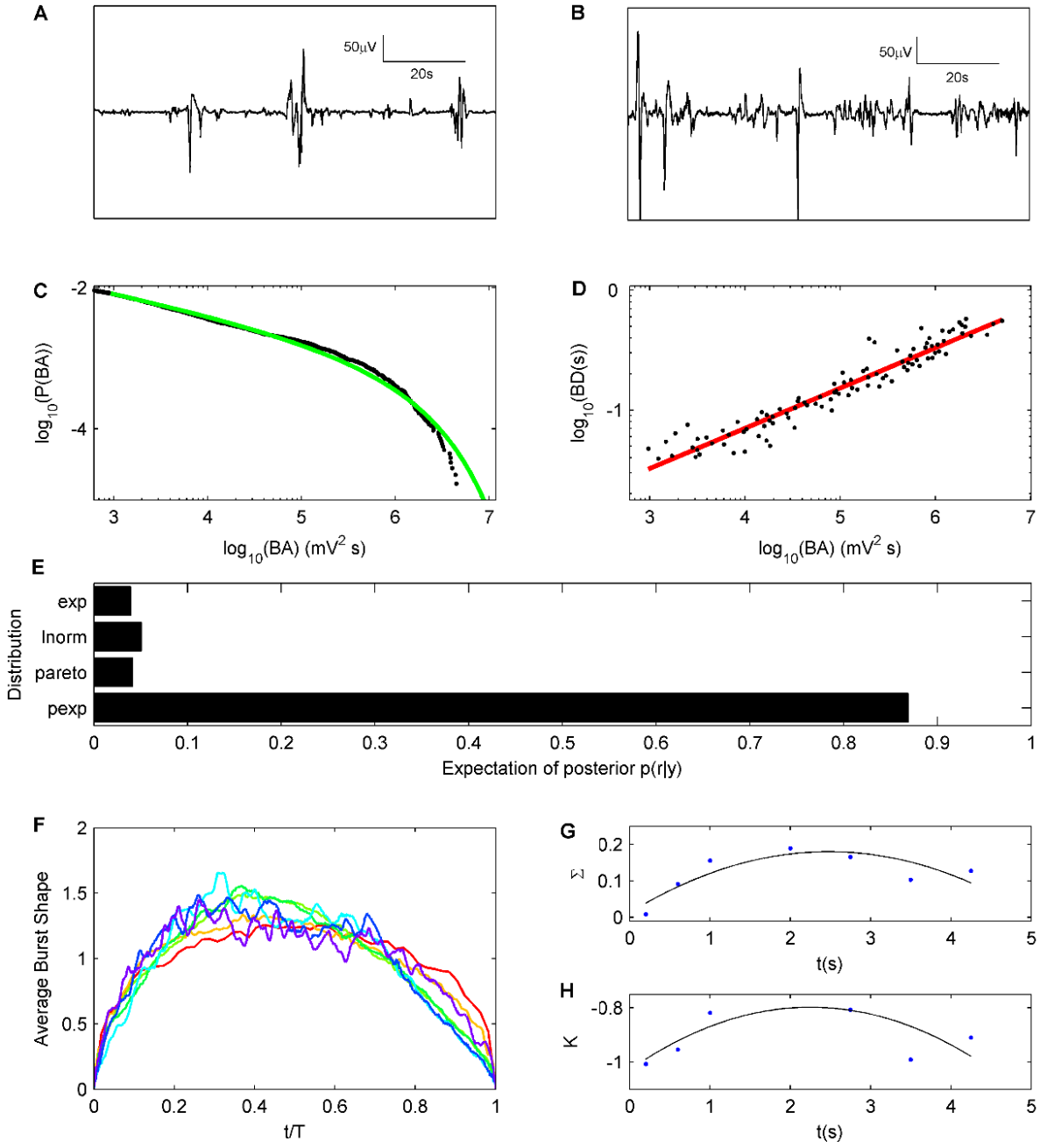

Figure 5.2 - Preterm EEG analysis results. (A) Typical recording of preterm infant EEG at 12 hours, showing discontinuous activity with clear bursts and inter-burst periods. (B) The same infant at 72 hours has an increase in background EEG activity with brief inter-burst periods. (C) The upper cumulative distribution (CDF) of burst areas with fit to an exponentially truncated power law (green). (D) Burst scaling relationship of burst areas (BA) and their respective durations (BD). Linear fit (red) in log-log coordinates. (E) Bayesian Model Selection (BMS) of 5 candidate heavy tailed models: Weibull distribution, exponential (exp), log-normal (lnorm), power law (pareto), and exponentially truncated power law (pexp). The posterior expectation gives the likelihood that the model (r) explains observed data events (y). (F) Average burst shapes at increasing burst durations T = 200 ms (red), 600 ms (yellow), 1 s (light green), 2 s (green), 2.75 s (cyan), 3.5 s (blue) and 4.25 s (purple). (G) Burst skewness (Σ) across timescales with a parabolic fit. (H) Burst kurtosis (K) across timescales fitted with a quadratic fit.

In summary, these analyses assert the presence of power law scaling in the bursty cortical activity of the preterm as soon as 12 hours after birth. Whilst the bursts converge toward simple shapes, there is a subtle but systematic change in burst symmetry and sharpness as a function of time scale. For the subsequent analyses, we extract three robust burst metrics: (1) slope (*S*) of the linear relationship between burst areas and burst durations in log-log coordinates; (2) change in symmetry (Σ) of bursts across timescales and (3) corresponding change in sharpness (K) of bursts across timescales. These metrics together capture the heterogeneity of bursts, their shape, size, and overall temporal evolution over the first few days of preterm infant life.

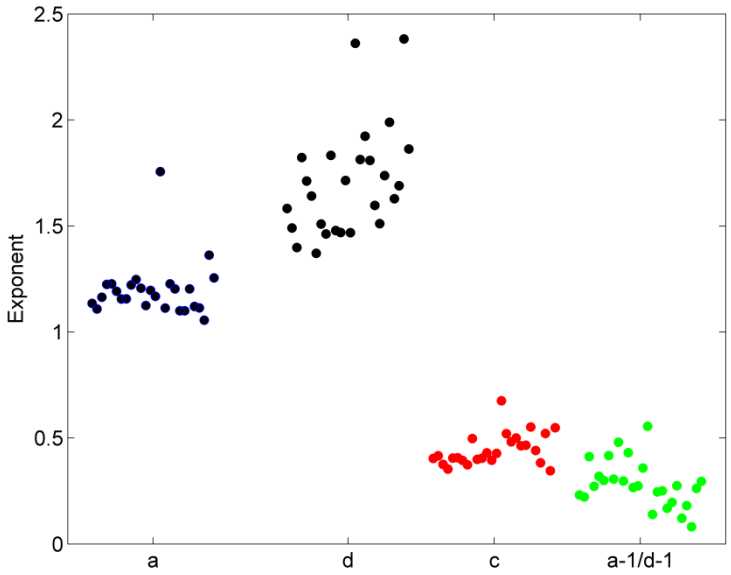

Figure 5.3 – Exponent interrelations for preterm EEG derived from statistical distributions of bursts at 12 hours. Scaling interrelations for exponents for area (a), duration (d), duration versus area (c), and the predicted relationship (a-1)/(d-1). A paired t-test reveals a significant difference ($p<0.01$) in the predicted relationships between exponents for slope (c) and a-1/d-1. Points are plotted with small horizontal offsets for clarity.

5.3.2 RELATIONSHIP OF BURST FEATURES TO GESTATIONAL AGE

Having established the presence of scale-free statistics, we next report on how the three markers of early cortical activity (scaling slope *S*; burst symmetry Σ; burst sharpness *K*) varied with gestational age (GA) in extremely preterm infants. At 12 hours, *S* values significantly co-varied with GA ($R=0.22$, $p<0.02$, Fig. 5.4A), with lower slopes occurring in the most preterm infants (22-24 weeks) and higher slopes in babies of a higher GA (25-28 weeks). Values of *S* did not co-vary with GA at 24, 48 and 72 hours after birth. Mean sharpness (*K*) for bursts (>2 s duration) also significantly correlated with GA at 12 hours ($R=0.29$, $p=0.0071$, Fig. 5.4B), but there was no correlation at 24, 48 and 72 hours. Mean symmetry (Σ) for bursts (>2 s duration) did not correlate with GA at any postnatal epoch period between 12 to 72 hours. The burst metrics *S* and *K* were also inversely

correlated at 12 hours such that lower *S* generally corresponded with higher *K* (R^2=0.50, *p*<0.00011, Fig. 5.4C). This relationship was present at each postnatal period (24 hours R=0.34, p<0.0003; 48 hours R= 0.18, p<0.007; 72 hours R=0.32, p<0.003).

At a postnatal age of 12 hours, average burst shapes showed a specific dependence on burst duration in the most immature infants (GA 22-24 weeks) (Fig. 5.4D) which was not present at later GA (25-28 weeks, Fig. 5.4E). In particular, the burst sharpness (*K*) at longer durations (>1 s duration) differs between these gestational ages. Further we find that *K* at mid-ranged burst durations significantly correlates with gestational age (Fig. 5.4F), specifically durations from 1 s – 2 s (p<0.017), 2 s - 2.75 s (p<0.0015) and 2.75 s to 3.5 s (p<0.049). Bursts shorter than 1 s and longer than 3.5 s do not show any significant dependence on GA. The measured features of bursts were hence specifically related to GA of the baby.

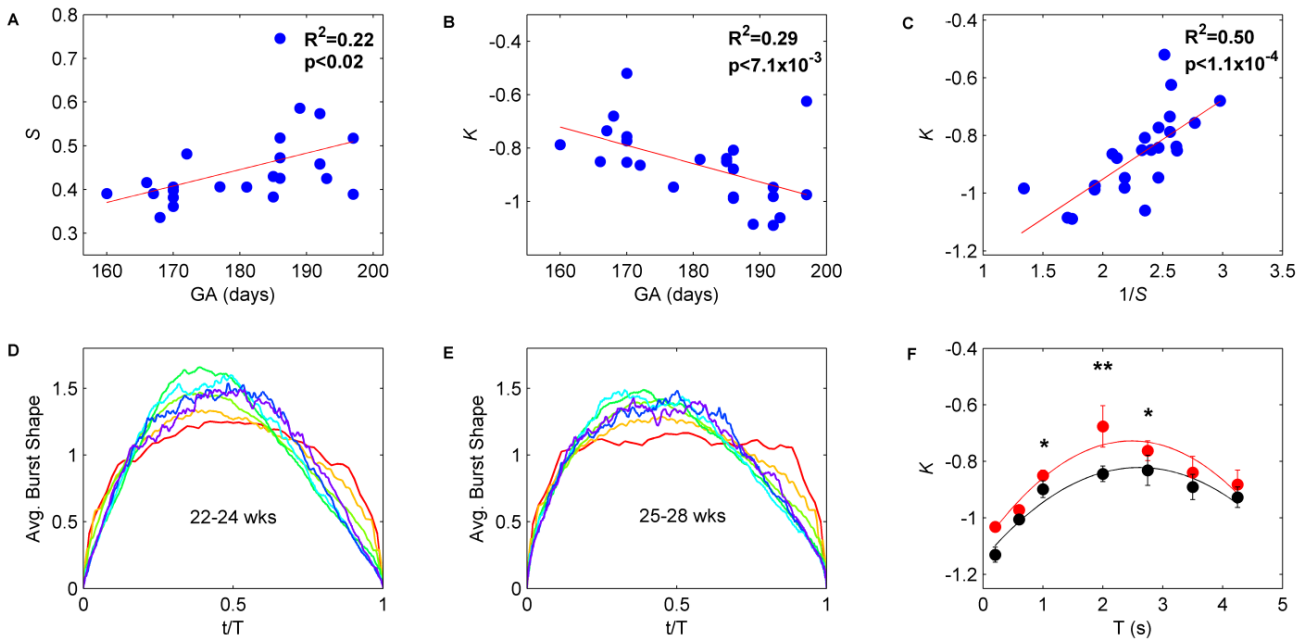

Figure 5.4 - Relationship of burst metrics with gestational age 12 hours after birth. Scatter plots of (A) Slope (*S*) versus GA, (B) Mean sharpness (*K*) of bursts >2 s duration versus GA, and (C) Inter-relationship of burst metrics *S* and *K* values. (D) Average burst shapes for a range of burst durations (from 200 ms - 6 s) show changes in sharpness values between (D) 22-24 weeks GA and (E) 25-28 weeks at 12 hours after birth. (F) Bursts are predominantly more kurtotic at middle timescales (1-3.5 s) in younger preterms (red line with standard error bars) compared with later ages (black line with standard error bars); * *p*<0.05, ** *p*<0.01.

In the early post-natal hours, these novel burst shape measures also significantly covaried with the traditional measure of scale-free activity, namely the power law exponent. In particular, the power law exponent co-varies with burst slope *S* and asymmetry Σ at both 12 hours (R^2=0.28, *p*=0.0077 and R^2=0.21, *p*=0.026, respectively) and 24 hours (R^2=0.5, *p*<0.001 and R^2=0.16, *p*=0.016, respectively). The power law exponent co-varies with burst sharpness *K* only at 24 hours (R^2=0.27, *p*<0.0012). There are no significant correlations at later post-natal hours.

5.3.3 BURST METRICS PREDICTIVE OF LONG-TERM OUTCOME

We next regressed these burst metrics against neurodevelopmental outcomes. In the human infant, this can be assessed by examining their correlations with long-term neurodevelopmental outcomes. Thus we examined the potential for *S*, *K* and Σ to predict three later outcomes at the age of 2 years: (1) the Mental Developmental Index (MDI), (2) the Psychomotor Index (PDI), and (3) composite outcome measures. These analyses are presented in Table 5.2. Of note, slope (S) values were predictive of MDI ($R=0.24$, $p<0.035$) as soon as 12 hours after birth, and was also predictive of composite outcome measures ($R=0.19$, $p<0.035$) at 72 hours. Mean sharpness (K) values for bursts (>2 s duration) at 12 hours were predictive of composite outcome ($R=0.29$, $p<0.007$). At 72 hours, K (bursts with >2 s duration) was predictive of all three outcome measures: MDI ($R=0.18$, $p<0.04$), PDI ($R=0.25$, $p<0.01$) and composite outcome ($R=0.18$, $p<0.034$). In contrast, mean symmetry (Σ) of bursts (>2 s duration) was only predictive at 72 hours of MDI ($R=0.28$, $p<0.01$) and PDI ($R=0.19$, $p<0.04$).

Metric	**MDI**		**PDI**		**Overall**	
	R	***p***	***R***	***p***	***R***	***p***
12 hours						
GA	**0.55**	**0.0002**	0.06	0.29	**0.32**	**0.003**
S	**0.24**	**0.035**	0.04	0.43	**0.19**	**0.035**
Σ	0.01	0.98	0.00	0.89	0.01	0.62
K	0.17	0.08	0.10	0.192	**0.29**	**0.007**
72 hours						
GA	**0.41**	**0.001**	0.17	0.05	0.09	0.147
S	0.08	0.19	0.11	0.12	**0.18**	**0.036**
Σ	**0.28**	**0.01**	**0.19**	**0.04**	0.14	0.067
K	**0.18**	**0.04**	**0.25**	**0.01**	**0.18**	**0.034**

Table 5.2 - Bivariate correlations (ANOVA) of burst metrics slope (S), skewness (Σ), and kurtosis (K) with Gestational Age, and Mental Developmental Index (MDI), Psychomotor Developmental Index (PDI) and overall Outcome (good/poor dichotomy).

Importantly, we find that both *S* and GA are correlated with MDI (Table 1). Further our burst metrics *S* and *K* are also correlated with GA (Fig. 5.5). In addition, we identified a weaker correlation of *K* with MDI at 12 hours (Table 5.1). This raises the possibility that the correlations of *S* and *K* with MDI arise only through the co-linearity of both variables with GA. Hence, we wanted to see whether our burst measures have independent predictive value over GA, which is already known in each given baby. This was done by assessing how GA affects the outcome prediction from burst measures. We employed statistical moderation (Baron and Kenny, 1986), to study via

general linear models (GLM) whether GA strengthens the causal relationship between burst variables *S* and *K* to MDI.

$$\text{MDI} = b_0 + b_1.S + b_2.\text{GA} + b_3.S.\text{GA} + \varepsilon_1. \quad (5.1)$$

$$\text{MDI} = b_{10} + b_{11}.K + b_{12}.\text{GA} + b_{13}.K.\text{GA} + \varepsilon_{12}. \quad (5.2)$$

Thus, for GLM (1) (with regression coefficients b_n): b_1 (2514) and b_2 (6.7) quantify the contributions of *S* and GA, respectively, and b_3 (-13.33) quantifies the interaction between both *S* and GA, where ε_1 (9.86) is the error term in the fit. This GLM (1) is highly significant in the case of *S* predicting MDI at 12 hours after birth (overall GLM (1): R'=0.75, p'=8.03x10^{-5}). In addition the value of b_3 is significant thus satisfying the condition for a moderating relationship (p<7.32x10^{-4}). Similarly, for GLM (2), b_{11} (-1133.2) and b_{12} (5.99) quantify the contributions of *K* and GA, respectively, and b_{13} (5.94) is highly significant (p<0.02): thus *K* is also highly predictive of MDI (overall GLM (2): R'=0.69, p'=4.26x10^{-4}, ε_{12}=11). Thus our metrics predict outcome even after taking into account the effect of GA, and the combined model yields a better predictor than either alone. Hence, formally, this relationship between *S* and MDI is moderated by GA. We represent these relationships using a simple path analysis diagram (Fig. 5.5).

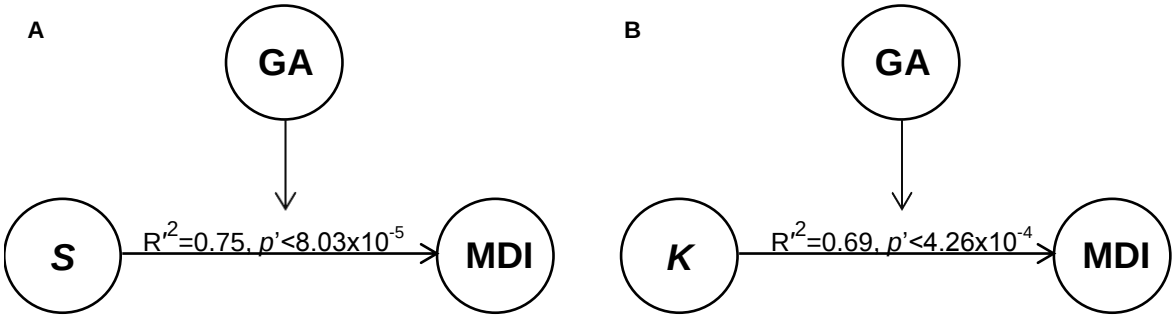

Figure 5.5 - Path analysis diagram of correlations at 12 hours showing how GA moderates (A) S to MDI and (B) *K* to MDI. Values of *S* and *K* at 12 hours are strongly influenced by GA in predicting mental development indices.

The relationships between burst metrics and clinical outcome measures at each postnatal time period are summarized in Figure 5.6. Over a 72 hour period, burst metrics significantly co-vary with composite outcome measure D1 (Fig. 5.6A to C) at some, but not at all postnatal ages. Dichotomizing MDI into sub-optimal and optimal MDI (D2) yields strong correlations at 12 hours for *S* (p<0.009) and *K* (p<0.03) values (Fig. 5.6D to F). To demonstrate the potential for burst metrics in diagnostic classification, we next assessed the sensitivity and specificity across a range of thresholds. These results were quantified using receiver operating characteristic (ROC) curves (Fig. 5.6G to I).

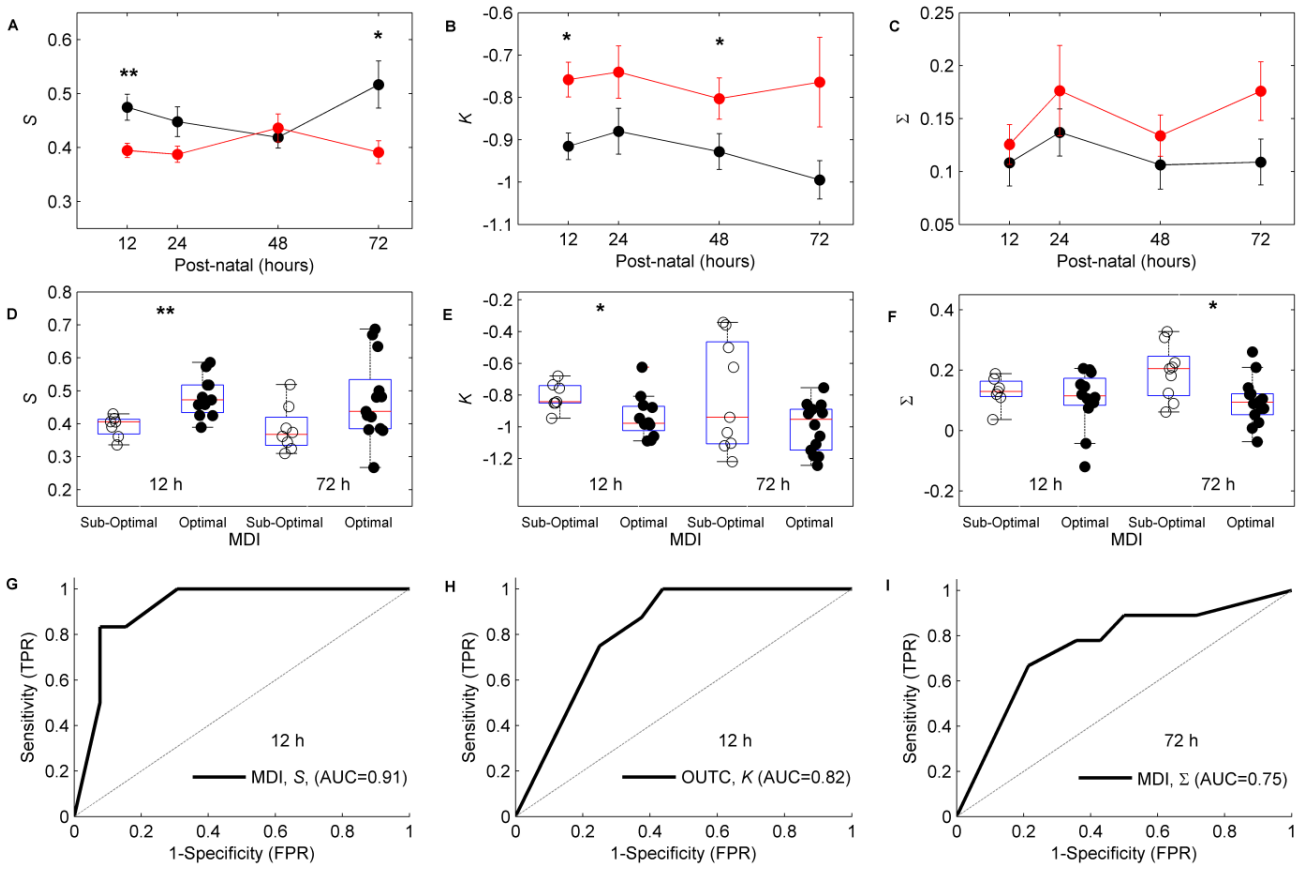

Figure 5.6 - Preterm EEG burst metrics versus clinical outcome over a 72 hour period. Mean values (circles) ±standard error bars (*p<0.05; **p<0.01), representing good (black) versus poor (red) composite outcome D1 for (A) *S* values, (B) Mean *K* values (>2 s duration), and (C) Mean Σ values (>2 s duration). Boxplots of sub-optimal (MDI<85) versus optimal (MDI>85) outcomes (D2) for (D) *S* values, (E) Mean *K* values (>2 s duration), and (F) Mean Σ values (>2 s duration) for post-natal ages of 12 hours (open circles) and 72 hours (filled circles). (G) ROC curve showing sensitivity (true positive rate, TPR) and specificity (false positive rate, FPR) at 12 hours for values of *S* predicting MDI. (H) ROC curve for values of *K* at 12 hours predicting the composite outcome. (I) ROC curve for values of Σ at 72 hours predicting MDI.

We observe very high accuracy (AUC=0.82) for kurtosis *K* as a predictor for the composite outcome (D1) and for the slope *S* at 12 hours as a predictor (AUC=0.91) for later optimal/suboptimal MDI outcome (D2). Values of slope S carry very high sensitivity for later MDI outcome (up to 100%), achieved with a specificity of close to 80%. At 72 hours, asymmetry Σ of bursts also predicts later optimal/suboptimal MDI outcome (D2) with a high accuracy (AUC=0.75).

Our analyses were conducted on lengthy epochs of relatively artifact-free clinical EEG (mean duration 116 minutes). In clinical practice, availability of such data is often restricted to briefer epochs. To test the sensitivity of our approach in such settings, we repeated our analyses restricted to the first 50% of each neonate's data (average of 58 min) as well as 25% (average of 30 min). The primary outcome measures remained significant on these shorter epochs. In particular for epochs of 50% their original duration, slope *S* predicted MDI (p<0.043) at 12 hours, whilst skew Σ and kurtosis *K* at 72 hours predicted MDI (p<0.0024 and p<0.019, respectively) and PDI (p<0.0098 and p<0.0034, respectively). Most of these outcome predictors dropped below significance for data of

duration less than 30 minutes. Predictors of the continuous outcome measures MDI and PDI were more robust to data down-sampling than the predictors of the composite outcome measure D1.

We also benchmarked our findings against more conventional measures of preterm EEG (Hayakawa *et al.*, 2001), namely, the burst count and the inter-burst intervals (IBIs). As per Table 5.1, we analyzed an average of 2376 bursts per epoch, with no significant differences across the four postnatal ages (12 to 72 hours, F=2.2, $p>0.096$). Similarly, IBIs were also statistically non-significant across postnatal ages (F=1.8, $p>0.16$). No statistically significant differences in IBIs and burst counts were found in infants with respect to the severity of outcomes and long-term injury (MDI, PDI and composite outcomes) at any of the four postnatal ages (12 to 72 hours, $p>0.24$ in all cases).

5.4 DISCUSSION

In this chapter, we establish that intermittent, spontaneous cortical bursts in the preterm brain exhibit scale-free properties. Moreover, the characteristic statistics of these bursting dynamics correlate with indices of longer term developmental outcome. Path analysis indicates that the relationship between these burst metrics and outcome is moderated by gestational age. Hence, this analysis identifies specific predictive properties of scale-free bursts in the preterm and their relationship to long term neurodevelopment. We also highlight the crucial temporal transitions in these scaling statistics that occur already between 12 and 72 hours after birth. Scale-free processes arising from cortical activity in the preterm may provide insight into infant brain behavior when normal gestation is interrupted. Further, statistics scale-free bursts in the preterm may reflect fundamental thalamo-cortical and cortico-cortical pathways which emerge during the gestational ages studied.

5.4.1 NEUROBIOLOGICAL UNDERPINNINGS OF EARLY SCALE-FREE BEHAVIOR

The presence of scale-free activity provides insight into system disturbances, potentially arising due to interplay between excitation and inhibition in cortical pathways and, more broadly, complex dynamics within neuronal networks, particularly in the face of scarce metabolic resources (Roberts et al. 2014a). In this study the results of scaling exponent interrelations suggest that early human brain activity self-organizes, transitioning between subcritical and critical states, though not entirely consistent with criticality. Early developing neuronal circuits have been studied in detail at the cellular level (Blankenship and Feller 2009; Hanganu-Opatz 2010; Kilb et al. 2011) but little is quantitatively known about systems level brain dynamics in neonatal brains. It has been established in in vivo tissue slices that a shift in endogenous balance results in spontaneous cortical bursts exhibiting "neuronal avalanches", occurring when a system is bordering on the cusp between stability and instability (Beggs and Plenz 2003). This avalanche-type behavior has been studied in a variety of neuronal recordings (Friedman et al. 2012; Meisel et al. 2012) highlighting that cortical activity may be generated via self-organized networks within the human cortex. In physical systems, self-organization further elucidates the unpredictable nature of a system at a critical state, resulting in fluctuations spanning a broad range of sizes (Sethna et al. 2001).

Recent neuroanatomical work has shown that major thalamo-cortical and cortico-cortical pathways are in the early stages of development during the first weeks of early preterm life (Kostović and Judaš 2010). Hence, the observed scale-free behavior of cortical activity arises in a brain network that is immaturely wired (early GA neonates) or where wiring is still undergoing intensive organization (later GA neonates). Indeed, our findings showed that cortical bursting dynamics are

different in infants prior to (GA < 24 weeks) versus those after (GA > 24 weeks) which aligns with the growth of first thalamo-cortical pathways (cf. Kostović and Judaš, 2010). Research using animal models shows that at early phases of cortical pathway development, these sparse connections give rise to intermittent spontaneous activity transients (SATs) – a characteristic feature of immature brain activity (Ben-Ari 2001; Blankenship and Feller 2009; Colonnese and Khazipov 2012; Hanganu-Opatz 2010; Khazipov and Luhmann 2006; Kilb et al. 2011; Vanhatalo and Kaila 2006). These events are thought to be the key functional driver of neuronal development where the deprivation of neurons leads to apoptotic cell death in experimental models (Kilb et al. 2011; Nimmervoll et al. 2013), while the overall level of bursting activity relates to prospective structural growth in the human preterm babies (Benders et al. 2014). Moreover, disruption of these events leads to disorganized thalamo-cortical connectivity and neuronal death (Catalano and Shatz 1998; Tolner et al. 2012). In this study, we demonstrate that features of cortical bursts in the early preterm do reflect immature cortical pathways which readily relate to neurodevelopmental consequences as indicated by our findings.

The recent observation of scale-free processes in hypoxic term infants with burst suppression (J. A. Roberts et al. 2014) opens novel insights into critical states of cortical activity under the constraints of metabolic depletion. Using similar methods and more stringent statistical tests (i.e., Bayesian model selection), the present study establishes that scale invariant distributions exist in preterm EEG data - a characteristic feature recently identified as a key, but challenging objective (Fransson et al. 2013). Our results thus provide insight into a neurodevelopment window in the early preterm, where classical scale-free processes characterize potential system disturbances in cortical pathways hours after birth.

5.4.2 TRANSITIONS IN BURST DYNAMICS AT EARLY GESTATIONAL AGES

Previous analyses of preterm EEG have established the developmental trajectory of burst properties, with an increase in their duration and decrease in their amplitudes with GA (André et al. 2010; Tolonen et al. 2007; Vanhatalo et al. 2005). The intra-burst activities are also known to change with development (André et al. 2010; Tolonen et al. 2007), as well as after medication (Malk et al. 2014) or brain lesions (Akihisa Okumura et al. 2002). These prior findings suggest that the burst shape analysis advanced in the present report may find diagnostic use in preterm babies, akin to evidence from full-term babies (see chapter 3 and chapter 4). In our study of preterm neonates, bursting statistics change substantially over the 72 hour period after birth, either in response to treatment in the NICU, spontaneous metabolic recovery, or conversely due to progression of underlying neuronal disturbances. Further clarifying how these burst metrics reveal critical periods that predict outcome is to be the focus of future work.

In the absence of solid ground-truth, the issue of pathophysiological versus physiological preterm EEG remains a difficult and vexed issue (cf. Kidkoro *et al.*, 2009). Based upon the our sensitivity analysis, the EEG in preterm neonates that are most likely to have a favorable outcome is characterized by bursts that are typically symmetric and relatively flat at long time scales (Figure 5.6B,C). Conversely, bursts in neonates with long term disability are skewed and highly kurtotic shortly after birth. Assuming that long term outcome correlates with the presence of post-natal pathophysiological EEG, these values provide promising benchmarks for future research that correlates features of surface EEG with invasive measures of existing underlying pathophysiology.

5.4.3 EARLY PREDICTION OF LONG-TERM NEURODEVELOPMENT

Early prediction of long-term neurodevelopmental outcome remains a major bedside challenge as very preterm infants that survive into early childhood have a high likelihood of developing mental disability or poor psychomotor performance at 2 years of age (Wood et al. 2000). The availability of outcome prediction within the first few days of life would allow early identification and provide the basis for improved guidance of intensive care interventions.

We observed significant relationships between statistical metrics of single channel EEG and later neurodevelopmental outcomes. Our results show that low slope values, moderated by the effect of gestational age, correlate with poor scores on the Mental Developmental Index (MDI, <85 on Bayley scales) or early death. We also show that higher burst sharpness (kurtosis), moderated by gestational age is indicative of poorer MDI. Importantly, our study quantifies the moderating role of gestational age on outcome. Thus, moderation was used to formally establish the effect of GA on our burst measures S and K. In the context of predicting likely neurocognitive outcome hours after preterm birth, this characterization of preterm EEG bursts is highly significant. Further we posit that these measures provide insight to the notion that system level disturbances (i.e., metabolic imbalance and poor synaptic connectivity) are acute reflections of the underlying neuronal circuitry in an immature cortex. It is also compatible with the interpretation that prenatal disturbances, such as placental infections or brain hemorrhages, predispose the child to adverse outcomes (H. K. Brown et al. 2013; Shapiro-Mendoza 2014), and that our present EEG metrics capture the immediate consequences of these system-level disturbances coupled with the gestational age of the infant. In the absence of acute complications, the preterm infant is considered to be metabolically stable by the third day of life (Klein 2002). Formal ROC curves, used to quantify sensitivity and specificity of later outcome prediction yielded promising results at both 12 and 72 hours after birth (Fig 5G-I). The finding of outcome prediction by 12 hours may be particularly important because of its potential implications for clinical management directly after birth. Prediction during the first day

of life may be crucial in terms of active and specific neuroprotective strategies. We find that at 72 hours, skew and kurtosis values are predictive of mental and psychomotor outcome. This may indicate that temporal changes in bursting behavior reflect the impact of metabolic disturbances on neuronal integrity and recovery. In contrast, traditional measures (of burst count and inter-burst interval) did not co-vary with post-natal age or predict later outcome.

Most prior studies have focused on measuring overall amplitudes at a limited bandwidth (aEEG). As reviewed above, this approach requires trained reviewers and is vulnerable to artifacts. Despite these limitations, a relationship to later outcomes has been established (Hellström-Westas and Rosén 2005; Olischar et al. 2004; Sisman et al. 2005; Wikström et al. 2012). These findings are compatible with the proposal that the total amount of brain activity is important for early brain health (see also (Benders et al. 2014).

5.4.4 METHODOLOGICAL CONSIDERATIONS AND FUTURE DIRECTIONS

A particular technical advantage in our methods is that they are based on analyzing extracted events (bursts). Hence they do not require fully continuous streams of EEG signal. This allows rejection of signal epochs with clear artifacts without loss of analytical reliability, which commonly challenges paradigms relying on continuous temporal behavior, such as vigilance state cyclicity (Stevenson et al. 2014) or broad spectrum power spectra (Fransson et al. 2013). The requirements of the algorithm are also computationally modest, depending only upon a simple algorithm for threshold detection, followed by resampling, averaging, and shape characterization. It would hence be quite feasible to implement the burst characterization on-line, giving a moving window predictor of outcome, which could then be integrated with other clinical variables to inform acute management. Whilst practical from a computational perspective, such an endeavor naturally rests upon future, large validation studies.

We can see two directions that warrant more detailed future studies. First, in establishing the presence of scale-free bursts in single-channel recordings, we focused entirely on the temporal properties of bursts. An aspect of SAT events in discontinuous preterm EEG is the spatial specificity of neonatal EEG signals (Odabaee et al. 2013), which may account for some of the observed variability in burst shapes in our single channel recordings due to varying spatial relations between cortical activity and scalp electrode positions. Future studies with higher density EEG will show whether sensitivity of burst shape analyses can be improved by better spatial sampling.

Second, the efficacy of quantitative EEG measures in the NICU is dependent upon disambiguating bursts of cortical origin (e.g. duration, area, and shape of SAT) from artifact type events (e.g. movement, respiration spikes, and amplifier noise). Recent studies have shown that more conventional quantification of burst occurrence (Benders et al. 2014) and the presence of vigilance

state cycling (a.k.a. sleep wake cycling; SWC) (Stevenson et al. 2014) may inform brain health. These methods recently became available with the validation of burst detectors (Palmu et al. 2010) and the development of cyclicity measures for preterm EEG monitoring (Stevenson et al. 2014). Future studies to this end will need to apply all methods to the same datasets to define their mutually added values in clinical applications.

Third, full band EEG recordings potentially offer substantial additional benefits over those presently analyzed. In particular, the slowest signal component (infra-slow) would likely allow detection of bursts of longer duration and greater area, hence expanding the upper bound in the corresponding probability distributions. Unfortunately, such data is not currently available from clinical datasets with long-term monitoring and outcome data, which were acquired with inbuilt hardware high-pass filters. The extension to full band recordings remains the objective of future research using new generation amplifiers.

Finally, we presently restrict our approach to analyses of a single (bipolar) electrode recording. Additional channels were available in some, but not all, of our neonates. Such additional data could potentially enhance the sensitivity of the proposed approach in two ways: First, by pooling across all channels, more bursts would be available and hence the confidence of our shape estimates would be greater. This improvement may be tempered somewhat by the fact that, in very early preterm babies, many underlying bursts would appear in several channels contemporaneously such that additional true degrees of freedom may be limited. Second, if many additional channels were present, additional analyses based on the spatiotemporal properties of avalanche-like activity would be possible. However this would require high quality, dense EEG recordings which are not presently available in the NICU.

In summary, the analysis of bursts of electrical activity in neonatal EEG using the techniques of scale-free systems shows potential for predicting long-term outcome in preterm infants. Further, combining information from burst shapes with gestational age strongly predicts later outcome. Finally, we highlight the subtle but important temporal changes in cortical bursting dynamics during the first early weeks of preterm development, as well as over the first days of postnatal life.

6.0 EARLY FEATURES OF ACUTE BRAIN INJURY IN THE PRETERM

ABSTRACT

Acute brain injury in the preterm, such as intraventricular haemorrhage, is a common occurrence in neonatal intensive care. In this study we characterize early cortical activity that indicates the presence of intraventricular hemorrhage (IVH) in preterm infants. Automated offline analyses of electroencephalography in 25 extremely preterm infants (23 to 28 weeks gestational age) included quantifiers of burst shapes: symmetry and sharpness, calculated for all burst durations, and conventional detection of inter-burst intervals and burst counts. Two contrasts of quantitative EEG data were performed: (1) Between neonates with (n=14) versus those without IVH (n=11), and (2) Before and after the ultrasound confirmation of IVH. Burst shape and asymmetry differed significantly for both clinical contrasts. Moreover, increasing levels of IVH severity corresponded with sharper, more asymmetric burst shapes. Clinical sensitivity and specificity testing of burst symmetry and sharpness revealed high true positive rates (Sensitivity: 82% and 88%, respectively) and low false positive rates (1-Specificity: 81% and 92%, respectively) in discriminating between infants with and without intraventricular hemorrhage. In contrast, conventional measures of inter-burst intervals and burst counts were not statistically significant for either contrast. Measures of early cortical burst shapes in the electroencephalogram offer a novel, real-time method to identify preterm infants at risk of intraventricular hemorrhage during their first days of life.

6.1 INTRODUCTION

Preterm infants are exposed to an increased risk of developing acute neurological disorders, such as germinal matrix and intraventricular hemorrhage (IVH), during the first few days of life (Ballabh 2010; Bolisetty et al. 2014). Common mechanisms that lead to IVH include failure of cerebral autoregulation (Milligan 1980; Volpe 2001b), hypoxic-ischemic insults, and sepsis (Volpe 2009). Prevention and management of IVH focuses on systemic circulatory stabilization and cardiorespiratory support, as well as correction of coagulopathies (Ballabh 2010; McCrea and Ment 2008). An acute injury such as a large IVH predisposes an infant to poor neurodevelopmental outcomes (Bolisetty et. al. 2014) such as cerebral palsy, developmental delay or hydrocephalus (Ballabh 2014). Hence, prevention or early detection of IVH holds promise of significantly improving neurodevelopmental outcomes in these vulnerable neonates.

Currently, the gold standard for IVH detection is cranial ultrasonography through the anterior fontanel (Bada et al. 1979; McCrea and Ment 2008), which is sensitive to lesions within hours to days after the occurrence of IVH. A timely therapeutic response to IVH requires a means of pre-empting IVH or detecting it as soon as it occurs, implying a need for continuous brain monitoring. Studies have shown that IVH may cause a qualitative change in EEG waveforms – as visually assessed (Hayakawa et al. 1999) - or in the background patterns of the electroencephalogram (EEG) (Chalak et al. 2011; Akihisa Okumura et al. 2002; Olischar et al. 2007). Continuous EEG recording is hence recognized as a clinically useful method for monitoring the preterm brain and is in widespread use (Olischar et al. 2004; Watanabe et al. 1999; Wikström et al. 2012). Identification of EEG features appropriate for automatic and objective analysis would greatly enhance the potential for this data to be used for real-time detection of impending IVH.

As reviewed in Chapter 2, the hallmark of early EEG activity in extremely preterm infants is the presence of intermittently occurring spontaneous activity transients (SATs), evident in the EEG trace as irregular high amplitude bursts of activity (André et al. 2010; Vanhatalo and Lauronen 2006). Normal preterm EEG activity is characterized by intermittent occurrence of activity with mixed frequency content, and the relatively silent EEG during the inter-burst (IBI) periods (André et al. 2010). In particular, extremely early preterm infants (<28 weeks gestational age) have characteristically dominant few second long epochs of low frequency activity (<1 Hz) with superimposed fast activity bouts, collectively called bursts, spontaneous activity transients (SAT) or delta brushes (Vanhatalo et al. 2006). Abnormalities in the preterm EEG are mostly seen as durations of the silent periods (André et al. 2010), however visually observed changes in the waveforms, such as positive rolandic sharp waves, have also been reported (Aso et al. 1993). This chapter builds upon the previous study of predicting long-term outcomes from preterm EEG during

the first days of life. In the present study, we hypothesize that quantitative measures of the early cortical bursts in the preterm EEG may acutely reflect, and even precede, the onset of IVH. Importantly, the findings presented in this chapter suggest that IVH may be detectable via bedside EEG monitoring prior to routine cranial ultrasound detection, hence our method opens a novel window to real-time monitoring as well as identifying neural mechanisms underlying IVH.

6.2 MATERIALS AND METHODS

In chapter 3, quantitative methods are used to rapidly analyze EEG bursts that occur after asphyxia in full-term infants. In Chapter 4 we found that specific changes in burst size are predictive of long-term outcome. These methods are fully automated and free from subjective qualitative assessments, thus enabling robust burst characterization, complementing conventional visually analyzed EEG measures such as the inter-burst interval (IBI) and burst counts (Wikstrom 2012, Hellstrom-Westas 2001).

6.2.1 DATA COLLECTION

We analyzed EEG recordings of 25 preterm infants (gestational age 23-28 weeks; Table 1) that were monitored during their first three days of life in the Neonatal Intensive Care Unit (NICU) at Lund University Hospital, Sweden. The infants constitute approximately half of the infants in a cohort of extremely preterm infants from which qualitative and quantitative (IBI and measures of suppression) EEG analyses have been previously published (Wikström 2011, Wikström 2012). Inclusion criteria for this analysis included clinically confirmed absence or presence of IVH via ultrasound at either day 1 or day 3 of life. Exclusion criteria for this study were based on unconfirmed ultrasound reports, infants greater than 28 weeks gestation and relatively artifact-free postnatal EEG epochs 12 to 72 hours. EEG was acquired at the biparietal P3-P4 derivation at a sampling rate of 256 Hz using a NicOne amplifier (Cardinal Healthcare, Nicolet Biomedical, Madison, WI, USA). Epochs of EEG (90-120 minutes) were selected at fixed post-natal time points of 12, 24, 48 and 72 hours from relatively artifact-free periods irrespective of vigilance state. Our quantitative EEG analysis focused on EEG epochs that preceded (pre-IVH) or followed (IVH) the confirmation of hemorrhage by ultrasound within the first three days of birth. The use of patient data for this study was approved by the Research Ethics Committee of the Lund University Hospital.

Cranial ultrasound was performed routinely on day 1 (0-24 postnatal hours) and day 3 (48-72 postnatal hours) (Ultrasound brand should be mentioned- I can find it in previous papers: LHW comment). Data were analyzed in three categories according to the severity of IVH: no IVH (grade 0); mild-moderate IVH (grades 1-2, i.e. germinal matrix hemorrhages or IVH without ventricular

dilatation, respectively); and severe IVH (grades 3-4, i.e. IVH with ventricular dilatation or intraparenchymal involvement, respectively) (Papile et al 1978). Contrasts on EEG analyses were then performed, comparing: i) infants with no IVH, ii) infants with IVH grades 1-2 and iii) IVH grades 3-4. EEG data were exported to MATLAB (Mathworks, Natick, MA, USA), band-pass filtered (0.2-20 Hz), and analyzed using conventional and custom algorithms (Roberts et al, 2014). Clinical details for each neonate are provided in Table 6.1.

		GA (weeks +days)	Birth Weight (g)	Apgar5[a]	US day 1 (0-24 h)	US day 2 (24-48 h)	US day 3 (0-48-72 h)
No IVH	1	26+6	854	6	0		0
	2	25+2	638	7	0		0
	3	27+1	854	8	0		0
	4	24+4	788	8	0		0
	5	27+3	840	7	0		0
	6	25+3	940	8	0		0
	7	27+3	950	9	0		0
	8	27+3	1148	8	0		0
	9	25+1	732	9	0		0
	10	25+5	946	5	0		0
	11	25+5	780	8	0		0
IVH (Gr 1 -2)	12	24+2	730	6	0		1
	13	24+2	646	5	2		2
	14	26+4	951	8	1		1
	15	25	725	6	0		2
	16	27	970	7	1		2
	17	23+5	584	9	0		2
	18	27+4	1092	6	-	2	2
	19	28+1	1230	7	-	2	2
	20	27+4	630	6	-	2	2
IVH (Gr 3 -4)	21	22+6	580	7	0		3
	22^	26+4	670	3	4		-
	23*	24+3	796	6	0		3
	24*	27	950	7	0	3	-
	25	24+2	730	6	3		-

Table 6.1 – Clinical summary of the preterm population analyzed for this study. Table legend: GA=gestational age, Apgar5= Apgar score at 5 minutes; [a] IVH and Apgar5 were significantly correlated (Wilcoxon ranksum test, $p<0.05$), Gr=Grade. Ultrasound labels: US= cranial ultrasound, 0=no IVH, 1=mild IVH, 2=moderate IVH, 3=severe IVH, 4=very severe IVH, "-"=no ultrasound examination, blank table entry=no ultrasound performed. ^= periventricular leukomalacia (25). *=bilateral IVH.

Contrasts on EEG analyses were then performed, comparing: i) infants with no IVH, ii) infants with IVH grades 1-2 (mild-moderate), and iii) IVH grades 3-4 (severe IVH). We also analyzed bursts from EEG epochs recorded prior to identification of the IVH by ultrasound to investigate whether burst shapes could indicate an impending or early onset phase of IVH. Thus, we compared all postnatal epochs with ultrasound confirmed IVH with epochs temporally precedent to hemorrhage confirmation. Hereafter, we refer to epochs with no hemorrhage as "no IVH", epochs prior to

ultrasound confirmed IVH as "preUS-IVH" and epochs with ultrasound confirmed IVH as "US-IVH". Thus for the data cohort, we identified 11 epochs as no IVH. Moreover, for mild-moderate IVH we identified 12 epochs as preUS-IVH grade 1-2 and 11 epochs as US-IVH grade 1-2. For severe IVH, we identified 6 epochs as preUS-IVH grade 3-4 and 4 epochs as US-IVH grade 3-4.

6.2.2 AVERAGE BURST SHAPES ANALYSIS OF INTRAVENTRICULAR HEMORRHAGE

We first applied conventional analyses, namely interburst interval (IBI) and burst counts for the three preterm populations as classified in Table 6.1. Following these conventional measures, we performed average shape analyses to analyze burst symmetry (skewness, Σ) and sharpness (kurtosis, *K*), across a wide range of burst durations (200 ms-6 s) (see Chapter 3). Statistical group comparisons of burst shape metrics were conducted using one-way analysis of variance (ANOVA).

To assess diagnostic accuracy of burst shapes to identify IVH, we estimated true positive and false positive rates across a range of Σ and K values, deriving corresponding receiver operating characteristic (ROC) curves. The ROC curves were further quantified by calculating the area under curve (AUC), a measure of diagnostic accuracy. We then summarized the clinical sensitivity and specificity of burst symmetry and sharpness values to discriminate between preUS-IVH, US-IVH and no IVH neonates. To validate the diagnostic accuracy of our measures, we performed two tests of data reliability for both Σ and K values. First, we used the leave-one-out cross validation test – a method where one single value in the sample set is tested against the rest of the samples. This process is iteratively repeated for each value to calculate the error in prediction, until all samples in the dataset have been tested, thus deriving an overall accuracy measure. Similarly, we also tested whether adding null data points in each sample set – group mean values of Σ and K in both no IVH and IVH infants, respectively –and derived the relevant sensitivity and specificity measures. Figure 6.1 shows a schematic for the analyses.

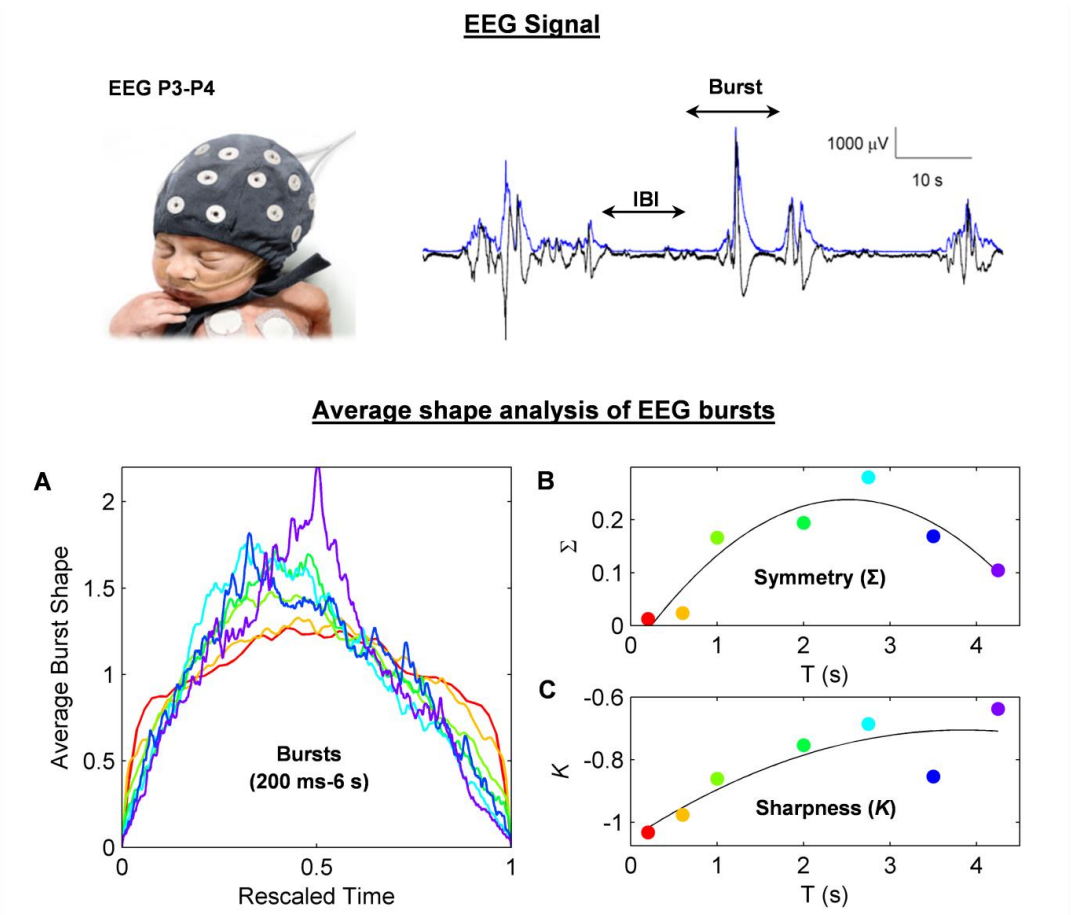

Figure 6.1 - Analysis schema for each EEG burst. (A) Bursts binned by duration (T) to seven groups and all bursts in a group are averaged, then re-scaled to have unit time and analyzed for their (B) change in shape symmetry (skewness) and (C) sharpness (kurtosis) across duration T. Durations in average burst shapes are here color coded to corresponding points in the skewness and kurtosis graphs: 200 ms (red), 600 ms (yellow), 1 s (light green), 2 s (cyan), 2.75 s (green), 3.5 s (purple) and greater than 4.25 s (blue). Solid lines show quadratic fits to skewness and kurtosis graphs across burst durations.

6.3 RESULTS

Visual assessment of EEG epochs did not significantly indicate any differences between no IVH and IVH infants. Conventional measures did not differ significantly across IVH (grades 1-2 and 3-4, respectively). For mean IBI of length >1 second ($F=0.08$, $p=0.92$) across normal and IVH populations revealed no statistically significant differences. Further, burst counts comparing short bursts ($F=0.43$, $p=0.65$ for bursts < 2 seconds) or long bursts ($F=0.12$, $p=0.88$ for bursts >2 seconds) were statistically insignificant (Fig. 6.2A and B). Inspection of the preterm EEG showed characteristic SATs with no visually apparent difference in the overall activity between the groups - that is no IVH (e.g. Fig. 6.2A) versus IVH (e.g. Fig. 6.3C). There were also no statistically significant differences in IBI or burst counts related to severity of IVH, gestational age, birth weight or 5-minute Apgar score.

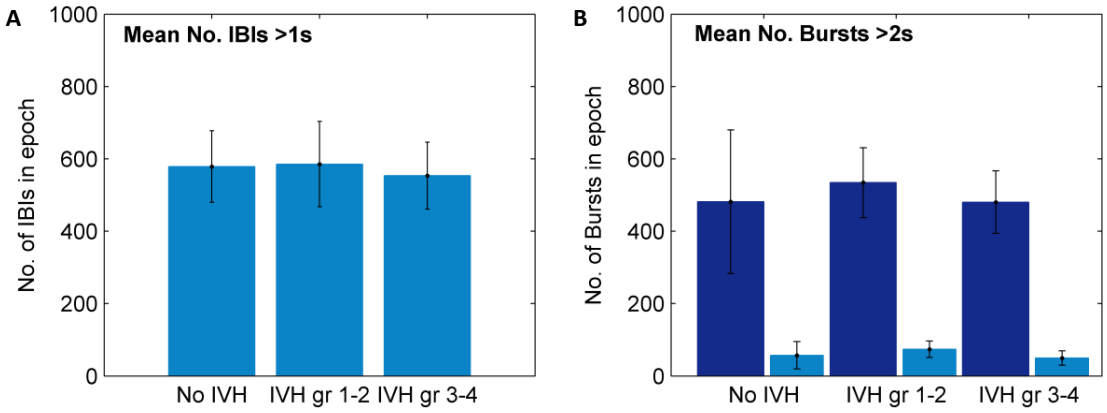

Figure 6.2 - Conventional analyses of preterm EEG (A) Mean number of IBIs longer than 1 second (±SEM) for the three IVH categories. No significant differences were found (Gr=grade). (B) Total burst counts (±SEM) demonstrating that short bursts (dark blue bar; 200 ms-2 s) and longer duration bursts (light blue bar; 2 s-6 s) in the three categories did not exhibit significant group differences.

The observable difference in EEG traces suggested infants with IVH grades 1-4 appeared to have higher amplitudes and greater burst areas than infants without IVH. These differences appeared more evident when we computed the instantaneous amplitude of the signals (see blue overlay traces in Fig. 6.3A and C). This observation appeared further confirmed by super-positioning hundreds of bursts (Fig. 6.3B and D). However, on closer inspection conventional mean amplitudes (F=0.54, p=0.59) and mean areas (F=1.81, p=0.18) for bursts (>1 s duration) did not significantly differ between groups. Thus we can firmly establish from these measures that conventional measures that burst counts, IBIs and amplitude changes are not effective for classifying between hemorrhagic and non-hemorrhagic presentation.

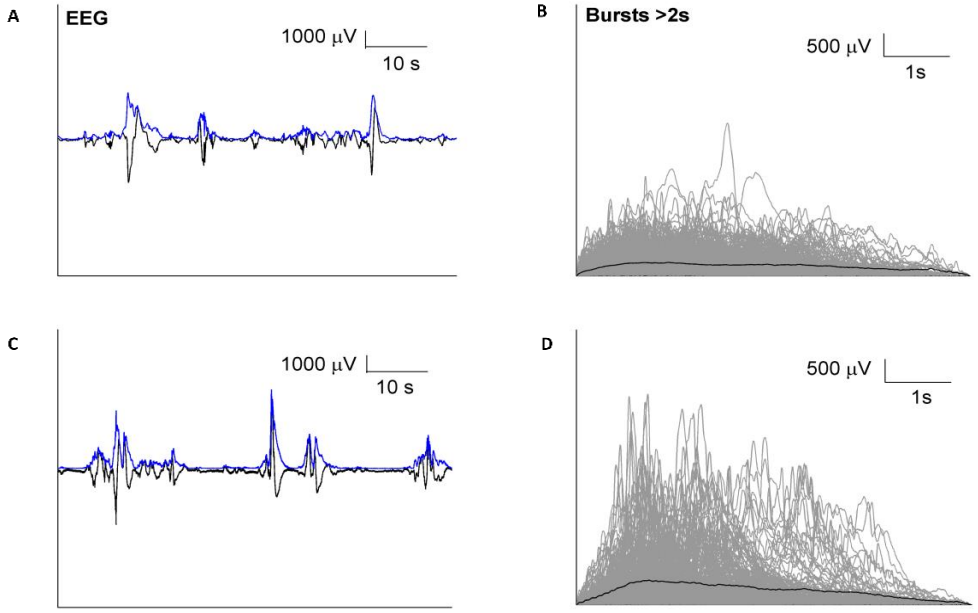

Figure 6.3 – Comparisons of EEG bursts in normal preterm and IVH preterms. (A) Example of EEG epoch (black) from infant with no IVH, with corresponding amplitude envelope (blue). (B) Overlay of all amplitude envelope signals (gray) and their mean (black) for a single infant with no IVH. (C) Example of EEG epoch for infant with IVH grade 2. (D) All amplitude envelopes for an infant with IVH grade 2.

6.3.1 BURST SHAPE ANALYSES

We next examined the change in average burst shape as a function of burst duration using measures of burst symmetry (Σ) and sharpness (K). Visual comparison of grand average burst shapes across burst durations shows clear differences between the three IVH groups. We also analyzed bursts from postnatal EEG prior to ultrasound screening to investigate whether burst activity indicates an onset of early IVH. Thus, we also analyzed each postnatal epoch with confirmed IVH with epochs temporally precedent to hemorrhage confirmation, referred hereafter as pre-IVH. For each IVH grouping we calculated average burst shapes for pre-IVH 1-2 and 3-4 compared with IVH grades 1-2 and 3-4, respectively (Fig. 6.4). Most notably, there was a strong increase in the sharpness of longer bursts (>2 s duration) with increasingly severe IVH. The longer bursts in infants with severe IVH (grades 3-4) were also asymmetric to the left, with sharper onset and slower decay compared to the bursts in infants with no or mild IVH (grades 1-2).

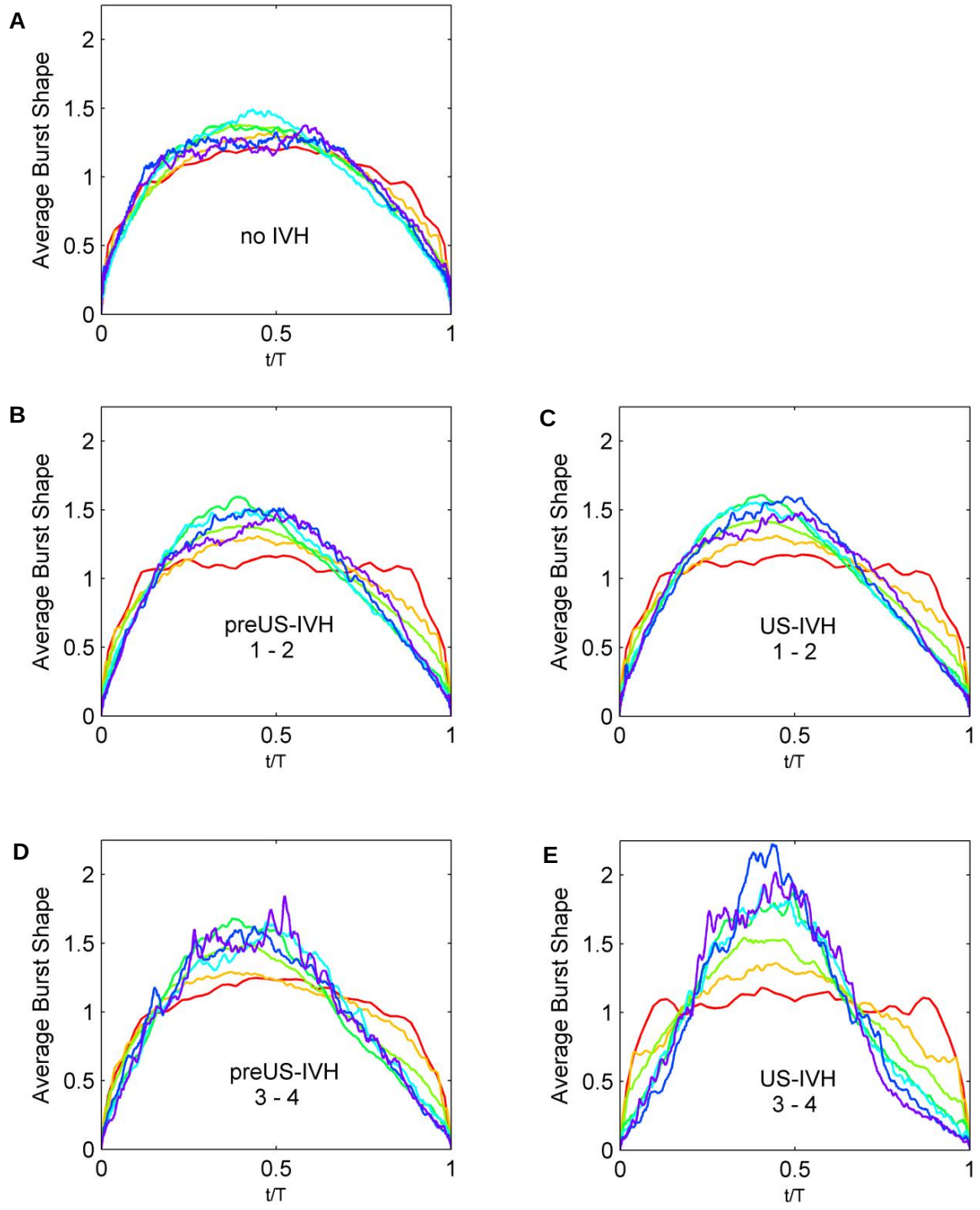

Figure 6.4 - Differences in average burst shape across burst durations for infants with no IVH compared to preUS-IVH and US-IVH. Color coding of burst duration (200 ms – 6 s) as per Figure 1. (A) Grand average burst shape of all infants with no IVH: Short and long bursts have similar symmetry and sharpness. (B) Infants classified as mild-moderate exhibit changes in average burst shape preUS-IVH over these burst durations hours before (C) presenting with grade 1 or 2 IVH. The onset of more severe hemorrhage is significantly noticeable in grand average shape features in infants (D) preUS-IVH and (E) US-IVH grades 3 or 4.

6.3.2 DIAGNOSTIC ACCURACY OF BURST SHAPE METRICS

Statistical comparison of burst shapes between the three groups - no IVH, mild-moderate IVH 1-2, and severe IVH 3-4 – showed that bursts in the IVH infants were significantly sharper (higher *K*) at most burst durations (Fig. 6.5A). Mean *K* values for bursts longer than 2 seconds differed markedly between no IVH and IVH epochs (preUS-IVH: F=22.23, $p=6.5x10^{-5}$, US-IVH:F=22.25, $p=8.5x10^{-5}$, Fig. 6.5B). We also observed that asymmetry (Σ) of mid-duration bursts (1 s-3.5 s) differed significantly between IVH infants versus no IVH infants (Fig. 6.5D). The difference in longer bursts (>2 s duration) was statistically significant between preUS-IVH and US-IVH infants when contrasted with no IVH infants (preUS-IVH: F=6.91, p=0.014, US-IVH: F=24.01, $p=5.23x10^{-5}$, Fig. 6.5E), indicating that IVH infants tend to have more asymmetric bursts. No significant difference was seen in Σ values between IVH severity grades (F=0.41, p=0.53).

The accuracy of burst shape metrics in identifying IVH was evaluated by use of receiver operating characteristics (ROC) for mean sharpness (*K*) (Fig. 6.5C), and symmetry (Σ) derived from longer bursts (>2 s duration) (Fig. 6.5F). We combined IVH 1-2 and IVH 3-4 (injury positive) in both preUS-IVH and US-IVH groups and compared these infants to infants who did not develop IVH for each burst measure. The overall accuracy estimated by area under the curve (AUC) was high in both groups (0.83-0.94). Importantly, sensitivity was fairly high (>80% and >60% for *K* and Σ, respectively) at all cutoff levels. A modest increase in sensitivity comes at a high price of substantial loss in specificity.

We then tested systematically a range of *K* and Σ values for long bursts (>2 s duration), and found high sensitivity and specificity at selected cutoff levels for all preUS-IVH and IVH groups. Specifically, for this dataset, in both preUS-IVH and US-IVH groups we find that for K very high sensitivity and specificity values are found at a cutoff of -0.99 (for K ranging between -1.06 to -0.98). Similarly, for Σ, sensitivity and specificity in preUS-IVH and US-IVH groups also remains high at a cutoff of 0.13 (for Σ ranging between 0.12 to 0.16). The validity of our results are confirmed our reliability tests where the leave-one-out and added data permutation analyses reveal that for both K and Σ values, sensitivity and specificity remain consistently high (>80% for K and Σ). Table 6.2 summarizes the highest sensitivity and specificity values found in the ROC analysis, along with the reliability tests employed.

		preUS-IVH		US-IVH
ROC analysis	K:	88.2%,91%	K:	86.7%, 90.9%
	Σ:	82.4%, 81.8 %	Σ:	80%, 90.9%
Leave-one-out	K:	83%,90.3%	K:	88%, 90.3%
permutation	Σ:	83%, 88.2%	Σ:	81%, 92.3%
Added data	K:	80%,91.9%	K:	88%, 91.9%
permutation	Σ:	80%, 88.2%	Σ:	82%, 91.7%

Table 6.2 - Sensitivity and specificity for different cutoffs in mean sharpness (*K*) and mean asymmetry (Σ) to predict no IVH or IVH at any grade. The top row shows the sensitivity and specificity of our main test statistics.The middle row shows the average sensitivity and specificity if leaving out any one of the subjects we reported. The lower row shows the values if further infants without the reported effect are added.

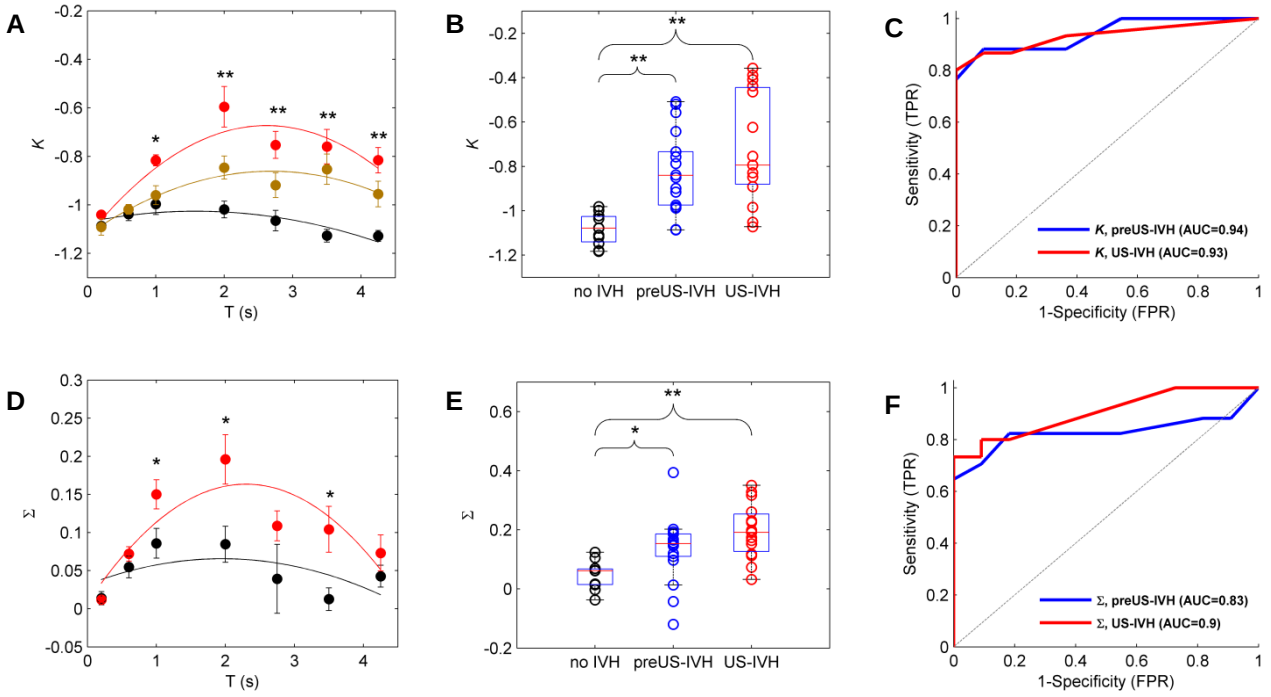

Figure 6.5 - Summary of statistical differences in burst features between infants with no IVH compared to those with any IVH grade. (* p<0.05; ** p<0.01). (A) Infants with no IVH (black) had lower mean *K* values over longer bursts than infants with IVH 1-2 (light brown) and IVH 3-4 (red). (B) Boxplots of no IVH (black circles) versus preUS-IVH (blue circles) and US-IVH (red circles) for mean values of *K* longer than 2 seconds, where open colored circles indicate individual data points. (C) ROC curves showing true positive rates (TPR) and false positive rates (FPR) for mean *K* derived from bursts >2 s in infants pre-IVH (yellow) and IVH (red); the Area Under Curve (AUC) values suggest a high predictive value. (D) Infants with no IVH (black) had lower mean Σ values over longer bursts as compared to infants with IVH (red). Error bars denote ±SEM. Solid curves are parabolic fits. (E) Boxplots of no IVH (black circles) versus preUS-IVH (blue circles) and US-IVH (red circles) for mean values of Σ longer than 2 seconds, where open colored circles indicate individual data points. (F) ROC curves for mean Σ for bursts >2 s for all grades of pre-IVH (yellow) and IVH (red) with the respective AUC values.

The combination of *K* and Σ values for long bursts (>2 s duration) were further tested by a method of classification in logistic regression model. In combining both burst features an even more accurate predictor is achieved, where for preUS-IVH and US-IVH, AUC values were 0.95 and 0.97.

The improvement in sensitivity and specificity suggests that edge cases (previously misclassified infants) were now detected by the combination of burst variables.

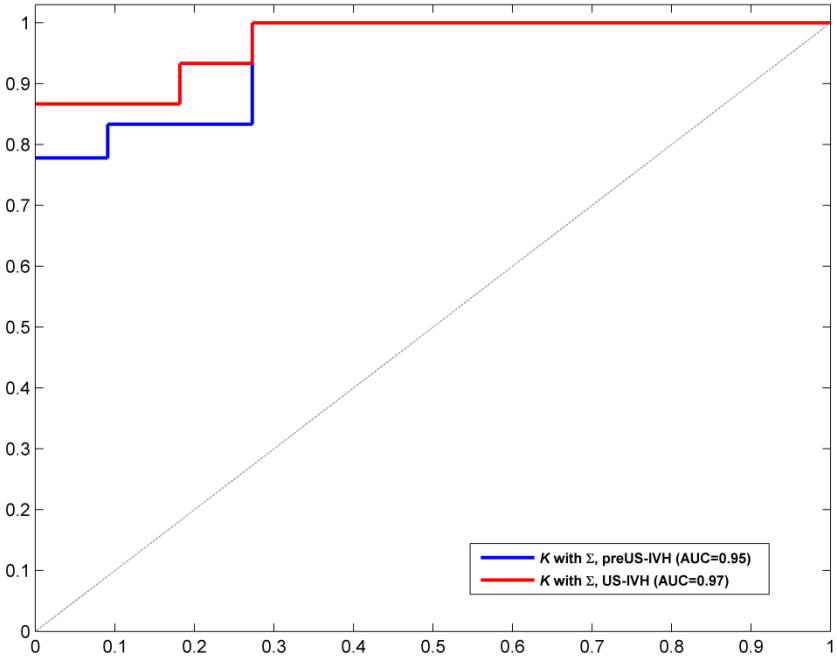

Figure 6.6 – Classification via logistic regression of burst sharpness (K) and skew values (Σ) values.

6.4 DISCUSSION

In this chapter we demonstrate that two novel features of early cortical activity in extremely preterm infants - burst shape and asymmetry - are sensitive indicators of intraventricular hemorrhage. Cortical burst shapes can be rapidly and automatically analyzed from continuously recorded EEG data: the presently used metrics are thus readily translatable back into the clinical setting. This study also shows a high diagnostic accuracy for identifying preterm IVH. Together, these findings hold promise for the everyday clinical challenge of real-time detection of impending IVH in extremely preterm infants and build on the prediction of long-term outcomes in Chapter 5.

Prior studies of EEG abnormalities in the presence of vascular lesions have focused on late EEG features, particularly the presence of positive rolandic sharp waves (PRS) (Clancy et al. 1984; A Okumura et al. 1999). These PRS waves are identified as sharp, discrete transients of short duration (≤400 ms), which provide a relatively reliable sign of previously experienced IVH and white matter injury. The overall levels of early aEEG/EEG activity were recently shown to be associated with early brain injury (Bowen et al. 2010; Chalak et al. 2011; Hellström-Westas et al. 2001; Akihisa Okumura et al. 2002; Olischar et al. 2007)' . Our objective and patient-wise adaptive analysis method found no significant quantitative differences between study groups in the conventional measures used in studies of aEEG markers during acute IVH, namely IBI and burst count. However, average burst shapes were significantly sharper and more asymmetric during the onset and occurrence of IVH as compared to infants without IVH. This suggests that the study of burst morphology in EEG may reflect disturbances in cortical activity prior to and during acute brain injury.

The observed changes in cortical burst shapes offer new insights into developmental neurobiology. Recent advances in experimental animal models have established that the early preterm EEG bursts are cortical events, spontaneous activity transients (SATs (Vanhatalo et al. 2005)), that play a crucial role in both neuronal survival and guidance of emerging network growth (Colonnese and Khazipov 2012; Hanganu-Opatz 2010). Studies in both animals (Brockmann et al. 2011; Colonnese and Khazipov 2012; Kilb et al. 2011) and humans(Omidvarnia et al. 2013) have shown that these events bind brain areas together, a necessary activity-dependent developmental mechanism for the developing brain connectome (Rubinov et al. 2009; L. I. Zhang and Poo 2001). It has also been demonstrated that the subplate layer in the developing cortex is responsible for orchestrating early cortical activity transients (Dupont et al. 2005). These mechanisms offer a potential developmental context to our finding - burst shapes were found to be most informative in the most severe, parenchymal brain lesions that extend to subplate or its vicinity (i.e., IVH grades 3-4). A change in the shape of scalp EEG bursts to sharper and leftward asymmetric forms could arise from a

compromised subplate function, or from lesions in cortico-cortical tracts in the white matter, both of which may render cortical bursts more focal. This complements the analysis in Chapter 3 where burst shapes may also arise from compromises in metabolic resources - a likely scenario at, or around the time of the occurrence of intra-ventricular hemorrhage.

Prior to routine clinical implementation, the methodology employed in this study requires validation from larger, independent patient cohorts that are monitored with EEG for several days after birth, with detailed accounts of clinical treatment, complications, outcome and other co-morbidities. Such studies, for example, would allow further confirmation of whether the current EEG metrics reveal as-yet–unmeasured existing IVH or are sensitive to precursors that predict the onset of IVH itself. For example, this could be achieved using frequent repeated ultrasounds. Therefore, larger data cohorts need to be targeted in confirming the utility of burst sharpness in EEG as a sensitive indicator of IVH. A larger cohort size necessitates a multicenter study or, optimally, sourcing existing datasets with similar data quality, clinical details, outcome related information.

Our present method offers possible solutions for common challenges in clinical applications of this kind in the neonatal intensive care environment. A particular technical advantage is that our method analyzes extracted EEG events (bursts) without a need for continuous, uninterrupted streams of EEG signal. This allows automated selection of sufficient quality, artifact-free EEG epochs, without compromising analytical reliability. Hence, our burst-shape metrics will allow reliable diagnostics derived from EEG monitoring, even during NICU treatment where EEG records are frequently prone to disruption by clinical care artifacts, which are a particular weakness of currently available algorithms for NICU EEG monitoring.

In conclusion, we demonstrate that burst shape and burst asymmetry in the early EEG are indicators of IVH in extremely preterm infants as soon as 12 hours after birth,. Early and accurate identification of abnormal burst shape and asymmetry may enable timely identification of infants at high risk for developing IVH, and may thus contribute to an increased understanding of pathophysiological mechanisms associated with IVH and targeted neuroprotective strategies.

7.0 GENERAL DISCUSSION AND CONCLUSIONS

7.1 OVERVIEW OF THE CONCLUSIONS OF THESIS

In this thesis, novel methods were developed to predict clinical outcome from neonatal brain activity soon after birth. The overarching message for this body of work is that the cortical activity of the neonate brain has inherently rich temporal structures, with cortical bursts belong to a widely occurring class of dynamics known as scale-free processes. Significantly, we find that scale-free burst dynamics yield predictive properties towards eventual neurodevelopmental outcome. These properties provide critical insight into fundamental neurophysiological mechanisms, such as constraints to metabolic supply and the development of cortical pathways.

Through a series of data driven cohort studies, this thesis addresses its principle aims and objectives in two neonate data cohorts: 1) term hypoxia, and 2) preterm birth. Here we revisit the aims and objectives in summarizing the insights provided by Chapter 2:

- To identify stochastic processes present in neonatal brain activity following full-term hypoxia through a detailed statistical characterization;
- To objectively extract signatures of bursts of cortical activity measured via the neonatal electroencephalogram (EEG) in full-term hypoxic and preterm neonates;
- To combine detailed statistical characterization and signatures of bursting cortical activity in order to predict clinical outcome in neonates.

In Chapter 3, I characterized the temporal information present during burst suppression in term hypoxic neonates. The statistical characterization of early brain activity is vital to its overall interpretation due its complex, stochastic nature. In utilizing a data-driven approach for thresholding data and extracting bursts, statistical distributions of burst durations and their sizes were found to be heavy tailed with power-law scaling regimes – a feature that is most commonly observed in physical systems. Next, exponents of burst size and duration were interrelated to reveal a fundamentally scale-free system operating near criticality. Significantly, I developed a novel method for characterizing the bursts during burst suppression to derive cortical signatures of recovery. The theory of crackling noise was linked to burst suppression, providing insight into how

neuronal resources are utilized following a period of complete quiescence. In analyzing average burst shapes at different time scales, burst suppression at longer time scales was found to have leftward asymmetry. Notably, as the neonates recover, there is a shift towards symmetrical bursting patterns at longer time scales, suggestive of a more scale invariant burst morphology. The findings of this chapter assert that bursts yield clinically informative properties in monitoring recovery of a hypoxic neonate. Thus, characterization of burst suppression data through empirical distribution functions from neonate EEG data yield closer approximations of underlying cortical behavior hours after birth. Further, the use of average burst shapes help identify cortical signatures of the neonate brain and understand the mechanisms involved in metabolic depletion.

In Chapter 4, I demonstrated the measure of scaling exponents from statistical distributions in post-hypoxia full-term infants in burst suppression to predict long-term clinical outcome following asphyxia. The provision of clinical hypothermia greatly affects the nature and interpretation of bedside EEG. Exponents of burst duration and burst size during early burst suppression were found to correlate significantly with neurodevelopmental findings at two years of age. Furthermore, this study steers away from previously conventional methods of burst suppression analysis, such as mean burst durations and inter-burst intervals. Hence, the scaling relationships of burst durations and sizes are vitally important to determining good and poor outcomes during post-hypoxic burst suppression.

In Chapter 5, I applied methods developed in Chapter 3 to demonstrate their utility in predicting long-term neurodevelopmental outcomes in extremely preterm infants. Early brain activity of the preterm, when normal gestation is interrupted, is inherently scale-free providing insight into cortical activity in the presence of immature cortical pathways. Specifically, scale-free properties of cortical bursts durations, their sizes and shapes are predictive of long term neurodevelopment outcomes. A combination of gestational age and scale-free burst variables provide a highly sensitive test in pre-empting neurocognitive outcome, i.e. Mental Development Index (MDI) at 2 years of age. Notably, this chapter first highlights the crucial temporal transitions in postnatal EEG burst statistics as early as 12 hours after birth, wherein gestational age plays a moderating role in influencing brain behavior and eventual outcome.

Chapter 6 shifts focus from long-term outcomes to acute injury observed in intensive care. This study revealed critical signatures of cortical bursts to predict the onset of acute brain haemorrhage in extremely preterm infants. Bedside monitoring of neonatal EEG in intensive care can be further complemented by measures of average burst shapes, irrespective of gestational age, to detect the early intraventricular haemorrhage. This chapter identifies significant change in cortical bursts via analyzing burst shapes across increasing burst durations, as opposed to conventional counts of bursts and inter-burst intervals. Furthermore, classification via a sensitivity and specificity analysis

reveals high true positive rates and low false positive rates: an important step in predicting acute brain injury in at-risk neonates.

Thus in summary, in both full-term HIE and preterm infants, early identification and characterization (within the first 72 hours) of poor neuropathology provides a significant time advantage in potentially informing types of clinical treatment. In future trials, analysis techniques such as those presented in this thesis may influence short-term treatment (i.e. use of anti-convulsant medication and hypothermia treatment). For long-term outcomes, EEG correlated with later imaging analysis may identify those infants at-risk of poor neurodevelopment in early childhood. Furthermore, early or interrupted birth of a newborn results in poor homeostatic control and maintenance of biochemical pathways (as highlighted in Chapter 2), resulting in multiple neuronal damage effects. In this aspect, the studies in the thesis (Chapters 3 to 6) focus primarily on utilizing EEG burst analysis at bedside in the first 72 hours to reveal these potential post-birth risk factors, of which some are potentially treatable (via metabolic replenishment and management).

7.2 CONTRIBUTIONS OF THIS THESIS

This thesis combines principles of physical systems and neuroscience with neonatal brain activity recordings to present an integration of novel methods in predicting clinical outcome soon after birth. Specifically, the techniques detailed in this work and cohort studies presented have been subjected to stringent statistical characterization and validation. Moreover, in identifying clinically relevant features of early brain activity, this thesis offers a data-driven approach to bedside monitoring of neonates.

In revisiting the key hypotheses presented, the contributions of this thesis to the field of neuroscience are:

1) Neonatal brain activity exhibits inherently scale-free processes; a ubiquitous signature of natural systems

Following term hypoxia and/or preterm birth, the statistical distributions of single-channel neonatal electroencephalographic data reveal inherently scale-free, exponentially truncated power-law regimes. As a neonate transitions from abnormal EEG towards a normal, continuous cortical activity pattern, these scale-free processes become shorter-ranged and sharply truncated, indicative of a system undergoing critical phase transitions following birth.

2) Scale-free behavior arising from neonate brain activity is consistent with systems that exhibit criticality and a more complex form of stochastic behavior known as crackling noise

In the term hypoxic brain I established that scaling relationships of cortical burst durations and their sizes, confirm a system consistent with criticality. Scaling relationships of cortical bursts in preterm brain activity are also consistent with a system that exhibits critical features, with robust scale-free processes. However, evidence suggests that although the statistical distributions of activity in the preterm brain are scale-free the activity does not meet exact criteria for criticality, instead displaying scale-specific changes in cortical bursting behavior. The presence of crackling noise elucidates upon fundamental mechanisms such as the self-organization of cortical bursts and neuronal resource constraints present following birth.

3) Properties of crackling noise in the neonate brain are inextricably linked with neurobiological processes, such as metabolic constraint and cortical pathway development

This thesis provides a significant contribution to identifying signatures of cortical activity via the analysis of average burst shapes in neonate EEG soon after birth. Here, properties of cortical bursts in both term hypoxic and preterm infants have state-dependant effects which speak to underlying neurobiological processes. Specifically, average burst shapes suggest a phase transition towards the resumption of healthy cortical activity following hypoxia, which reflects a fundamental reorganization of metabolic supply. In the preterm, average burst shapes correlate with gestational age and acute brain injury, reflecting an immature cortical network during recovery.

Furthermore, the contributions of this thesis to the field of neonatal brain monitoring are:

4) Characterizing early neonate brain activity through analysis of scale-free and crackling noise dynamics yields highly predictive properties for potential neurodevelopmental outcomes.

This thesis identifies a direct clinical utility for extracting scale-free distributions and properties of crackling noise from neonate EEG data. Notably, scaling relationships of cortical bursts and average burst shapes aid in delineating between abnormal from healthy cortical signatures. This is a novel contribution in clinically classifying at-risk neonate populations such as term hypoxic and preterm infants. The methods detailed in this thesis provide a translatable approach in the automated analysis of bedside EEG. This approach potentially guides the clinician in predicting the risk for acute brain injury and long-term neurodevelopmental outcomes during neonatal intensive care.

7.3 CONCLUDING REMARKS AND FUTURE WORK

There are specific areas of this thesis that warrant future work. For this dissertation I focused primarily on routinely used biparietal electrode derivations of EEG data. From a statistical point of view, in Chapter 3, empirical distribution functions of bursts could be compared with detrended fluctuation analysis, a technique used to identify long-range correlations in time series of adult EEG (Linkenkaer-Hansen et al. 2001; Palva et al. 2013). Long-range correlations and spatial evolution of cortical bursting would likely be informative in improving understanding of abnormal cortical activity patterns. Here, an understanding of global and focal cortical connections in the neonate could be enhanced by source localization analysis (Roche-Labarbe et al. 2008) and functional connectivity of resting-state networks (Omidvarnia et al. 2013). Moreover, given that scale-specific phase transitions are observed in temporal EEG data, increased spatial topology could further motivate an understanding for traveling wave mechanisms, changes in power-law scaling and cortical burst propagation (Nunez and Srinivasan 2014; Patten et al. 2012). It is important to note however that characterization of spatiotemporal dynamics in the neonate requires a far denser array of scalp electrodes than is usually used in neonatal intensive care settings (Odabaee et al. 2013).

In examining selected periods of postnatal EEG after birth, this thesis identifies heterogeneous burst scaling regimes which require investigation. Through calculating average burst shapes, we establish the change in burst dynamics between abnormal states of activity (pathological or preterm) and healthier states (continuous, rhythmic EEG). Reliability analyses conducted in each study revealed that within a minimum of 20 minutes, EEG epochs produce reliable numbers of bursts which can be robustly characterized with the calculation of average burst shapes. Future measures of reliability need to recapitulate criticality theory with the variations in burst shapes, in particular bursts at short time scales which show the greatest variability (< 1 s). In this regard, it may be useful to employ measures which are targeted towards identifying fast frequency activity in conjunction with average burst shape analysis (Palmu et al. 2010; Palmu 2015). To formally understand the mechanisms of recovery, specifically how neurobiological processes speak to metabolic replenishment and cortical pathway development, more continuous streams of data are required for analysis. Here, recordings of animal models, such as prolonged hypoxia effects in piglet EEG (Nakamura et al. 2013; D. Zhang et al. 2012), could be used to further establish the effects of oxygen deprivation, hemodynamic blood flow contributing to abnormal cortical activity patterns, such as burst suppression.

In chapter 3, a phenomenological model for burst generation was used, whereby sequences of alternating bursts and suppression were not explicitly modelled. This type of modelling provides a practical yet mechanistic interpretation of how energy is transformed and maintained, drawing

parallels with velocities of ferromagnetic domains (Zapperi et al. 2005). Ideally, model-driven approaches such as a bifurcation analysis could build upon previously detailed neuronal models of the cortex, further elucidating upon activity ranging between microscopic and macroscopic scales (Breakspear et al. 2006; Da Silva et al. 2003; Freyer et al. 2009; J. Roberts and Robinson 2012; Victor et al. 2011). The presence of large-scale dynamics, such as the types of temporal EEG analyzed in this thesis, requires a large scale model such as a mean field approach to effectively capture and track the changes in recovery of brain activity. Furthermore, a more insightful method would investigate coupling between variables of metabolic supply and neuronal activity to better understand newborn neuropathology. Currently identified metabolic variables such as oxygen availability and ion (Na^+/K^+, Cl^-) concentrations have shown to be coupled with the cortical excitability of neurons (Cressman Jr et al. 2009; Hajos et al. 2009; Ivanov and Zilberter 2011). Furthermore, the hypothesis of this model would be to assert the mutual coupling between brain dynamics and metabolic function. Thus, formal, unifying approaches to neural computational modelling will ultimately inform our understanding of early neurophysiological drive and brain health, providing a more sophisticated framework for empirical interpretation (J. W. Brown 2014).

From a clinical context, cohort studies presented in chapters 5 through to 7 have potential avenues for future work. Identifying larger neonatal populations of EEG data following birth asphyxia and preterm birth would assist in building a strong and identifying case for the predictive utility of methods applied. Prospective studies could be used to identify the critical time windows in which signatures of electrical bursts, such as burst shape and scaling, in combination with interburst interval detection are most predictive of outcome (Matic et al. 2014). Furthermore, testing this study's methodology in prospective cohorts would provide an indication of diagnostic efficacy during bedside monitoring. The promise of such trials include a more rapid and robust characterization of burst and interburst activity, which for short-term management could be used to trigger a cranial ultrasound for IVH identification or in the long-term indicate likely neurodevelopmental outcomes. Moreover, such studies would provide a more sensitive test of background EEG abnormality that may temporally precede current monitoring methods, e.g. brain imaging via ultrasound or MRI. Importantly, the use of these methods would provide highly focused EEG metrics based on relatively short epochs of data (between 30-60 minutes), rather than hours of continuously recorded EEG (which are then subjected to laborious visual assessment), enabling these prospective study designs.

Further validation of current techniques should also exploit existing clinical datasets. In this respect, potential EEG datasets from multicentre trials similar to the neonate populations analyzed in this thesis have been identified for future collaboration. These datasets have collected neonate brain activity with other bedside monitored signals such as cardiorespiratory response (e.g. heart rate,

CO_2, respiratory function. The proposed hypotheses in both full-term hypoxic infants and preterm infants would be the evolution of scale-free dynamics during impaired cardiorespiratory response and its link with short-term outcomes and pathophysiology. Moreover, subtle nuances of neonate EEG such as sleep patterns (REM, non-REM) and characterization of salient cortical patterns such as seizure activity, i.e. status epilepticus, will yield more informative markers of brain health and outcome prediction. Other routinely monitored bedside monitoring such as electrocardiograms (ECG/EKG) and respiration rate may elucidate upon the link between cardiorespiratory drive and neuronal dynamics, i.e. heart-rate variability with associated changes to neonate EEG (Massaro et al. 2014; Matić et al. 2013). These types of analysis will further reveal insights into how scale-free dynamics are linked to core neurophysiological processes, including how energy resources are managed in early electroencephalographic patterns of at-risk newborns.

To conclude, in this body of work I have demonstrated that universal scaling properties which are found in naturally occurring phenomena, such as earthquakes and avalanches, exist in the neonate brain soon after birth. Notably, early cortical activity signatures are fundamentally scale-free and consistent with systems undergoing critical phase transitions. These transitions are scale-specific and temporally evolving as a neonate recovers - providing evidence of underlying neurobiological processes in the early human brain. Significantly, clinically informative properties can be readily extracted from single-channel derivations of neonatal electroencephalography, allowing for a prediction of neurodevelopmental outcomes. Thus, the applications for the novel methods presented in this thesis extend toward the bedside monitoring of at-risk neonates, and further, the potential for guided postnatal treatment and management.

REFERENCES

Aarnoudse-Moens, Cornelieke Sandrine Hanan, Weisglas-Kuperus, Nynke, van Goudoever, Johannes Bernard, and Oosterlaan, Jaap (2009), 'Meta-analysis of neurobehavioral outcomes in very preterm and/or very low birth weight children', *Pediatrics,* 124 (2), 717-28.

Abend, Nicholas S and Licht, Daniel J (2008), 'Predicting outcome in children with hypoxic ischemic encephalopathy', *Pediatric Critical Care Medicine,* 9 (1), 32-39.

Aburn, Matthew J, Holmes, CA, Roberts, James A, Boonstra, Tjeerd W, and Breakspear, Michael (2012), 'Critical fluctuations in cortical models near instability', *Frontiers in physiology,* 3.

Alderliesten, Thomas, Nikkels, Peter GJ, Benders, Manon JNL, de Vries, Linda S, and Groenendaal, Floris (2013), 'Antemortem cranial MRI compared with postmortem histopathologic examination of the brain in term infants with neonatal encephalopathy following perinatal asphyxia', *Archives of Disease in Childhood-Fetal and Neonatal Edition,* 98 (4), F304-F09.

Amzica, Florin (2009), 'Basic physiology of burst-suppression', *Epilepsia,* 50 (s12), 38-39.

André, Monique, Lamblin, M-D, d'Allest, Anne-Marie, Curzi-Dascalova, Lilia, Moussalli-Salefranque, F, Nguyen The Tich, S, Vecchierini-Blineau, M-F, Wallois, F, Walls-Esquivel, E, and Plouin, P (2010), 'Electroencephalography in premature and full-term infants. Developmental features and glossary', *Neurophysiologie Clinique/Clinical Neurophysiology,* 40 (2), 59-124.

Arnold, Matthias, Doering, Axel, Witte, Herbert, Dörschel, Jens, and Eisel, Michael (1996), 'Use of adaptive Hilbert transformation for EEG segmentation and calculation of instantaneous respiration rate in neonates', *Journal of clinical monitoring,* 12 (1), 43-60.

Aso, Kosaburo, Abdab-Barmada, Mamdouha, and Scher, Mark S (1993), 'EEG and the neuropathology in premature neonates with intraventricular hemorrhage', *Journal of Clinical Neurophysiology,* 10 (3), 304-13.

Back, Stephen A and Miller, Steven P (2014), 'Brain injury in premature neonates: A primary cerebral dysmaturation disorder?', *Annals of neurology,* 75 (4), 469-86.

Bada, Henrietta S, Hajjar, Waleed, Chua, Carlos, and Sumner, David S (1979), 'Noninvasive diagnosis of neonatal asphyxia and intraventricular hemorrhage by Doppler ultrasound', *The Journal of pediatrics,* 95 (5), 775-79.

Badawi, Nadia, Kurinczuk, Jennifer J, Keogh, John M, Alessandri, Louisa M, O'Sullivan, Fiona, Burton, Paul R, Pemberton, Patrick J, and Stanley, Fiona J (1998), 'Antepartum risk factors for newborn encephalopathy: the Western Australian case-control study', *Bmj,* 317 (7172), 1549-53.

Bak, Per and Tang, Chao (1989), 'Earthquakes as a self-organized critical phenomenon', *Journal of Geophysical Research: Solid Earth (1978–2012),* 94 (B11), 15635-37.

Bak, Per, Tang, Chao, and Wiesenfeld, Kurt (1987), 'Self-organized criticality: An explanation of the 1/f noise', *Physical Review Letters,* 59 (4), 381-84.

Baldassarri, Andrea, Colaiori, Francesca, and Castellano, Claudio (2003), 'Average shape of a fluctuation: Universality in excursions of stochastic processes', *Physical Review Letters*, 90 (6), 060601.

Ballabh, Praveen (2010), 'Intraventricular hemorrhage in premature infants: mechanism of disease', *Pediatric research*, 67 (1), 1-8.

--- (2014), 'Pathogenesis and Prevention of Intraventricular Hemorrhage', *Clinics in perinatology*, 41 (1), 47-67.

Beck, Stacy, Wojdyla, Daniel, Say, Lale, Betran, Ana Pilar, Merialdi, Mario, Requejo, Jennifer Harris, Rubens, Craig, Menon, Ramkumar, and Van Look, Paul FA (2010), 'The worldwide incidence of preterm birth: a systematic review of maternal mortality and morbidity', *Bulletin of the World Health Organization*, 88 (1), 31-38.

Beggs, John M and Plenz, Dietmar (2003), 'Neuronal avalanches in neocortical circuits', *The Journal of Neuroscience*, 23 (35), 11167-77.

Beggs, John M and Timme, Nicholas (2012), 'Being critical of criticality in the brain', *Frontiers in physiology*, 3.

Bell, Angela H, McClure, BG, McCullagh, PJ, and McClelland, RJ (1991), 'Variation in power spectral analysis of the EEG with gestational age', *Journal of Clinical Neurophysiology*, 8 (3), 312-19.

Ben-Ari, Yehezkel (2001), 'Developing networks play a similar melody', *Trends in neurosciences*, 24 (6), 353-60.

Benayoun, Marc, Cowan, Jack D, van Drongelen, Wim, and Wallace, Edward (2010), 'Avalanches in a stochastic model of spiking neurons', *PLoS computational biology*, 6 (7), e1000846.

Benders, Manon J, Palmu, Kirsi, Menache, Caroline, Borradori-Tolsa, Cristina, Lazeyras, Francois, Sizonenko, Stephane, Dubois, Jessica, Vanhatalo, Sampsa, and Hüppi, Petra S (2014), 'Early Brain Activity Relates to Subsequent Brain Growth in Premature Infants', *Cerebral Cortex*, bhu097.

Bhattacharyya, Sourya, Biswas, Arunava, Mukherjee, Jayanta, Majumdar, Arun Kumar, Majumdar, Bandana, Mukherjee, Suchandra, and Singh, Arun Kumar (2011), 'Feature selection for automatic burst detection in neonatal electroencephalogram', *Emerging and Selected Topics in Circuits and Systems, IEEE Journal on*, 1 (4), 469-79.

Birkeland, KW and Landry, CC (2002), 'Power-laws and snow avalanches', *Geophysical Research Letters*, 29 (11), 49-1-49-3.

Blankenship, Aaron G and Feller, Marla B (2009), 'Mechanisms underlying spontaneous patterned activity in developing neural circuits', *Nature Reviews Neuroscience*, 11 (1), 18-29.

Blencowe, Hannah, Cousens, Simon, Oestergaard, Mikkel Z, Chou, Doris, Moller, Ann-Beth, Narwal, Rajesh, Adler, Alma, Vera Garcia, Claudia, Rohde, Sarah, and Say, Lale (2012), 'National, regional, and worldwide estimates of preterm birth rates in the year 2010 with time trends since 1990 for selected countries: a systematic analysis and implications', *The Lancet*, 379 (9832), 2162-72.

Bolisetty, Srinivas, Dhawan, Anjali, Abdel-Latif, Mohamed, Bajuk, Barbara, Stack, Jacqueline, and Lui, Kei (2014), 'Intraventricular hemorrhage and neurodevelopmental outcomes in extreme preterm infants', *Pediatrics,* 133 (1), 55-62.

Bonifacio, Sonia L, Glass, Hannah C, Peloquin, Susan, and Ferriero, Donna M (2011), 'A new neurological focus in neonatal intensive care', *Nature Reviews Neurology,* 7 (9), 485-94.

Bourgeois, JP (1997), 'Synaptogenesis, heterochrony and epigenesis in the mammalian neocortex', *Acta Paediatrica,* 86 (S422), 27-33.

Bowen, Jennifer R, Paradisis, Mary, and Shah, Dharmesh (2010), 'Decreased aEEG continuity and baseline variability in the first 48 hours of life associated with poor short-term outcome in neonates born before 29 weeks gestation', *Pediatric research,* 67 (5), 538-44.

BrainFacts.org (2014), *BrainFacts.org: Brain Development*. <http://www.brainfacts.org/~/media/Brainfacts/Article%20Multimedia/Brain%20Basics/Brain%20Development/BrainDevt.ashx>.

Brandon Westover, M, Shafi, Mouhsin M, Ching, ShiNung, Chemali, Jessica J, Purdon, Patrick L, Cash, Sydney S, and Brown, Emery N (2013), 'Real-time segmentation of burst suppression patterns in critical care EEG monitoring', *Journal of neuroscience methods,* 219 (1), 131-41.

Breakspear, M, Roberts, JA, Terry, John R, Rodrigues, S, Mahant, N, and Robinson, PA (2006), 'A unifying explanation of primary generalized seizures through nonlinear brain modeling and bifurcation analysis', *Cerebral Cortex,* 16 (9), 1296-313.

Brenner, RP, Schwartzman, RJ, and Richey, ET (1975), 'Prognostic significance of episodic low amplitude or relatively isoelectric EEG patterns', *Diseases of the nervous system,* 36 (10), 582-87.

Brockmann, Marco D, Pöschel, Beatrice, Cichon, Nicole, and Hanganu-Opatz, Ileana L (2011), 'Coupled oscillations mediate directed interactions between prefrontal cortex and hippocampus of the neonatal rat', *Neuron,* 71 (2), 332-47.

Brown, Hilary K, Speechley, Kathy Nixon, Macnab, Jennifer, Natale, Renato, and Campbell, M Karen (2013), 'Neonatal morbidity associated with late preterm and early term birth: the roles of gestational age and biological determinants of preterm birth', *International journal of epidemiology*, dyt251.

Brown, Joshua W (2014), 'The tale of the neuroscientists and the computer: why mechanistic theory matters', *Frontiers in neuroscience,* 8.

Bryce, Jennifer, Boschi-Pinto, Cynthia, Shibuya, Kenji, and Black, Robert E (2005), 'WHO estimates of the causes of death in children', *The Lancet,* 365 (9465), 1147-52.

Callaghan, William M, MacDorman, Marian F, Rasmussen, Sonja A, Qin, Cheng, and Lackritz, Eve M (2006), 'The contribution of preterm birth to infant mortality rates in the United States', *Pediatrics,* 118 (4), 1566-73.

Catalano, Susan M and Shatz, Carla J (1998), 'Activity-dependent cortical target selection by thalamic axons', *Science,* 281 (5376), 559-62.

Chalak, Lina F, Sikes, Natalie C, Mason, Melanie J, and Kaiser, Jeffrey R (2011), 'Low-voltage aEEG as predictor of intracranial hemorrhage in preterm infants', *Pediatric neurology,* 44 (5), 364-69.

Chialvo, Dante R (2010), 'Emergent complex neural dynamics', *Nature Physics,* 6 (10), 744-50.

Ching, ShiNung, Purdon, Patrick L, Vijayan, Sujith, Kopell, Nancy J, and Brown, Emery N (2012), 'A neurophysiological–metabolic model for burst suppression', *Proceedings of the National Academy of Sciences,* 109 (8), 3095-100.

Clancy, Robert R, Tharp, Barry R, and Enzman, Dieter (1984), 'EEG in premature infants with intraventricular hemorrhage', *Neurology,* 34 (5), 583-83.

Clauset, Aaron, Shalizi, Cosma Rohilla, and Newman, Mark EJ (2009), 'Power-law distributions in empirical data', *SIAM review,* 51 (4), 661-703.

Colaiori, Francesca (2008), 'Exactly solvable model of avalanches dynamics for Barkhausen crackling noise', *Advances in Physics,* 57 (4), 287-359.

Colaiori, Francesca, Baldassarri, Andrea, and Castellano, Claudio (2004), 'Average trajectory of returning walks', *Physical Review E,* 69 (4), 041105.

Colonnese, Matthew and Khazipov, Rustem (2012), 'Spontaneous activity in developing sensory circuits: implications for resting state fMRI', *Neuroimage,* 62 (4), 2212-21.

Cowan, Frances, Rutherford, Mary, Groenendaal, Floris, Eken, Paula, Mercuri, Eugenio, Bydder, Graeme M, Meiners, Linda C, Dubowitz, Lilly, and de Vries, Linda S (2003), 'Origin and timing of brain lesions in term infants with neonatal encephalopathy', *The Lancet,* 361 (9359), 736-42.

Cressman Jr, John R, Ullah, Ghanim, Ziburkus, Jokubas, Schiff, Steven J, and Barreto, Ernest (2009), 'The influence of sodium and potassium dynamics on excitability, seizures, and the stability of persistent states: I. Single neuron dynamics', *Journal of computational neuroscience,* 26 (2), 159-70.

Da Silva, Fernando Lopes, Blanes, Wouter, Kalitzin, Stiliyan N, Parra, Jaime, Suffczynski, Piotr, and Velis, Demetrios N (2003), 'Epilepsies as dynamical diseases of brain systems: basic models of the transition between normal and epileptic activity', *Epilepsia,* 44 (s12), 72-83.

de Arcangelis, Lucilla, Perrone-Capano, Carla, and Herrmann, Hans J (2006), 'Self-organized criticality model for brain plasticity', *Physical review letters,* 96 (2), 028107.

Deluca, Anna and Corral, Álvaro (2013), 'Fitting and goodness-of-fit test of non-truncated and truncated power-law distributions', *Acta Geophysica,* 61 (6), 1351-94.

Dupont, Erwan, Hanganu, Ileana L, Kilb, Werner, Hirsch, Silke, and Luhmann, Heiko J (2005), 'Rapid developmental switch in the mechanisms driving early cortical columnar networks', *Nature,* 439 (7072), 79-83.

Eeg-Olofsson, Orvar (1980), 'Longitudinal developmental course of electrical activity of brain', *Brain and Development,* 2 (1), 33-44.

Eguiluz, Victor M, Chialvo, Dante R, Cecchi, Guillermo A, Baliki, Marwan, and Apkarian, A Vania (2005), 'Scale-free brain functional networks', *Physical review letters,* 94 (1), 018102.

Evans, AS Rigby, P. Hamilton, N. Titchiner, DMB Hall, K (2001), 'The relationships between neonatal encephalopathy and cerebral palsy: a cohort study', *Journal of Obstetrics & Gynecology*, 21 (2), 114-20.

Feldman, Ruth and Eidelman, Arthur I (2006), 'Neonatal state organization, neuromaturation, mother-infant interaction, and cognitive development in small-for-gestational-age premature infants', *Pediatrics*, 118 (3), e869-e78.

Fellman, Vineta and Raivio, Kari O (1997), 'Reperfusion injury as the mechanism of brain damage after perinatal asphyxia', *Pediatric research*, 41 (5), 599-606.

Flisberg, A, Kjellmer, I, Löfhede, J, Lindecrantz, Kaj, and Thordstein, M (2011), 'Prognostic capacity of automated quantification of suppression time in the EEG of post-asphyctic full-term neonates', *Acta Paediatrica*, 100 (10), 1338-43.

Fransson, Peter, Metsäranta, Marjo, Blennow, Mats, Åden, Ulrika, Lagercrantz, Hugo, and Vanhatalo, Sampsa (2013), 'Early development of spatial patterns of power-law frequency scaling in fMRI resting-state and EEG data in the newborn brain', *Cerebral cortex*, 23 (3), 638-46.

Frette, Vidar, Christensen, Kim, Malthe-Sørenssen, Anders, Feder, Jens, Jøssang, Torstein, and Meakin, Paul (1996), 'Avalanche dynamics in a pile of rice', *Nature*, 379 (6560), 49-52.

Freyer, Frank, Aquino, Kevin, Robinson, Peter A, Ritter, Petra, and Breakspear, Michael (2009), 'Bistability and non-Gaussian fluctuations in spontaneous cortical activity', *The Journal of Neuroscience*, 29 (26), 8512-24.

Friedman, Nir, Ito, Shinya, Brinkman, Braden AW, Shimono, Masanori, DeVille, RE Lee, Dahmen, Karin A, Beggs, John M, and Butler, Thomas C (2012), 'Universal critical dynamics in high resolution neuronal avalanche data', *Physical Review Letters*, 108 (20), 208102.

Fuller, Patrick M, Gooley, Joshua J, and Saper, Clifford B (2006), 'Neurobiology of the sleep-wake cycle: sleep architecture, circadian regulation, and regulatory feedback', *Journal of biological rhythms*, 21 (6), 482-93.

Gluckman, Peter D, Wyatt, John S, Azzopardi, Denis, Ballard, Roberta, Edwards, A David, Ferriero, Donna M, Polin, Richard A, Robertson, Charlene M, Thoresen, Marianne, and Whitelaw, Andrew (2005), 'Selective head cooling with mild systemic hypothermia after neonatal encephalopathy: multicentre randomised trial', *The Lancet*, 365 (9460), 663-70.

Goldenberg, Robert L, Culhane, Jennifer F, Iams, Jay D, and Romero, Roberto (2008), 'Epidemiology and causes of preterm birth', *The lancet*, 371 (9606), 75-84.

Graven, Stanley N and Browne, Joy V (2008), 'Sleep and brain development: the critical role of sleep in fetal and early neonatal brain development', *Newborn and Infant Nursing Reviews*, 8 (4), 173-79.

Greisen, G, Hellstrom-Westas, Lena, Lou, H, Rosén, Ingmar, and Svenningsen, NW (1987), 'EEG depression and germinal layer haemorrhage in the newborn', *Acta Paediatrica*, 76 (3), 519-25.

Greisen, Gorm and Børch, K (2001), 'White matter injury in the preterm neonate: the role of perfusion', *Developmental neuroscience*, 23 (3), 209-12.

Grigg-Damberger, Madeleine M, Coker, Steven B, Halsey, Carey L, and Anderson, Craig L (1989), 'Neonatal burst suppression: its developmental significance', *Pediatric Neurology,* 5 (2), 84-92.

Gutenberg, Beno and Richter, Charles F (1945), 'Seismicity of the earth (supplementary paper)', *Geological Society of America Bulletin,* 56 (6), 603-67.

Haimovici, Ariel, Tagliazucchi, Enzo, Balenzuela, Pablo, and Chialvo, Dante R. (2013), 'Brain Organization into Resting State Networks Emerges at Criticality on a Model of the Human Connectome', *Physical Review Letters,* 110 (17), 178101.

Hajos, Norbert, Ellender, Tommas J, Zemankovics, Rita, Mann, Edward O, Exley, Richard, Cragg, Stephanie J, Freund, Tamás F, and Paulsen, Ole (2009), 'Maintaining network activity in submerged hippocampal slices: importance of oxygen supply', *European Journal of Neuroscience,* 29 (2), 319-27.

Haldeman, Clayton and Beggs, John M (2005), 'Critical branching captures activity in living neural networks and maximizes the number of metastable states', *Physical review letters,* 94 (5), 058101.

Hallberg, B, Grossmann, K, Bartocci, M, and Blennow, M (2010), 'The prognostic value of early aEEG in asphyxiated infants undergoing systemic hypothermia treatment', *Acta Paediatrica,* 99 (4), 531-36.

Hanganu-Opatz, Ileana L (2010), 'Between molecules and experience: role of early patterns of coordinated activity for the development of cortical maps and sensory abilities', *Brain research reviews,* 64 (1), 160-76.

Hayakawa, Fumio, Okumura, Akihisa, Kato, Toru, Kuno, Kuniyoshi, and Watanabe, Kazuyoshi (1999), 'Determination of timing of brain injury in preterm infants with periventricular leukomalacia with serial neonatal electroencephalography', *Pediatrics,* 104 (5), 1077-81.

He, Biyu J (2014), 'Scale-free brain activity: past, present, and future', *Trends in cognitive sciences*.

He, Biyu J., Zempel, John M., Snyder, Abraham Z., and Raichle, Marcus E. (2010), 'The Temporal Structures and Functional Significance of Scale-free Brain Activity', *Neuron,* 66 (3), 353-69.

Hellström-Westas, Lena and Rosén, Ingmar (2005), 'Electroencephalography and brain damage in preterm infants', *Early human development,* 81 (3), 255-61.

--- (2006), 'Continuous brain-function monitoring: state of the art in clinical practice', *Seminars in Fetal and Neonatal Medicine* (11: Elsevier), 503-11.

Hellström-Westas, Lena, Rosén, Ingmar, and Svenningsen, NW (1991), 'Cerebral function monitoring during the first week of life in extremely small low birthweight (ESLBW) infants', *Neuropediatrics,* 22 (01), 27-32.

Hellström-Westas, Lena, De Vries, Linda S, and Rosén, Ingmar (2003), *An atlas of amplitude-integrated EEGs in the newborn* (Parthenon Publishing Group).

Hellström-Westas, Lena, Klette, H, Thorngren-Jerneck, Kristina, and Rosén, Ingmar (2001), 'Early prediction of outcome with aEEG in preterm infants with large intraventricular hemorrhages', *Neuropediatrics,* 32 (06), 319-24.

Herculano-Houzel, Suzana (2011), 'Scaling of brain metabolism with a fixed energy budget per neuron: implications for neuronal activity, plasticity and evolution', *PLoS One,* 6 (3), e17514.

Holmes, Gregory, Rowe, Jonelle, Hafford, James, Schmidt, Ruth, Testa, Marcia, and Zimmerman, Andrew (1982), 'Prognostic value of the electroencephalogram in neonatal asphyxia', *Electroencephalography and clinical neurophysiology,* 53 (1), 60-72.

Hull, J and Dodd, K (1992), 'Falling incidence of hypoxic-ischaemic encephalopathy in term infants', *BJOG: An International Journal of Obstetrics & Gynaecology,* 99 (5), 386-91.

Iadecola, Costantino and Nedergaard, Maiken (2007), 'Glial regulation of the cerebral microvasculature', *Nature neuroscience,* 10 (11), 1369-76.

Innocenti, Giorgio M and Price, David J (2005), 'Exuberance in the development of cortical networks', *Nature Reviews Neuroscience,* 6 (12), 955-65.

Ivanov, Anton and Zilberter, Yuri (2011), 'Critical state of energy metabolism in brain slices: the principal role of oxygen delivery and energy substrates in shaping neuronal activity', *Frontiers in neuroenergetics,* 3.

Iwasaki, N, Hamano, K, Okada, Y, Horigome, Y, Nakayama, J, Takeya, T, Takita, H, and Nose, T (1997), 'Volumetric quantification of brain development using MRI', *Neuroradiology,* 39 (12), 841-46.

Kadanoff, Leo P, Nagel, Sidney R, Wu, Lei, and Zhou, Su-min (1989), 'Scaling and universality in avalanches', *Physical Review A,* 39 (12), 6524.

Kaiser, JR, Gauss, CH, Pont, MM, and Williams, DK (2006), 'Hypercapnia during the first 3 days of life is associated with severe intraventricular hemorrhage in very low birth weight infants', *Journal of perinatology,* 26 (5), 279-85.

Kessler, Sudha Kilaru, Topjian, Alexis A, Gutierrez-Colina, Ana M, Ichord, Rebecca N, Donnelly, Maureen, Nadkarni, Vinay M, Berg, Robert A, Dlugos, Dennis J, Clancy, Robert R, and Abend, Nicholas S (2011), 'Short-term outcome prediction by electroencephalographic features in children treated with therapeutic hypothermia after cardiac arrest', *Neurocritical care,* 14 (1), 37-43.

Khazipov, Rustem and Luhmann, Heiko J (2006), 'Early patterns of electrical activity in the developing cerebral cortex of humans and rodents', *Trends in neurosciences,* 29 (7), 414-18.

Kidokoro, H, Kubota, T, Hayashi, N, Hayakawa, M, Takemoto, K, Kato, Y, and Okumura, A (2010), 'Absent cyclicity on aEEG within the first 24 h is associated with brain damage in preterm infants', *Neuropediatrics,* 41 (06), 241-45.

Kilb, Werner, Kirischuk, Sergei, and Luhmann, Heiko J (2011), 'Electrical activity patterns and the functional maturation of the neocortex', *European Journal of Neuroscience,* 34 (10), 1677-86.

Kinouchi, Osame and Copelli, Mauro (2006), 'Optimal dynamical range of excitable networks at criticality', *Nature Physics,* 2 (5), 348-51.

Klein, Catherine J (2002), 'Nutrient requirements for preterm infant formulas', *The Journal of nutrition,* 132 (6), 1395S-577S.

Kostović, Ivica and Jovanov-Milošević, Nataša (2006), 'The development of cerebral connections during the first 20–45 weeks' gestation', *Seminars in Fetal and Neonatal Medicine* (11: Elsevier), 415-22.

Kostović, Ivica and Judaš, Miloš (2007), 'Transient patterns of cortical lamination during prenatal life: do they have implications for treatment?', *Neuroscience & Biobehavioral Reviews,* 31 (8), 1157-68.

--- (2010), 'The development of the subplate and thalamocortical connections in the human foetal brain', *Acta Paediatrica,* 99 (8), 1119-27.

Kurinczuk, Jennifer J, White-Koning, Melanie, and Badawi, Nadia (2010), 'Epidemiology of neonatal encephalopathy and hypoxic–ischaemic encephalopathy', *Early human development,* 86 (6), 329-38.

Lagercrantz, Hugo, Hanson, Mark A, Ment, Laura R, and Peebles, Donald M (2010), *The newborn brain: neuroscience and clinical applications* (Cambridge University Press).

Lamblin, MD, Andre, M, Challamel, MJ, Curzi-Dascalova, L, d'Allest, AM, De Giovanni, E, Moussalli-Salefranque, F, Navelet, Y, Plouin, P, and Radvanyi-Bouvet, MF (1999), '[Electroencephalography of the premature and term newborn. Maturational aspects and glossary]', *Neurophysiologie clinique= Clinical neurophysiology,* 29 (2), 123-219.

Larroque, Béatrice, Marret, S, Ancel, Pierre-Yves, Arnaud, Catherine, Marpeau, Loic, Supernant, Karine, Pierrat, Véronique, Rozé, Jean-Christophe, Matis, Jacqueline, and Cambonie, Gilles (2003), 'White matter damage and intraventricular hemorrhage in very preterm infants: the EPIPAGE study', *The Journal of pediatrics,* 143 (4), 477-83.

Lauritzen, Martin, Mathiesen, Claus, Schaefer, Katharina, and Thomsen, Kirsten J (2012), 'Neuronal inhibition and excitation, and the dichotomic control of brain hemodynamic and oxygen responses', *Neuroimage,* 62 (2), 1040-50.

Laurson, Lasse and Alava, MJ (2006), '1⁄ f noise and avalanche scaling in plastic deformation', *Physical Review E,* 74 (6), 066106.

Lazar, LM, Milrod, LM, Solomon, GE, and Labar, DR (1999), 'Asynchronous pentobarbital-induced burst suppression with corpus callosum hemorrhage', *Clinical neurophysiology,* 110 (6), 1036-40.

Lenroot, Rhoshel K and Giedd, Jay N (2006), 'Brain development in children and adolescents: insights from anatomical magnetic resonance imaging', *Neuroscience & Biobehavioral Reviews,* 30 (6), 718-29.

Levene, M, Blennow, M, Whitelaw, A, Hankø, E, Fellman, V, and Hartley, R (1995), 'Acute effects of two different doses of magnesium sulphate in infants with birth asphyxia', *Archives of Disease in Childhood-Fetal and Neonatal Edition,* 73 (3), F174-F77.

Levina, Anna, Herrmann, J Michael, and Geisel, Theo (2007), 'Dynamical synapses causing self-organized criticality in neural networks', *Nature Physics,* 3 (12), 857-60.

Lewis, Laura D, Ching, ShiNung, Weiner, Veronica S, Peterfreund, Robert A, Eskandar, Emad N, Cash, Sydney S, Brown, Emery N, and Purdon, Patrick L (2013), 'Local cortical dynamics of burst suppression in the anaesthetized brain', *Brain*, 136 (9), 2727-37.

Linkenkaer-Hansen, Klaus, Nikouline, Vadim V, Palva, J Matias, and Ilmoniemi, Risto J (2001), 'Long-range temporal correlations and scaling behavior in human brain oscillations', *The Journal of neuroscience*, 21 (4), 1370-77.

Löfhede, Johan, Löfgren, Nils, Thordstein, Magnus, Flisberg, Anders, Kjellmer, Ingemar, and Lindecrantz, Kaj (2008), 'Classification of burst and suppression in the neonatal electroencephalogram', *Journal of neural engineering*, 5 (4), 402.

Löfhede, Johan, Thordstein, Magnus, Löfgren, Nils, Flisberg, Anders, Rosa-Zurera, Manuel, Kjellmer, Ingemar, and Lindecrantz, Kaj (2010), 'Automatic classification of background EEG activity in healthy and sick neonates', *Journal of neural engineering*, 7 (1), 016007.

Lukatch, Heath S, Kiddoo, Cynthia E, and MacIver, M Bruce (2005), 'Anesthetic-induced burst suppression EEG activity requires glutamate-mediated excitatory synaptic transmission', *Cerebral Cortex*, 15 (9), 1322-31.

Malamud, Bruce D, Morein, Gleb, and Turcotte, Donald L (1998), 'Forest fires: an example of self-organized critical behavior', *Science*, 281 (5384), 1840-42.

Malk, Kaija, Metsäranta, Marjo, and Vanhatalo, Sampsa (2014), 'Drug effects on endogenous brain activity in preterm babies', *Brain and Development*, 36 (2), 116-23.

Mandelbrot, Benoît B and Hudson, Richard L (2004), 'The (mis) behavior of markets: A Fractal View of Risk', *Ruin, and Reward—Basic Books*.

Marret, Stéphane, Parain, Dominique, Ménard, Jean-François, Blanc, Thierry, Devaux, Anne-Marie, Ensel, Pierre, Fessard, Claude, and Samson-Dollfus, Dominique (1997), 'Prognostic value of neonatal electroencephalography in premature newborns less than 33 weeks of gestational age', *Electroencephalography and clinical neurophysiology*, 102 (3), 178-85.

Massaro, An Nguyen, Govindan, Rathinaswamy B, Al-Shargabi, T, Andescavage, Nickie N, Metzler, M, Chang, Taeun, Glass, P, and Du Plessis, Adre J (2014), 'Heart rate variability in encephalopathic newborns during and after therapeutic hypothermia', *Journal of Perinatology*.

Massobrio, Paolo, de Arcangelis, Lucilla, Pasquale, Valentina, Jensen, Henrik J, and Plenz, Dietmar (2015), 'Criticality as a signature of healthy neural systems', *Frontiers in systems neuroscience*, 9.

Matic, Vladimir, Cherian, Perumpillichira J, Koolen, Ninah, Naulaers, Gunnar, Swarte, Renate M, Govaert, Paul, Van Huffel, Sabine, and De Vos, Maarten (2014), 'Holistic approach for automated background EEG assessment in asphyxiated full-term infants', *Journal of neural engineering*, 11 (6), 066007.

Matić, Vladimir, Cherian, Perumpillichira J, Widjaja, Devy, Jansen, Katrien, Naulaers, Gunnar, Van Huffel, Sabine, and De Vos, Maarten (2013), 'Heart Rate Variability in Newborns with Hypoxic Brain Injury', *Oxygen Transport to Tissue XXXV* (Springer), 43-48.

Mazzoni, Alberto, Broccard, Frédéric D, Garcia-Perez, Elizabeth, Bonifazi, Paolo, Ruaro, Maria Elisabetta, and Torre, Vincent (2007), 'On the dynamics of the spontaneous activity in neuronal networks', *PloS one*, 2 (5), e439.

McCrea, Heather J and Ment, Laura R (2008), 'The diagnosis, management, and postnatal prevention of intraventricular hemorrhage in the preterm neonate', *Clinics in perinatology*, 35 (4), 777-92.

McKelvey, Bill and Andriani, Pierpaolo (2005), 'Why Gaussian statistics are mostly wrong for strategic organization', *Strategic Organization*, 3 (2), 219-28.

Mehta, Amit P, Mills, Andrea C, Dahmen, Karin A, and Sethna, James P (2002), 'Universal pulse shape scaling function and exponents: Critical test for avalanche models applied to Barkhausen noise', *Physical Review E*, 65 (4), 046139.

Meisel, Christian and Gross, Thilo (2009), 'Adaptive self-organization in a realistic neural network model', *Physical Review E*, 80 (6), 061917.

Meisel, Christian, Storch, Alexander, Hallmeyer-Elgner, Susanne, Bullmore, Ed, and Gross, Thilo (2012), 'Failure of adaptive self-organized criticality during epileptic seizure attacks', *PLoS computational biology*, 8 (1), e1002312.

Merkle, Florian T and Alvarez-Buylla, Arturo (2006), 'Neural stem cells in mammalian development', *Current opinion in cell biology*, 18 (6), 704-09.

Miller, Kai J, Sorensen, Larry B, Ojemann, Jeffrey G, and Den Nijs, Marcel (2009), 'Power-law scaling in the brain surface electric potential', *PLoS computational biology*, 5 (12), e1000609.

Miller, SP, Weiss, J, Barnwell, A, Ferriero, DM, Latal-Hajnal, B, Ferrer-Rogers, A, Newton, N, Partridge, JC, Glidden, DV, and Vigneron, DB (2002), 'Seizure-associated brain injury in term newborns with perinatal asphyxia', *Neurology*, 58 (4), 542-48.

Milligan, DWA (1980), 'Failure of autoregulation and intraventricular haemorrhage in preterm infants', *The Lancet*, 315 (8174), 896-98.

Morley, George Malcolm (2005), 'Birth brain injury: Etiology and prevention Part I: Hypoxic-ischemic encephalopathy and cerebral palsy', *Medical Veritus*, 2, 500-06.

Moser, MB (1999), 'Making more synapses: a way to store information?', *Cellular and Molecular Life Sciences CMLS*, 55 (4), 593-600.

Nakamura, Shinji, Kusaka, Takashi, Yasuda, Saneyuki, Ueno, Masaki, Miki, Takanori, Koyano, Kosuke, Nakamura, Makoto, Okada, Hitoshi, Okazaki, Kaoru, and Isobe, Kenichi (2013), 'Cerebral blood volume combined with amplitude-integrated EEG can be a suitable guide to control hypoxic/ischemic insult in a piglet model', *Brain and Development*, 35 (7), 614-25.

Nash, KB, Bonifacio, SL, Glass, HC, Sullivan, JE, Barkovich, AJ, Ferriero, DM, and Cilio, MR (2011), 'Video-EEG monitoring in newborns with hypoxic-ischemic encephalopathy treated with hypothermia', *Neurology*, 76 (6), 556-62.

Niedermeyer, E, Sherman, David L, Geocadin, Romergryko J, Hansen, H Christian, and Hanley, Daniel F (1999), 'The burst-suppression electroencephalogram', *Clinical EEG (electroencephalography)*, 30 (3), 99.

Niedermeyer, Ernst and da Silva, FH Lopes (2005), *Electroencephalography: basic principles, clinical applications, and related fields* (Lippincott Williams & Wilkins).

Nimmervoll, Birgit, White, Robin, Yang, Jenq-Wei, An, Shuming, Henn, Christopher, Sun, Jyh-Jang, and Luhmann, Heiko J (2013), 'LPS-induced microglial secretion of TNFα increases activity-dependent neuronal apoptosis in the neonatal cerebral cortex', *Cerebral Cortex*, 23 (7), 1742-55.

Nunez, Paul L and Srinivasan, Ramesh (2014), 'Neocortical dynamics due to axon propagation delays in cortico-cortical fibers: EEG traveling and standing waves with implications for top-down influences on local networks and white matter disease', *Brain research*, 1542, 138-66.

O'Reilly, Deirdre, Navakatikyan, Michael A, Filip, Marcia, Greene, Deirdre, and Van Marter, Linda J (2012), 'Peak-to-peak amplitude in neonatal brain monitoring of premature infants', *Clinical Neurophysiology*, 123 (11), 2139-53.

Odabaee, Maryam, Freeman, Walter J, Colditz, Paul B, Ramon, Ceon, and Vanhatalo, Sampsa (2013), 'Spatial patterning of the neonatal EEG suggests a need for a high number of electrodes', *NeuroImage*, 68, 229-35.

Okumura, A, Hayakawa, F, Kato, T, Kuno, K, and Watanabe, K (1999), 'Positive rolandic sharp waves in preterm infants with periventricular leukomalacia: their relation to background electroencephalographic abnormalities', *Neuropediatrics*, 30 (06), 278-82.

Okumura, Akihisa, Hayakawa, Fumio, Kato, Toru, Kuno, Kuniyoshi, and Watanabe, Kazuyoshi (2002), 'Developmental outcome and types of chronic-stage EEG abnormalities in preterm infants', *Developmental Medicine & Child Neurology*, 44 (11), 729-34.

Olischar, Monika, Klebermass, Katrin, Waldhoer, Thomas, Pollak, Arnold, and Weninger, Manfred (2007), 'Background patterns and sleep-wake cycles on amplitude-integrated electroencephalography in preterms younger than 30 weeks gestational age with peri-/intraventricular haemorrhage', *Acta Paediatrica*, 96 (12), 1743-50.

Olischar, Monika, Klebermass, Katrin, Kuhle, Stefan, Hulek, Margot, Kohlhauser, Christina, Rücklinger, Ernst, Pollak, Arnold, and Weninger, Manfred (2004), 'Reference values for amplitude-integrated electroencephalographic activity in preterm infants younger than 30 weeks' gestational age', *Pediatrics*, 113 (1), e61-e66.

Omidvarnia, Amir, Fransson, Peter, Metsäranta, Marjo, and Vanhatalo, Sampsa (2013), 'Functional bimodality in the brain networks of preterm and term human newborns', *Cerebral Cortex*, bht120.

Palmu, Kirsi (2015), 'Event detection in preterm electroencephalography', (Aalto University).

Palmu, Kirsi, Kirjavainen, Turkka, Stjerna, Susanna, Salokivi, Tommi, and Vanhatalo, Sampsa (2013), 'Sleep wake cycling in early preterm infants: Comparison of polysomnographic recordings with a novel EEG-based index', *Clinical Neurophysiology*, 124 (9), 1807-14.

Palmu, Kirsi, Wikström, Sverre, Hippeläinen, Eero, Boylan, Geraldine, Hellström-Westas, Lena, and Vanhatalo, Sampsa (2010), 'Detection of 'EEG bursts' in the early preterm EEG: visual vs. automated detection', *Clinical Neurophysiology*, 121 (7), 1015-22.

Palva, J Matias, Zhigalov, Alexander, Hirvonen, Jonni, Korhonen, Onerva, Linkenkaer-Hansen, Klaus, and Palva, Satu (2013), 'Neuronal long-range temporal correlations and avalanche dynamics

are correlated with behavioral scaling laws', *Proceedings of the National Academy of Sciences*, 110 (9), 3585-90.

Papanikolaou, Stefanos, Bohn, Felipe, Sommer, Rubem Luis, Durin, Gianfranco, Zapperi, Stefano, and Sethna, James P (2011), 'Universality beyond power laws and the average avalanche shape', *Nature Physics*, 7 (4), 316-20.

Papile, Lu-Ann, Burstein, Jerome, Burstein, Rochelle, and Koffler, Herbert (1978), 'Incidence and evolution of subependymal and intraventricular hemorrhage: a study of infants with birth weights less than 1,500 gm', *The Journal of pediatrics*, 92 (4), 529-34.

Pasquale, V, Massobrio, P, Bologna, LL, Chiappalone, M, and Martinoia, S (2008), 'Self-organization and neuronal avalanches in networks of dissociated cortical neurons', *Neuroscience*, 153 (4), 1354-69.

Patten, Timothy M, Rennie, Christopher J, Robinson, Peter A, and Gong, Pulin (2012), 'Human cortical traveling waves: dynamical properties and correlations with responses', *PloS one*, 7 (6), e38392.

Peirano, Patricio, Algarín, Cecilia, and Uauy, Ricardo (2003), 'Sleep-wake states and their regulatory mechanisms throughout early human development', *The Journal of pediatrics*, 143 (4), 70-79.

Perković, Olga, Dahmen, Karin, and Sethna, James P (1995), 'Avalanches, Barkhausen noise, and plain old criticality', *Physical review letters*, 75 (24), 4528.

Pisarenko, VF and Sornette, D (2003), 'Characterization of the frequency of extreme earthquake events by the generalized Pareto distribution', *Pure and Applied Geophysics*, 160 (12), 2343-64.

Priesemann, Viola, Valderrama, Mario, Wibral, Michael, and Le Van Quyen, Michel (2013), 'Neuronal avalanches differ from wakefulness to deep sleep–evidence from intracranial depth recordings in humans', *PLoS computational biology*, 9 (3), e1002985.

Roberts, JA and Robinson, PA (2012), 'Quantitative theory of driven nonlinear brain dynamics', *Neuroimage*, 62 (3), 1947-55.

Roberts, James A, Iyer, Kartik K, Finnigan, Simon, Vanhatalo, Sampsa, and Breakspear, Michael (2014), 'Scale-free bursting in human cortex following hypoxia at birth', *The Journal of Neuroscience*, 34 (19), 6557-72.

Robinson, PA, Rennie, CJ, Phillips, AJK, Kim, JW, and Roberts, JA (2010), 'Phase transitions in physiologically-based multiscale mean-field brain models', *Modeling Phase Transitions in the Brain* (Springer), 179-201.

Roche-Labarbe, Nadège, Aarabi, Ardalan, Kongolo, Guy, Gondry-Jouet, Catherine, Dümpelmann, Matthias, Grebe, Reinhard, and Wallois, Fabrice (2008), 'High-resolution electroencephalography and source localization in neonates', *Human brain mapping*, 29 (2), 167-76.

Rubinov, Mikail, Sporns, Olaf, van Leeuwen, Cees, and Breakspear, Michael (2009), 'Symbiotic relationship between brain structure and dynamics', *BMC neuroscience*, 10 (1), 55.

Rubinov, Mikail, Sporns, Olaf, Thivierge, Jean-Philippe, and Breakspear, Michael (2011), 'Neurobiologically realistic determinants of self-organized criticality in networks of spiking neurons', *PLoS computational biology*, 7 (6), e1002038.

Rümelin, Werner (1982), 'Numerical treatment of stochastic differential equations', *SIAM Journal on Numerical Analysis*, 604-13.

Sabir, Hemmen, Jary, Sally, Tooley, James, Liu, Xun, and Thoresen, Marianne (2012), 'Increased inspired oxygen in the first hours of life is associated with adverse outcome in newborns treated for perinatal asphyxia with therapeutic hypothermia', *The Journal of pediatrics*, 161 (3), 409-16.

Salhab, Walid A, Wyckoff, Myra H, Laptook, Abbot R, and Perlman, Jeffrey M (2004), 'Initial hypoglycemia and neonatal brain injury in term infants with severe fetal acidemia', *Pediatrics*, 114 (2), 361-66.

Sarnat, Harvey B and Sarnat, Margaret S (1976), 'Neonatal encephalopathy following fetal distress: a clinical and electroencephalographic study', *Archives of neurology*, 33 (10), 696-705.

Savitzky, Abraham and Golay, Marcel JE (1964), 'Smoothing and differentiation of data by simplified least squares procedures', *Analytical chemistry*, 36 (8), 1627-39.

Schafer, Ronald W (2011), 'What is a Savitzky-Golay filter?[lecture notes]', *Signal Processing Magazine, IEEE*, 28 (4), 111-17.

Schumacher, Eva M, Westvik, Asbjorn S, Larsson, Pål G, Lindemann, Rolf, Westvik, Jostein, and Stiris, Tom A (2011), 'Feasibility of long-term continuous EEG monitoring during the first days of life in preterm infants: an automated quantification of the EEG activity', *Pediatric research*, 69, 413-17.

Schuster, Heinz Georg, Plenz, Dietmar, and Niebur, Ernst (2014), *Criticality in Neural Systems* (Weinheim, Germany: John Wiley & Sons).

Sethna, James P, Dahmen, Karin A, and Myers, Christopher R (2001), 'Crackling noise', *Nature*, 410 (6825), 242-50.

Shankaran, Seetha (2002), 'The postnatal management of the asphyxiated term infant', *Clinics in perinatology*, 29 (4), 675-92.

Shankaran, Seetha, Laptook, Abbot R, Ehrenkranz, Richard A, Tyson, Jon E, McDonald, Scott A, Donovan, Edward F, Fanaroff, Avroy A, Poole, W Kenneth, Wright, Linda L, and Higgins, Rosemary D (2005), 'Whole-body hypothermia for neonates with hypoxic–ischemic encephalopathy', *New England Journal of Medicine*, 353 (15), 1574-84.

Shapiro-Mendoza, Carrie K (2014), 'Commentary: Mediation and moderation analyses: a novel approach to exploring the complex pathways between maternal medical conditions, preterm birth and associated newborn morbidity risk', *International journal of epidemiology*, dyt285.

Shew, Woodrow L, Yang, Hongdian, Petermann, Thomas, Roy, Rajarshi, and Plenz, Dietmar (2009), 'Neuronal avalanches imply maximum dynamic range in cortical networks at criticality', *The Journal of Neuroscience*, 29 (49), 15595-600.

Shew, Woodrow L, Yang, Hongdian, Yu, Shan, Roy, Rajarshi, and Plenz, Dietmar (2011), 'Information capacity and transmission are maximized in balanced cortical networks with neuronal avalanches', *The Journal of neuroscience*, 31 (1), 55-63.

Shewmon, D Alan (2000), 'Coma prognosis in children: Part II: clinical application', *Journal of Clinical Neurophysiology*, 17 (5), 467-72.

Shriki, Oren, Alstott, Jeff, Carver, Frederick, Holroyd, Tom, Henson, Richard NA, Smith, Marie L, Coppola, Richard, Bullmore, Edward, and Plenz, Dietmar (2013), 'Neuronal Avalanches in the Resting MEG of the Human Brain', *The Journal of Neuroscience*, 33 (16), 7079-90.

Shu, Yousheng, Hasenstaub, Andrea, and McCormick, David A (2003), 'Turning on and off recurrent balanced cortical activity', *Nature*, 423 (6937), 288-93.

Sinclair, DB, Campbell, M, Byrne, P, Prasertsom, W, and Robertson, CMT (1999), 'EEG and long-term outcome of term infants with neonatal hypoxic-ischemic encephalopathy', *Clinical neurophysiology*, 110 (4), 655-59.

Sisman, Jülide, Campbell, Deborah E, and Brion, Luc P (2005), 'Amplitude-integrated EEG in preterm infants: maturation of background pattern and amplitude voltage with postmenstrual age and gestational age', *Journal of perinatology*, 25 (6), 391-96.

Smith, Gillian C, Gutovich, Jordan, Smyser, Christopher, Pineda, Roberta, Newnham, Carol, Tjoeng, Tiong H, Vavasseur, Claudine, Wallendorf, Michael, Neil, Jeffrey, and Inder, Terrie (2011), 'Neonatal intensive care unit stress is associated with brain development in preterm infants', *Annals of neurology*, 70 (4), 541-49.

Sood, Beena G, McLaughlin, Kathleen, and Cortez, Josef (2015), 'Near-infrared spectroscopy: Applications in neonates', *Seminars in Fetal and Neonatal Medicine* (Elsevier).

Sornette, Didier and Cont, Rama (1997), 'Convergent multiplicative processes repelled from zero: power laws and truncated power laws', *Journal de Physique I*, 7 (3), 431-44.

Spasojević, Djordje, Bukvić, Srdjan, Milošević, Sava, and Stanley, H Eugene (1996), 'Barkhausen noise: Elementary signals, power laws, and scaling relations', *Physical Review E*, 54 (3), 2531.

Spector, Jonathan M and Daga, Subhash (2008), 'Preventing those so-called stillbirths', *Bulletin of the World Health Organization*, 86 (4), 315-16.

Spitzmiller, R Edwin, Phillips, Tonya, Meinzen-Derr, Jareen, and Hoath, Steven B (2007), 'Amplitude-integrated EEG is useful in predicting neurodevelopmental outcome in full-term infants with hypoxic-ischemic encephalopathy: a meta-analysis', *Journal of child neurology*, 22 (9), 1069-78.

Staley, Kevin J, Longacher, Mark, Bains, Jaideep S, and Yee, Audrey (1998), 'Presynaptic modulation of CA3 network activity', *Nature neuroscience*, 1 (3), 201-09.

Stephan, Klaas Enno, Penny, Will D, Daunizeau, Jean, Moran, Rosalyn J, and Friston, Karl J (2009), 'Bayesian model selection for group studies', *Neuroimage*, 46 (4), 1004-17.

Steriade, M, Amzica, F, and Contreras, D (1994), 'Cortical and thalamic cellular correlates of electroencephalographic burst-suppression', *Electroencephalography and clinical neurophysiology*, 90 (1), 1-16.

Steriade, Mircea, Gloor, PLRR, Llinas, RR, Lopes da Silva, FH, and Mesulam, M-M (1990), 'Basic mechanisms of cerebral rhythmic activities', *Electroencephalography and clinical neurophysiology*, 76 (6), 481-508.

Stevenson, Nathan J, Palmu, Kirsi, Wikström, Sverre, Hellström-Westas, Lena, and Vanhatalo, Sampsa (2014), 'Measuring brain activity cycling (BAC) in long term EEG monitoring of preterm babies', *Physiological Measurement*, 35 (7), 1493.

Steyn-Ross, Moira L, Steyn-Ross, D Alistair, Sleigh, James W, and Liley, DTJ (1999), 'Theoretical electroencephalogram stationary spectrum for a white-noise-driven cortex: Evidence for a general anesthetic-induced phase transition', *Physical Review E*, 60 (6), 7299.

Stiles, Joan and Jernigan, Terry L (2010), 'The basics of brain development', *Neuropsychology review*, 20 (4), 327-48.

Stumpf, Michael PH and Porter, Mason A (2012), 'Critical truths about power laws', *Science*, 335 (6069), 665-66.

Sur, Mriganka and Rubenstein, John LR (2005), 'Patterning and plasticity of the cerebral cortex', *Science*, 310 (5749), 805-10.

Tabak, Joël, O'Donovan, Michael J, and Rinzel, John (2006), 'Differential control of active and silent phases in relaxation models of neuronal rhythms', *Journal of computational neuroscience*, 21 (3), 307-28.

Tagin, Mohamed A, Woolcott, Christy G, Vincer, Michael J, Whyte, Robin K, and Stinson, Dora A (2012), 'Hypothermia for neonatal hypoxic ischemic encephalopathy: an updated systematic review and meta-analysis', *Archives of pediatrics & adolescent medicine*, 166 (6), 558-66.

Tataranno, Maria Luisa, Alderliesten, Thomas, de Vries, Linda S, Groenendaal, Floris, Toet, Mona C, Lemmers, Petra MA, van Bel, Frank, and Benders, Manon JNL (2015), 'Early Oxygen-Utilization and Brain Activity in Preterm Infants'.

Ter Horst, Hendrik J, Sommer, Constanze, Bergman, Klasien A, Fock, Johanna M, Van Weerden, Tiemen W, and Bos, Arend F (2004), 'Prognostic significance of amplitude-integrated EEG during the first 72 hours after birth in severely asphyxiated neonates', *Pediatric research*, 55 (6), 1026-33.

Tetzlaff, Christian, Okujeni, Samora, Egert, Ulrich, Wörgötter, Florentin, and Butz, Markus (2010), 'Self-organized criticality in developing neuronal networks', *PLoS computational biology*, 6 (12), e1001013.

Thordstein, M, Flisberg, Anders, Löfgren, Nils, Bågenholm, Ralph, Lindecrantz, K, Wallin, BG, and Kjellmer, Ingemar (2004), 'Spectral analysis of burst periods in EEG from healthy and post-asphyctic full-term neonates', *Clinical neurophysiology*, 115 (11), 2461-66.

Thoresen, Marianne, Hellström-Westas, Lena, Liu, Xun, and de Vries, Linda S (2010), 'Effect of hypothermia on amplitude-integrated electroencephalogram in infants with asphyxia', *Pediatrics*, 126 (1), e131-e39.

Thrane, N, Wismer, J, Konstantin-Hansen, H, and Gade, S (1995), 'Practical use of the Hilbert transform', *B&K Application Note No. bo0437-11*.

Toet, MC, Hellström-Westas, L, Groenendaal, F, Eken, P, and De Vries, LS (1999), 'Amplitude integrated EEG 3 and 6 hours after birth in full term neonates with hypoxic–ischaemic encephalopathy', *Archives of Disease in Childhood-Fetal and Neonatal Edition,* 81 (1), F19-F23.

Tolner, Else A, Sheikh, Aminah, Yukin, Alexey Y, Kaila, Kai, and Kanold, Patrick O (2012), 'Subplate neurons promote spindle bursts and thalamocortical patterning in the neonatal rat somatosensory cortex', *The Journal of Neuroscience,* 32 (2), 692-702.

Tolonen, M, Palva, JM, Andersson, S, and Vanhatalo, S (2007), 'Development of the spontaneous activity transients and ongoing cortical activity in human preterm babies', *Neuroscience,* 145 (3), 997-1006.

Vairavan, Srinivasan, Eswaran, Hari, Haddad, Naim, Rose, Douglas F, Preissl, Hubert, Wilson, James D, Lowery, Curtis L, and Govindan, Rathinaswamy B (2009), 'Detection of discontinuous patterns in spontaneous brain activity of neonates and fetuses', *Biomedical Engineering, IEEE Transactions on,* 56 (11), 2725-29.

Van Baar, Anneloes L, Van Wassenaer, Aleid G, Briët, Judy M, Dekker, Friedo W, and Kok, Joke H (2005), 'Very preterm birth is associated with disabilities in multiple developmental domains', *Journal of pediatric psychology,* 30 (3), 247-55.

Van der Knaap, Marjo S and Valk, Jaap (2005), *Magnetic resonance of myelination and myelin disorders* (Springer).

van Putten, Michel JAM and van Putten, Maurice HPM (2010), 'Uncommon EEG burst-suppression in severe postanoxic encephalopathy', *Clinical neurophysiology,* 121 (8), 1213-19.

van Rooij, Linda GM, Toet, Mona C, Osredkar, Damjan, van Huffelen, Alexander C, Groenendaal, Floris, and de Vries, Linda S (2005), 'Recovery of amplitude integrated electroencephalographic background patterns within 24 hours of perinatal asphyxia', *Archives of Disease in Childhood-Fetal and Neonatal Edition,* 90 (3), F245-FF51.

Vanhatalo, Sampsa and Lauronen, Leena (2006), 'Neonatal SEP–back to bedside with basic science', *Seminars in Fetal and Neonatal Medicine* (11: Elsevier), 464-70.

Vanhatalo, Sampsa and Kaila, Kai (2006), 'Development of neonatal EEG activity: from phenomenology to physiology', *Seminars in Fetal and Neonatal Medicine* (11: Elsevier), 471-78.

Vanhatalo, Sampsa, Palva, J Matias, Andersson, Sture, Rivera, Claudio, Voipio, Juha, and Kaila, Kai (2005), 'Slow endogenous activity transients and developmental expression of K+–Cl− cotransporter 2 in the immature human cortex', *European Journal of Neuroscience,* 22 (11), 2799-804.

Victor, Jonathan D, Drover, Jonathan D, Conte, Mary M, and Schiff, Nicholas D (2011), 'Mean-field modeling of thalamocortical dynamics and a model-driven approach to EEG analysis', *Proceedings of the National Academy of Sciences,* 108 (Supplement 3), 15631-38.

Volpe, Joseph J (2001a), 'Perinatal brain injury: from pathogenesis to neuroprotection', *Mental retardation and developmental disabilities research reviews,* 7 (1), 56-64.

--- (2001b), 'Neurobiology of periventricular leukomalacia in the premature infant', *Pediatric research,* 50 (5), 553-62.

--- (2003), 'Cerebral white matter injury of the premature infant—more common than you think', *Pediatrics,* 112 (1), 176-80.

--- (2008), *Neurology of the Newborn* (fifth edn.; Chicago: Saunders Elsevier Health Sciences.).

--- (2009), 'Brain injury in premature infants: a complex amalgam of destructive and developmental disturbances', *The Lancet Neurology,* 8 (1), 110-24.

Vuong, Quang H (1989), 'Likelihood ratio tests for model selection and non-nested hypotheses', *Econometrica: Journal of the Econometric Society*, 307-33.

Walls-Esquivel, E, Vecchierini, MF, Héberlé, C, and Wallois, F (2007), 'Electroencephalography (EEG) recording techniques and artefact detection in early premature babies', *Neurophysiologie Clinique/Clinical Neurophysiology,* 37 (5), 299-309.

Walsh, BH, Murray, DM, and Boylan, GB (2011), 'The use of conventional EEG for the assessment of hypoxic ischaemic encephalopathy in the newborn: a review', *Clinical neurophysiology,* 122 (7), 1284-94.

Wang, Yunhua and Agarwal, Rajeev (2007), 'Automatic detection of burst suppression', *Engineering in Medicine and Biology Society, 2007. EMBS 2007. 29th Annual International Conference of the IEEE* (IEEE), 553-56.

Watanabe, Kazuyoshi, Hayakawa, Fumio, and Okumura, Akihisa (1999), 'Neonatal EEG: a powerful tool in the assessment of brain damage in preterm infants', *Brain and Development,* 21 (6), 361-72.

Watkins, AMC, West, CR, and Cooke, RWI (1989), 'Blood pressure and cerebral haemorrhage and ischaemia in very low birthweight infants', *Early human development,* 19 (2), 103-10.

Weisman, Omri, Magori-Cohen, Reuma, Louzoun, Yoram, Eidelman, Arthur I, and Feldman, Ruth (2011), 'Sleep-wake transitions in premature neonates predict early development', *Pediatrics*, 128 (4), 706-14.

Wertheim, DFP, Eaton, DG, Oozeer, RC, Connell, JA, Dubowitz, LMS, Dubowitz, V, Willetts, R, and Wootton, R (1991), 'A new system for cotside display and analysis of the preterm neonatal electroencephalogram', *Developmental Medicine & Child Neurology,* 33 (12), 1080-86.

West, Claire R, Harding, Jane E, Williams, Christopher E, Gunning, Mark I, and Battin, Malcolm R (2006), 'Quantitative electroencephalographic patterns in normal preterm infants over the first week after birth', *Early human development,* 82 (1), 43-51.

Westover, M Brandon, Ching, Shinung, Kumaraswamy, Vishakhadatta M, Akeju, Seun Oluwaseun, Pierce, Eric, Cash, Sydney S, Kilbride, Ronan, Brown, Emery N, and Purdon, Patrick L (2015), 'The Human Burst Suppression Electroencephalogram of Deep Hypothermia', *Clinical Neurophysiology*.

WHO (2013), 'Preterm Birth, Fact Sheet No. 363'.

Wikström, Sverre, Pupp, Ingrid Hansen, Rosén, Ingmar, Norman, Elisabeth, Fellman, Vineta, Ley, David, and Hellström-Westas, Lena (2012), 'Early single-channel aEEG/EEG predicts outcome in very preterm infants', *Acta Paediatrica,* 101 (7), 719-26.

Witte, H, Putsche, P, Schwab, K, Eiselt, M, Helbig, M, and Suesse, T (2004), 'On the spatio-temporal organisation of quadratic phase-couplings in ‘trace alternant’EEG pattern in full-term newborns', *Clinical neurophysiology*, 115 (10), 2308-15.

Wood, Nicholas S, Marlow, Neil, Costeloe, Kate, Gibson, Alan T, and Wilkinson, Andrew R (2000), 'Neurologic and developmental disability after extremely preterm birth', *New England Journal of Medicine*, 343 (6), 378-84.

Zapperi, Stefano, Castellano, Claudio, Colaiori, Francesca, and Durin, Gianfranco (2005), 'Signature of effective mass in crackling-noise asymmetry', *Nature Physics*, 1 (1), 46-49.

Zhang, Dandan, Hou, Xinlin, Liu, Yunfeng, Zhou, Congle, Luo, Yuejia, and Ding, Haiyan (2012), 'The utility of amplitude-integrated EEG and NIRS measurements as indices of hypoxic ischaemia in the newborn pig', *Clinical Neurophysiology*, 123 (8), 1668-75.

Zhang, Li I and Poo, Mu-ming (2001), 'Electrical activity and development of neural circuits', *Nature Neuroscience*, 4, 1207-14.

Zilberter, Yuri, Zilberter, Tanya, and Bregestovski, Piotr (2010), 'Neuronal activity< i> in vitro</i> and the< i> in vivo</i> reality: the role of energy homeostasis', *Trends in pharmacological sciences*, 31 (9), 394-401.

APPENDIX A – SECTION 1: CDF'S OF BURST SIZES

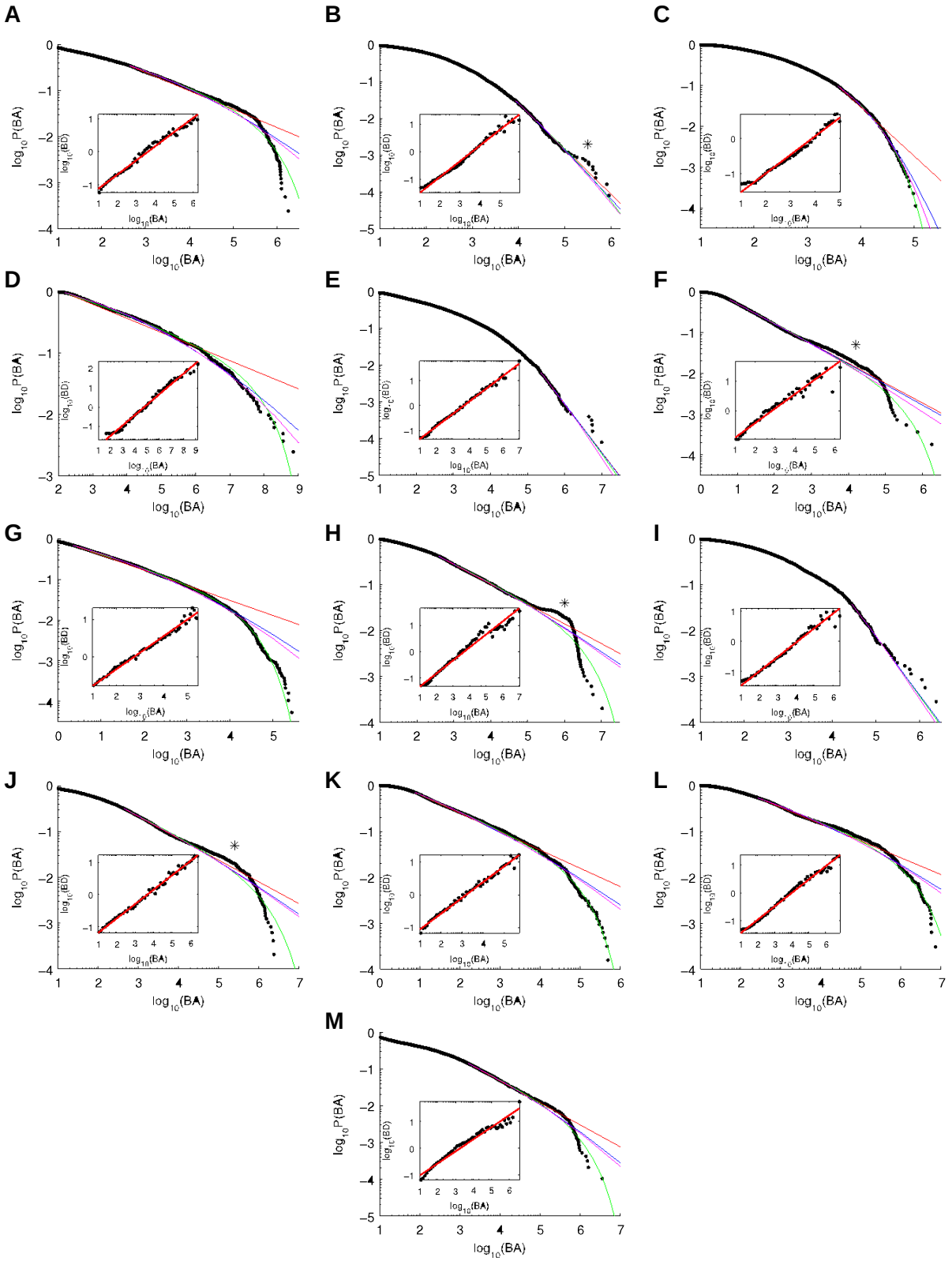

A-1 - Burst area distributions for all burst suppression recordings. A–M, Upper CDFs of burst area (BA, black) for all infants 1–13, respectively, with fits to Pareto (red), log-normal (blue), Weibull (magenta), and exponentially truncated ower-law (green) distributions. Asterisks denote "knees" showing an excess of bursts above the background trend. Insets, Scaling relationships between burst durations and burst areas (black; points are medians after binning both axes), with least-squares linear fit in double-logarithmic coordinates (red). BD, Burst duration.

APPENDIX A – SECTION 2: CDF'S OF BURST DURATIONS

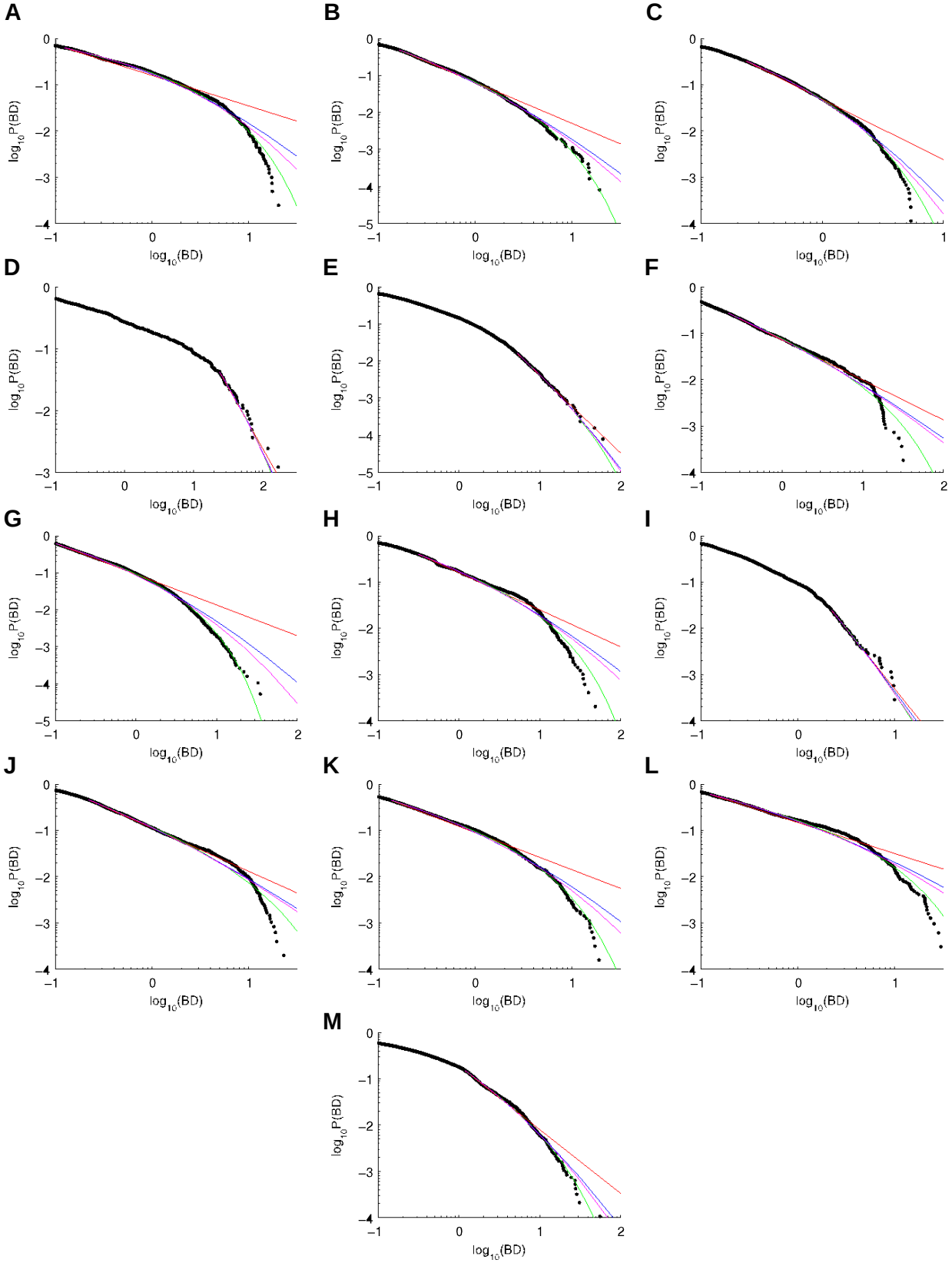

A-2 - Burst duration distributions for all burst suppression recordings. A–M, Upper CDFs of burst duration (BD; black) for all infants 1–13, respectively, with fits to Pareto (red), log-normal (blue), Weibull (magenta), and exponentially truncated power-law (green) distributions.

APPENDIX B – SECTION 1: OUTCOMES TABLE

Subjects		EEG Recordings					Clinical outcome			
Gestational age (weeks+days), weight (g)	**pH at birth, Apgar (Ap) (1/5/10min)**	**Infant**	**Sex**	**Duration of EEG epoch (mins)**	**Cooling onset (hours: mins)**	**EEG epoch onset (hours: mins)**	**MRI findings (Th = thalamus, BG = basal ganglia)**	**Early Neurology**	**Later outcome (age, years and months)**	**Outcome class**
39+4 3780	7.07 1/04/2005	1	m	30	3:48	4:34	Normal	-	mild abn in vision and fine motor skills 3y2m	2
39+2 3390	6.95 1/01/2005	2	m	120	0:01	1:20	*Excluded from main analysis due to lack of follow-up data*			
34+5 2525	6.71 0/0/6	3	m	120	2:24	4:39	bilateral Th lesion	myoclonic epilepsy, spastic hemiplegia	mild hemiplegia and epilepsy 2y	3
40+1 3030	6.76 2/04/2004	4	m	100	4:00	5:44	*Excluded from main analysis due to lack of follow-up data*			
40+0 3830	7.02 2/03/2005	5	m	330	11:00	15:54	extensive bilateral Th lesion & BG lesion	infantile spasms, dystonic CP, mental retardation	severe CP 2y	4
40+3	6.93	6	m	120	11:00	15:55	brain normal, mild subdural hematoma	mild abn in gross & fine motor skills, visual perception & speech, behavior	Normal	1

3960	1/04/2005							al issues	2y9m	
40+3 5778	7.1 0/0/1	7	m	90	3:03	3:07	Th lesion	died	-	4
41+4 3625	6.89 2/03/2005	8	m	120	3:34	5:56	normal MRI	normal at 1y	Normal 2y2m	1
40+1 3190	6.86 1/01/2001	9	f	180	4:37	5:53	severe Th lesion	died		4
41+3 2688	6.8 2/02/2005	10	f	120	3:15	8:32	severe Th lesion & cortical lesion	lost in follow-up (hospital transfer)	motor dysfunction, affects speech 3y3m	*2*
36+4 3374	6.68 0/2/3	11	f	160	2:23	11:55	extensive Th lesion & BG lesions	infantile spasms, dyskinetic CP	severe CP 3y1m	4
41+1 3260	7.13 Ap not known	12	f	40	3:54	4:59	*Excluded from main analysis due to lack of follow-up data*			
38+1 3300	6.84 1/04/2005	15	m	35	3:02	3:58	right Th lesion sign increase	normal at 11m	Normal 1y5m	1
36+1 2430	7.3 1/04/2005	16	m	70	3:20	17:45	normal	-	mild abnormality 1y7m	1
41+0 3510	6.9 5/06/2006	17	m	60	2:05	4:16	normal	-	Normal 13m	2
39+3 3550	7.15 1/01/2001	18	m	60	2:58	3:26	normal	-	Normal 12m	1
39+5 3645	6.85 3/04/2006	19	f	70	2:49	4:27	normal	-	Normal 12m	1

40+2 3520	6.87 0/0/1	20	m	210	2:26	2:38	extensive bilateral Th & BG lesion	died		4

APPENDIX B – SECTION 2: SUPPLEMENTAL MATERIALS

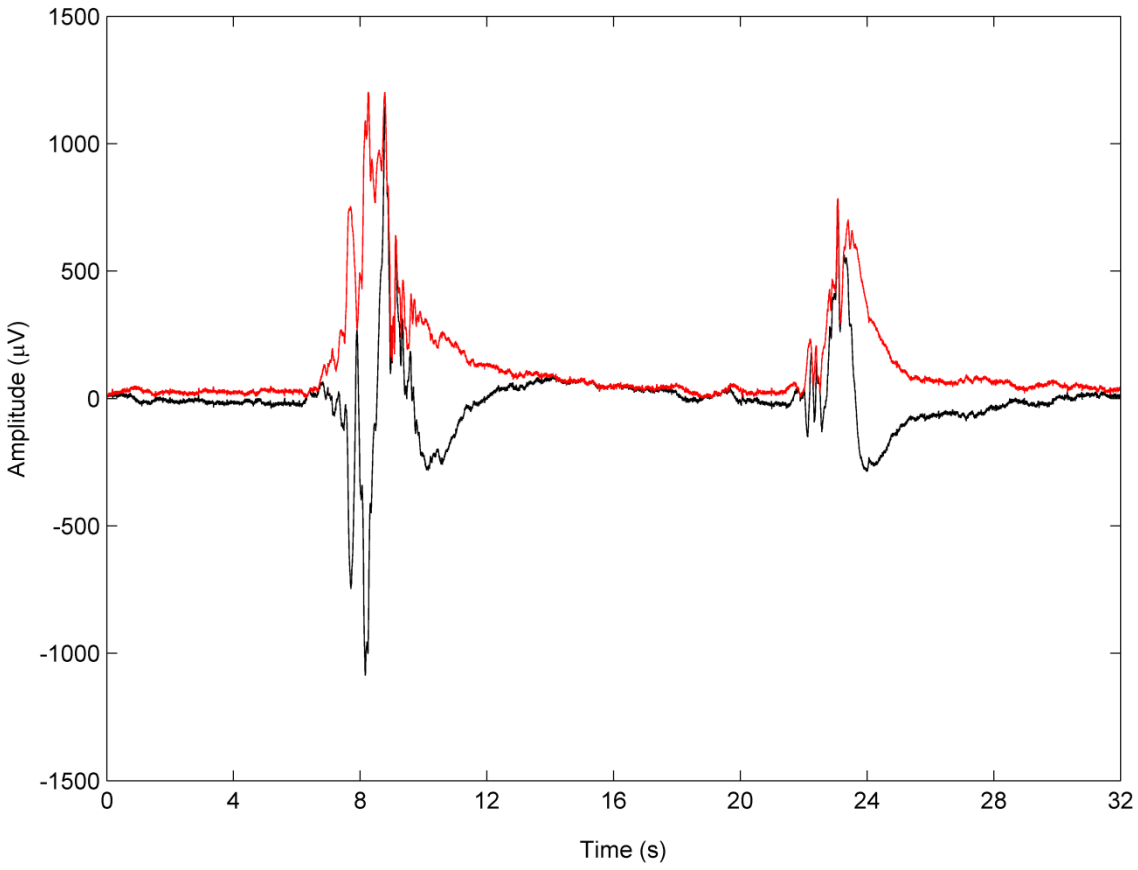

Supplementary Figure 1. This example EEG (P3-P4 derivation) demonstrates how the instantaneous EEG amplitude (red; amplitude at each time point) was computed using the Hilbert transform, a well-established method. The instantaneous power was then computed from the amplitude by taking its square at each time sample (see Fig. 1C).

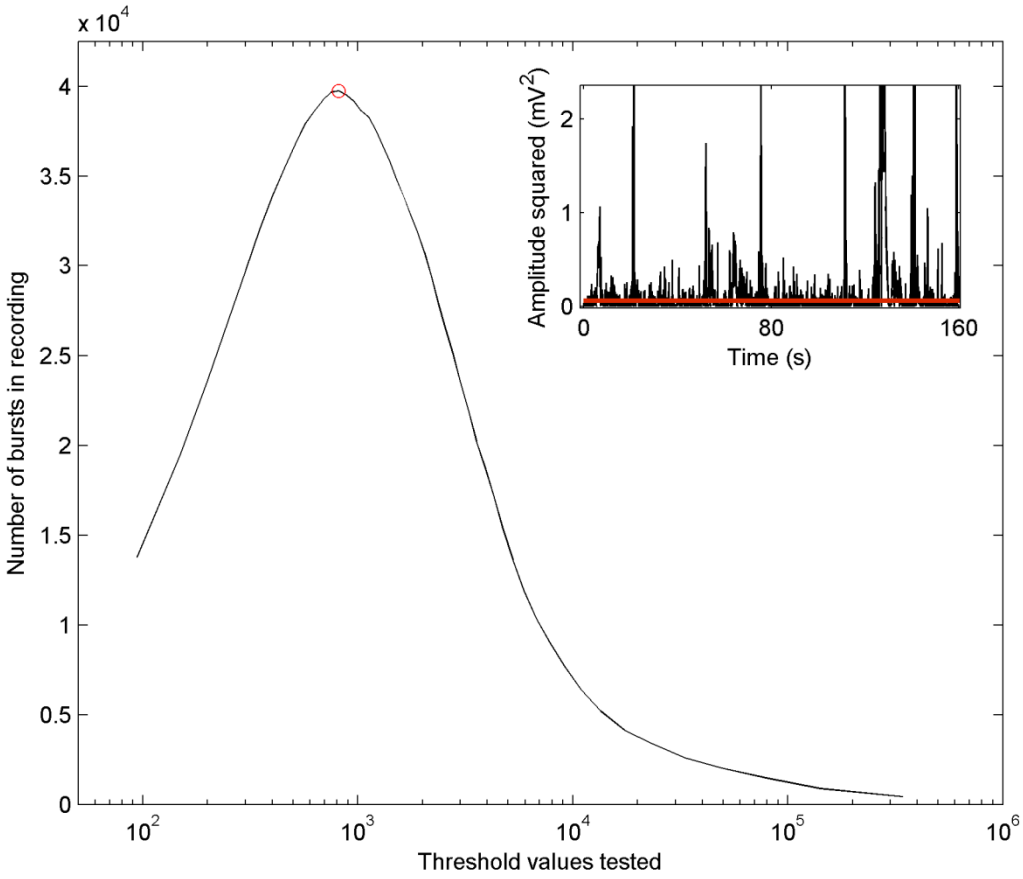

Supplementary Figure 2. In order to maximize objectivity in our analysis, we developed a burst detection algorithm that automatically identifies a threshold for each recording. A burst is defined as a series of consecutive time points beginning where the signal crosses above threshold and ending where the signal next crosses below threshold. The thresholding algorithm involves scanning through a wide range of thresholds (*x* axis) and counting the number of bursts for each threshold (*y* axis). The identified threshold is that which yields the most bursts (red circle). This procedure overcomes the proven ambiguity in visual burst detection (Palmu et al. 2010) as it yields reproducible and mathematically-unambiguous bursts. Inset: example instantaneous power signal (black) and its identified threshold (red).

1 Palmu, K. *et al.* Detection of 'EEG bursts' in the early preterm EEG: visual vs. automated detection. *Clinical Neurophysiology* **121**, 1015-1022 (2010).

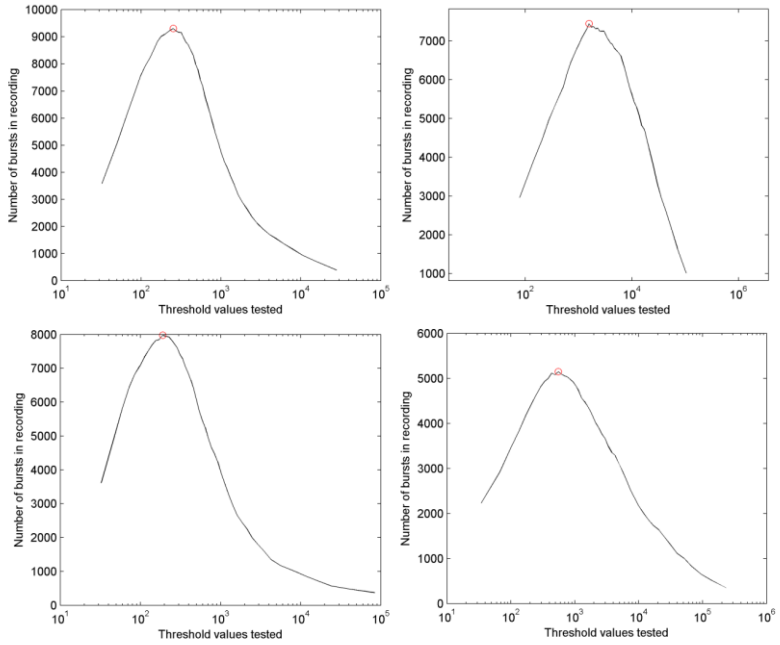

Supplementary Figure 3. Four additional examples of infant recordings showing reliability of our automated adaptive thresholding algorithm. In each case (and this was the case for all data sets) the relationship between threshold and the number of bursts follows the same unimodal form yielding one threshold value (red circles) that maximizes the number of bursts detected.

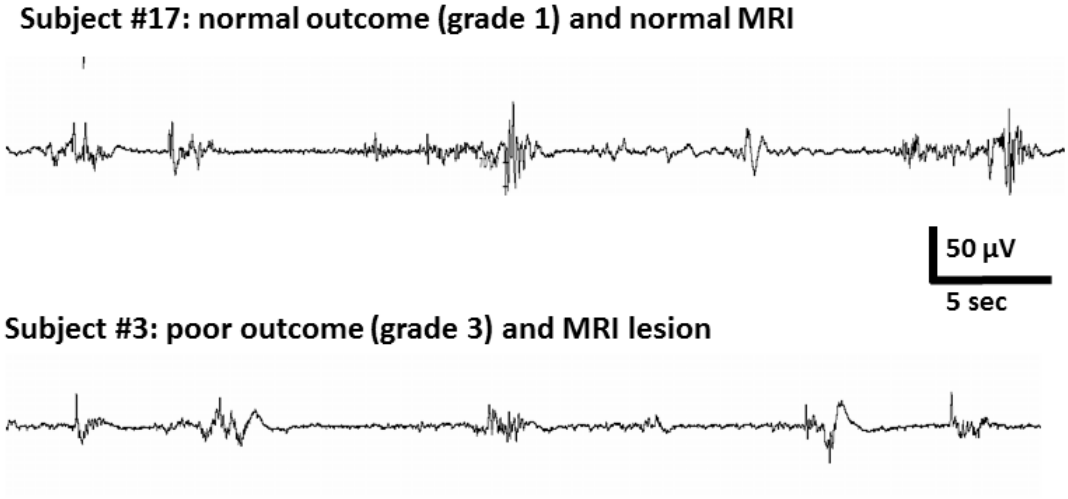

Supplementary Figure 4. These EEG examples show 45 s epochs of BS recordings in two babies that had either normal (above) or abnormal (lower) outcomes. In our overall dataset we observe that burst events span a wide range of durations, with a substantial number of long bursts with durations longer than 2 s (the sixteen babies in our outcome groups yielded an average of 236 long bursts each).

APPENDIX C – SECTION 1: STATISTICAL DISTRIBUTIONS IN PRETERM EEG DATA

N	Study ID	Onset age (+hrs)	Gestational Age (wks)	Notable features of distribution	Scaling exponent		Area v Durs slope		Outcome information					Presence of Seizures (N=0, Y=1)
					α.pexp	LLR	Slope	GOF	IVH1	IVH3	MDI	PDI	NOS	
1	47	12	22	With cut-off, good fit	1.27	-52.94	0.40	0.90	0	N/A	N/A	N/A	N/A	0
		24		Loss of powerlaw scaling	1.54	-7.87	0.43	0.96						
		48		Loss of powerlaw scaling	1.51	-5.40	0.60	0.57						
2	27	12	23	Fit suggests emergence	1.60	-6.83	0.38	0.95	0	0	50	53	59.3	1
		24		With cut-off, good fit	1.26	-122.73	0.35	0.96						
		48		Loss of powerlaw scaling	3.37	0.00	0.35	0.97						
		72		Slightly supercritical knee	1.32	-84.82	0.33	0.97						
3	40	12	23	No powerlaw scaling	2.05	-1.27	0.41	0.97	0	2	86	80	72	0
		24			2.75	-0.37	0.43	0.98						
		48			1.86	-2.39	0.41	0.95						
		72			2.57	-0.59	0.55	0.63						
4	6	12	24	With cut-off, good fit	1.30	-94.93	0.42	0.95	3	N/A	N/A	N/A	N/A	0
		24		With cut-off, good fit	1.33	-80.25	0.40	0.96						

		48		With cut-off, good fit	1.34	-81.27	0.40	0.95						
		72		Slightly supercritical knee	1.31	-91.64	0.37	0.94						
5	7	12	24	Supercritical knee	1.26	-52.19	0.41	0.92	3	N/A	N/A	N/A	N/A	0
6	17	24	24	Fit suggests emergence	1.35	-32.09	0.35	0.95	3	1	50	50	48.8	1
		48		With cut-off, good fit	1.47	-12.30	0.35	0.90						
		72		Slightly supercritical knee	1.35	-22.07	0.31	0.93						
7	25	12	24	No powerlaw scaling	1.98	-1.65	0.51	0.94	0	0	103	88	75.5	1
		24			1.99	-0.72	0.55	0.58						
		48			2.77	0.00	0.40	0.94						
8	34	12	24	No powerlaw scaling	1.80	-2.53	0.39	0.98	0	0	N/A	N/A	N/A	1
		24		Slightly supercritical knee	1.47	-24.07	0.42	0.67						
9	49	12	24	With cut-off, good fit	1.33	-55.60	0.35	0.94	0	0	56	80	64	0
		24		Slightly supercritical knee	1.27	-41.28	0.32	0.74						
		48		Loss of powerlaw scaling	3.33	-0.09	0.48	0.79						
		72		No powerlaw scaling	1.16	-4.76	0.44	0.46						
10	53	24	24	With cut-off, good fit	1.25	-96.11	0.36	0.96	0	0	72	80	71.5	1
		48		Slightly supercritical	1.16	-158.23	0.37	0.97						
11	61	12	24	With cut-off, good fit	1.22	-153.21	0.38	0.94	2	2	76	96	72.5	1

		24		Slightly supercritical knee	1.38	-39.33	0.37	0.95						
		48		No powerlaw scaling	0.86	-17.41	0.40	0.72						
		72		No powerlaw scaling	1.85	-1.99	0.36	0.95						
12	13	24	25	With cut-off, good fit	1.47	-37.00	0.40	0.95	0	N/A	50	N/A	N/A	0
		48		No powerlaw scaling	1.39	-16.97	0.50	0.93						
		72		Slightly supercritical knee	1.27	-113.18	0.37	0.95						
13	14	24	25	With cut-off, truncation	1.41	-4.28	0.40	0.93	0	0	61	88	67	0
		48		With cut-off, truncation	1.29	-71.36	0.41	0.88						
14	15	12	25	With cut-off	1.35	-31.37	0.39	0.75	0	0	72	80	78	1
		24		No powerlaw scaling	2.12	0.00	0.47	0.57						
		48		Supercritical knee	1.35	-23.82	0.39	0.52						
		72		Slightly supercritical knee	1.41	-44.12	0.50	0.58						
15	19	24	25	No powerlaw scaling	4.66	-0.01	0.38	0.89	0	0	106	84	78	0
		48			1.44	-8.25	0.38	0.89						
		72			1.72	-1.65	0.41	0.96						
16	39	48	25	No powerlaw scaling	2.31	-1.41	0.45	0.92	0	0	50	50	63.3	1
		72			2.11	-0.19	0.30	0.28						
17	44	48	25	No powerlaw scaling	1.01	-1.37	0.55	0.72	0	0	102	114	74	0

18	45	12	25		2.74	0.00	0.40	0.98	0	0	82	99	78	0
		48		No powerlaw scaling	2.59	0.00	0.39	0.98						
		72			0.97	-7.21	0.47	0.94						
19	50	24	25	Supercritical knee	1.52	-32.56	0.47	0.77	0	0	106	76	74.9	0
		48		Loss of scaling	1.46	-28.28	0.39	0.45						
20	51	24	25	No powerlaw scaling	5.21	0.00	0.43	0.97	0	0	N/A	N/A	N/A	0
		48			3.19	-0.06	0.48	0.90						
21	54	48	25	No powerlaw scaling	2.31	-0.50	0.44	0.84	0	0	94	103	78	0
22	58	24	25	With cut-off, good fit	1.26	-98.01	0.37	0.95	0	2	54	61	62	1
		48		Loss of scaling	2.50	-0.57	0.41	0.97						
		72		No powerlaw scaling	1.96	0.00	0.27	0.28						
23	62	24	25	No powerlaw scaling	3.17	0.00	0.49	0.79	0	0	94	88	73.5	1
		48		With cut-off, good fit	1.16	-183.47	0.41	0.94						
		72		With cut-off, good fit	1.17	-172.08	0.39	0.95						
24	11	12	26	With cut-off, slight trun	1.19	-244.66	0.43	0.93	0	N/A	88	72	75	0
		24		No powerlaw scaling	4.06	0.00	0.40	0.96						
		48		No powerlaw scaling	3.12	-0.18	0.47	0.97						
		72		No powerlaw scaling	3.59	0.00	0.44	0.97						

25	12	24	26	Supercritical knee	1.34	-65.30	0.35	0.96	4	N/A	N/A	N/A	N/A	N/A
		48		Supercritical knee, bimodal?	1.40	-22.13	0.36	0.88						
26	26	12	26	No powerlaw scaling	2.97	-0.20	0.69	0.83	1	1	106	92	78	0
		24		No powerlaw scaling	2.51	-0.62	0.55	0.87						
		48		No powerlaw scaling	2.65	-0.48	0.55	0.88						
		72		Fit suggests emergence	1.14	-75.98	0.78	0.79						
27	29	12	26	No powerlaw scaling	2.57	-0.76	0.43	0.95	N/A	0	80	72	71.5	1
		24		No powerlaw scaling	1.10	-3.84	0.39	0.96						
		48		Supercritical knee	1.27	-61.76	0.34	0.95						
28	30	12	26	With cut-off, good fit	1.24	-127.56	0.39	0.95	0	4	N/A	N/A	N/A	1
		48		No powerlaw scaling	2.51	-0.05	0.48	0.76						
29	57	12	26	No powerlaw scaling	1.42	-4.64	0.53	0.83	1	1	106	103	78	0
		24			2.36	-0.60	0.46	0.62						
		48			2.75	-0.25	0.54	0.82						
		72			3.03	0.00	0.53	0.75						
30	63	12	26	No powerlaw scaling	2.35	0.00	0.47	0.95	0	N/A	94	88	72	0
		24		With cut-off, good fit	1.19	-82.52	0.38	0.76						
		48		No powerlaw scaling	2.10	0.00	0.43	0.92						

		72		No powerlaw scaling	2.15	-1.07	0.49	0.95						
31	9	12	27	No powerlaw scaling	1.96	-2.49	0.47	0.97	0	0	112	121	75.6	1
		24		With cut-off, good fit	1.34	-85.90	0.36	0.96						
		48		Loss of scaling	2.11	-1.46	0.32	0.24						
32	23	24	27	Supercritical knee	1.36	-55.59	0.32	0.93	0	0	82	92	78	0
		48		No powerlaw scaling	2.84	-0.22	0.46	0.82						
33	24	24	27	No powerlaw scaling	3.37	-0.10	0.55	0.97	0	0	68	84	65	1
		48		No powerlaw scaling	2.08	-1.66	0.47	0.61						
34	33	12		No powerlaw scaling	1.46	-6.40	0.45	0.97	0	0	102	84	74	1
		24	27	No powerlaw scaling	3.36	-0.04	0.44	0.97						
		72		No powerlaw scaling	-0.58	-2.79	0.42	0.98						
35	41	12	27	Slightly supercritical knee	1.48	-75.16	0.55	0.94	0	0	96	88	71	1
		24		Slightly supercritical knee	1.43	-93.23	0.51	0.91						
		48		No powerlaw scaling	2.78	-0.31	0.50	0.85						
		72		No powerlaw scaling	2.24	-0.03	0.45	0.69						
36	60	12	27	No powerlaw scaling	2.86	-0.21	0.48	0.56	1	2	92	80	74.2	1
		24		No powerlaw scaling	3.37	-0.04	0.53	0.50						
		48		Fit suggests emergence	1.10	-37.34	0.52	0.86						

		72		Fit suggests emergence	1.26	-33.00	0.50	0.86						
37	64	12	27	No powerlaw scaling	1.67	-4.71	0.45	0.78	2	2	104	92	73	1
		24		With cut-off, good fit	1.41	-34.20	0.37	0.88						
		48		No powerlaw scaling	1.45	-5.11	0.31	0.65						
		72		No powerlaw scaling	1.84	-1.26	0.39	0.77						
38	20	48	28	Slightly supercritical?	1.62	-13.63	0.45	0.64	0	0	111	92	78	0
39	21	12	28	Slightly supercritical knee	1.22	-135.16	0.38	0.97	0	0	118	81	78	1
		24		Slightly supercritical knee	1.23	-160.43	0.37	0.98						
		48		No powerlaw scaling	5.97	0.00	0.42	0.98						
		72		No powerlaw scaling	2.45	-1.17	0.39	0.96						
40	35	12	28	Supercritical knee	1.57	-16.59	0.34	0.77	0	0	100	103	68.6	0
		24		Loss of scaling	2.22	-1.75	0.42	0.83						
		48		No powerlaw scaling	3.53	-0.13	0.40	0.97						
		72		No powerlaw scaling	2.37	-0.67	0.38	0.96						
41	36	12	28	No powerlaw scaling	2.39	0.00	0.51	0.73	0	0	94	96	74	0
		24		Fit suggests emergence	1.68	-19.45	0.50	0.88						
42	55	12	28		0.66	-2.49	0.52	0.95	2	3	100	76	73.5	1
		24		No powerlaw scaling	1.36	-9.64	0.45	0.97						

		48			0.94	-3.62	0.44	0.96						
43	22	48	30	Fit suggests presence	1.65	-0.43	0.36	0.78	N/A	0	84	92	78	0
		72		Fit suggests presence	1.69	-2.29	0.41	0.47						
44	38	24	30	No powerlaw scaling	2.57	-0.17	0.52	0.75	0	0	102	100	73.8	0
		48		No powerlaw scaling	2.21	-0.91	0.53	0.79						